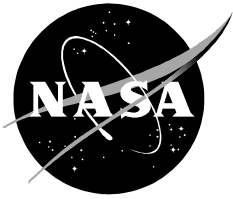NASA/TM—20220017246

Performance, Inflow, and Tip Loss Characteristics of Rotors with Discontinuous Steps in Twist and Lift at the Blade-Tips

Larry A. Young
Ames Research Center, Moffett Field, California

February 2023

NASA STI Program ... in Profile

Since its founding, NASA has been dedicated to the advancement of aeronautics and space science. The NASA scientific and technical information (STI) program plays a key part in helping NASA maintain this important role.

The NASA STI program operates under the auspices of the Agency Chief Information Officer. It collects, organizes, provides for archiving, and disseminates NASA's STI. The NASA STI program provides access to the NTRS Registered and its public interface, the NASA Technical Reports Server, thus providing one of the largest collections of aeronautical and space science STI in the world. Results are published in both non-NASA channels and by NASA in the NASA STI Report Series, which includes the following report types:

- TECHNICAL PUBLICATION. Reports of completed research or a major significant phase of research that present the results of NASA Programs and include extensive data or theoretical analysis. Includes compilations of significant scientific and technical data and information deemed to be of continuing reference value. NASA counter-part of peer-reviewed formal professional papers but has less stringent limitations on manuscript length and extent of graphic presentations.

- TECHNICAL MEMORANDUM. Scientific and technical findings that are preliminary or of specialized interest, e.g., quick release reports, working papers, and bibliographies that contain minimal annotation. Does not contain extensive analysis.

- CONTRACTOR REPORT. Scientific and technical findings by NASA-sponsored contractors and grantees.

- CONFERENCE PUBLICATION. Collected papers from scientific and technical conferences, symposia, seminars, or other meetings sponsored or co-sponsored by NASA.

- SPECIAL PUBLICATION. Scientific, technical, or historical information from NASA programs, projects, and missions, often concerned with subjects having substantial public interest.

- TECHNICAL TRANSLATION. English-language translations of foreign scientific and technical material pertinent to NASA's mission.

Specialized services also include organizing and publishing research results, distributing specialized research announcements and feeds, providing information desk and personal search support, and enabling data exchange services.

For more information about the NASA STI program, see the following:

- Access the NASA STI program home page at http://www.sti.nasa.gov

- E-mail your question to help@sti.nasa.gov

- Phone the NASA STI Information Desk at 757-864-9658

- Write to:
  NASA STI Information Desk
  Mail Stop 148
  NASA Langley Research Center
  Hampton, VA 23681-2199

NASA/TM—20220017246
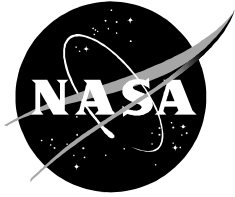
Performance, Inflow, and Tip Loss Characteristics of Rotors with Discontinuous Steps in Twist and Lift at the Blade-Tips

Larry A. Young
Ames Research Center, Moffett Field, California

February 2023

ACKNOWLEDGMENTS

TABLE OF CONTENTS

LIST OF FIGURES

NOMENCLATURE

B	Inboard-blade rotor thrust loss factor, includes interactional aerodynamic contribution of outboard tip section on inboard-blades
b	Span of tip outboard of the twist/lift discontinuity, nondimensionalized with respect to rotor radius
C_T	Total rotor thrust coefficient
C_{Tt}	Tip thrust coefficient
r	Rotor radial station, from zero at rotor axis to one at blade tip, nondimensionalized
r_{ac}	Outboard tip section spanwise aerodynamic center location, assumed to be at tip mid-span
s_i, s_o	Spacing of two-dimensional vortex sheets representing the rotor wake for the inboard and outboard tip regions of the rotor
w	Complex potential used in the derived extended-Prandtl inflow model
α_i	Uniform induced inflow estimate for tip based on momentum theory
$\Delta\theta$ or $\Delta\theta_{Tip}$	Tip index angle relative to the inboard-rotor blade, radians, positive nose up
$\lambda(r)$	Rotor nonuniform inflow distribution, as a function of radial station
λ_i	Uniform induced inflow estimate for inboard rotor, based on momentum theory
λ_t	Effective tip inflow angle, which includes the interactional aerodynamic contribution of the inboard-blades
μ	Rotor axial-flow advance ratio
$\varphi(...)$	Extended Prandtl indexed-tip proprotor inflow function

Performance, Inflow, and Tip Loss Characteristics of Rotors with Discontinuous Steps in Twist and Lift at the Blade-Tips

Larry A. Young

Ames Research Center

SUMMARY

This paper examines the inflow and tip-loss characteristics of rotors incorporating indexed blade-tips that have discontinuous steps in twist or lift distribution. An extension of the classic two-dimensional Prandtl tip loss analysis is derived for indexed-tip rotors and proprotors. Additionally, parametric analysis of tip span and indexed-tip twist-steps was performed using computational fluid dynamics for hover and high-speed axial-flow conditions for proprotors. The intent of this work is to define a new class of active-rotor-twist-control designs for proprotors that avoids unnecessary aeroperformance compromises for rotor twist distributions for proprotors in all phases of flight.

INTRODUCTION

Optimizing proprotor hover figure of merit and cruise propulsive efficiency is crucial to the success of a variety of VTOL aircraft—including tiltrotor, tiltwing, and tail-sitter aircraft in their manned and unmanned configurations. It is well known that proprotor twist distributions are a compromise between the ideal distributions for the two different operating conditions and flight regimes. Classic rotor theory can even be employed to define "ideal" and "optimum" twist distributions for hover and axial-flow cruise. A key aspect of the problem lies in how to mechanically provide—safely and efficiently—such variable (twist-rate) rotor geometry.

In the 1980s, passive-rotor-control devices called respectively the constant-lift rotor and the free-tip rotor (FTR) were explored at NASA Ames Research Center (Refs. 1-5). The FTR used indexed-tips with pitch angles passively determined by aerodynamic tip forces being counterbalanced by mechanisms that had constant-torque outputs, including various forms of near constant-torsion springs. Analytical work followed by rotor hover and edgewise forward flight wind tunnel test campaign studies were conducted. During the 1990s, both active- and passive-rotor-control approaches to aeroelastic-tailored rotors were explored by NASA and academia (Refs. 6 and 7). These rotors were designed to couple rotor torsional moments, and twist, to rotor tensile forces from centrifugal force loading—and thereby to rotor revolutions per minute (RPM)—to yield different rotor twist distributions as a function of helicopter- and airplane-mode RPM. Additionally, some limited work, e.g., Reference 8, performed on piezoelectric-driven tailored rotor work in the 1990s showed some promise, but were ultimately deemed to be impracticable for the specific design implementations studied.

1

As an alternate approach, it is proposed that the large body of work directed towards electromechanical actuators on servo-flaps for active rotors (e.g., Refs. 9 and 10) be adapted to directly drive rotor indexed-tips to prescribed quasi-steady pitch angles as a function of vehicle operating conditions (refer to Fig. 1). If proven feasible, such an approach would result in a safe and efficient mechanical implementation. Even then, the unique aspects of discrete twist jumps enabled by indexed-tips versus continuous twist distributions require a fundamental reexamination of the hover and axial-flow aeroperformance characteristics of such discrete indexed-tip propellers and proprotors.

This work provides a fundamental analytical and computational investigation of the hover and axial-flow cruise performance for propellers and proprotors with indexed-tips.
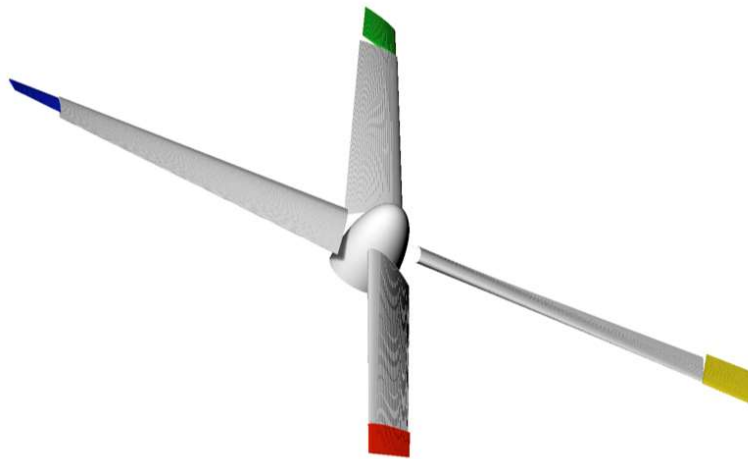
Figure 1. Actuator-driven indexed-tip proprotors.

POSSIBLE APPLICATIONS OF THIS WORK

It is widely recognized that tiltrotor proprotors have twist distributions that reflect a compromise between the optimum distributions for hover and high-speed airplane-mode flight. Several competing conceptual approaches have been proposed in the literature for changing/modifying the effective twist of rotors to enhance aerodynamic performance (for example, the extension-twist coupled rotor, Refs. 6 and 7). Other concepts that change the effective twist of the rotor include servo-flaps, embedded flaps, and controllable-twist rotors. One of the earliest proposals on the "constant lift rotor" concept was established in 1979, where a rotor used active or passive control to change rotor twist through discrete steps in tip index angle (Ref. 11). The free-tip rotor concept, which used passive free-pitching tips, was proposed for improving helicopter performance (Ref. 1). The indexed-tip proprotor concept discussed in this paper is based, in part, on that early work.

Figures 1 and 2 are conceptual sketches of an indexed-tip proprotor. In general, an indexed-tip proprotor would have the same characteristics as a conventional proprotor—high solidity and highly twisted rotor blades. The difference being, of course, that an actuator mechanism embedded in the rotor blades will index the tips to their optimum pitch angles, per pilot or flight-control input, throughout the aircraft operating envelope. The length of the indexed-tip span will likely range from 5 to 20 percent of the rotor radius. Actuator control loads and tip centrifugal force will be the limiting factors for the tip size. The tips would be trimmed to maximize rotor efficiency and/or thrust capability.

(a)

(b)

3
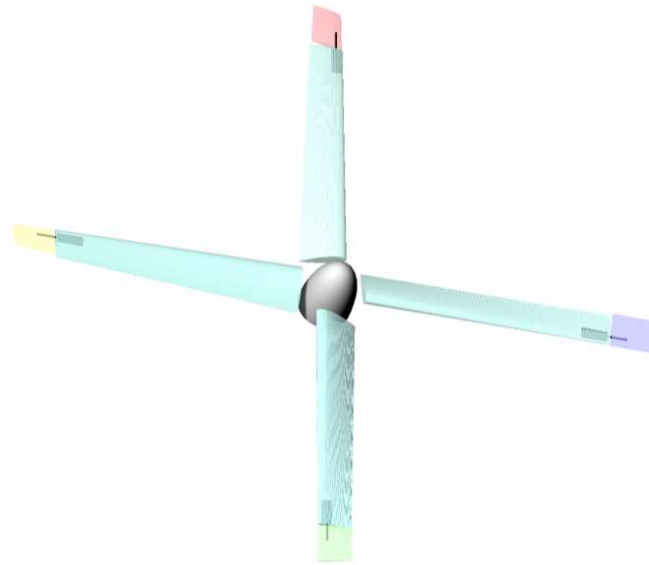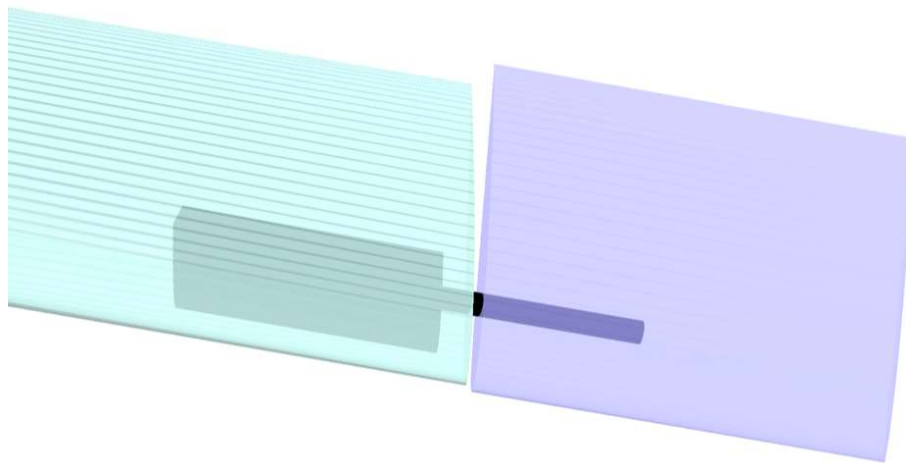
(c)

Figure 2. Indexed-tip mechanical implementation: (a) view of the proprotor, (b) close-up of indexed-tip, and (c) indexed-tip mechanism.

All of the proposed indexed-tip $\Delta\theta$ actuation is very low-frequency, being effected over many rotor revolutions; N-per-Rev control is not being proposed in this paper. The above proposed servo-actuator approach to indexed-tip proprotor $\Delta\theta$ control during flight not only potentially allows for improved efficiency in hover and axial-flow forward flight but thrust augmentation (above that of non-actuated baseline rotor) in those regimes. Finally, though this paper will focus on these two aspects of improved efficiency and thrust augmentation in hover and axial flow conditions, the ability to actuate the indexed-tip setting during proprotor transition/conversion from tiltrotor helicopter- to airplane-mode also has advantages. As proprotors are highly twisted for best aeroperformance during hover and airplane-mode, in edgewise helicopter-mode slightly twisted, near-linear, blade twist rates are more advantageous from both an aeroperformance and structural load perspective. Accordingly, actuating the indexed-tips to reduce the overall twist rate during transition/conversion might be beneficial. The study of indexed-tip $\Delta\theta$ actuation in proprotor transition/conversion is left to future work.

INFLOW ANALYSIS DERIVATION

The most critical aspect of the analysis is predicting the interactional aerodynamic contribution of the indexed-tip on the inboard-rotor and vice versa. All other aspects of the analysis involve modest extensions of blade element and axial momentum theory for the indexed-tip proprotor application.

The analytical treatment of the indexed-tip interactional aerodynamics is based upon an extension of Prandtl's two-dimensional vortex sheet wake analysis for rotor tip losses due to finite blades (Ref. 12). Reexamination of Prandtl's work has led to the conclusion that the Prandtl's analysis can be generalized to predict the upwash outboard of rotor tips and, further, this upwash expression can be adapted for application to the indexed-tip/inboard-rotor interactional aerodynamics problem.

4

Figure 3 shows the two-dimensional vortex sheet model used in the indexed-tip proprotor interactional aerodynamics analysis. The individual elements of the wake model correspond to one of three flow fields superimposed over each other. Superposition of the individual potential flow fields captures the key flow features for indexed-proprotors. The resulting spanwise rotor inflow distribution is shown in Figure 4a-c for a range of tip/blade loading ratios. The tip loading in the figure varies from zero to where the tip is uniformly loaded with respect to the inboard-rotor, i.e., $C_{Tt} = (2-b)bC_T$. The rotor inflow distribution trends from this analysis compare very well qualitatively to predicted and measured downwash distributions for nonrotating indexed-tip and semi-span wing configurations (Ref. 3). Equations 1a-b are the solution for the nonuniform inflow distribution for the complete rotor, based on the vortex sheet model of Figure 3.

The junction between the inboard-blade and the indexed-tip can be physically implemented in one of two ways: (1) discontinuous jump or (2) a smooth transition. The below extended Prandtl analysis assumes a discontinuous jump.
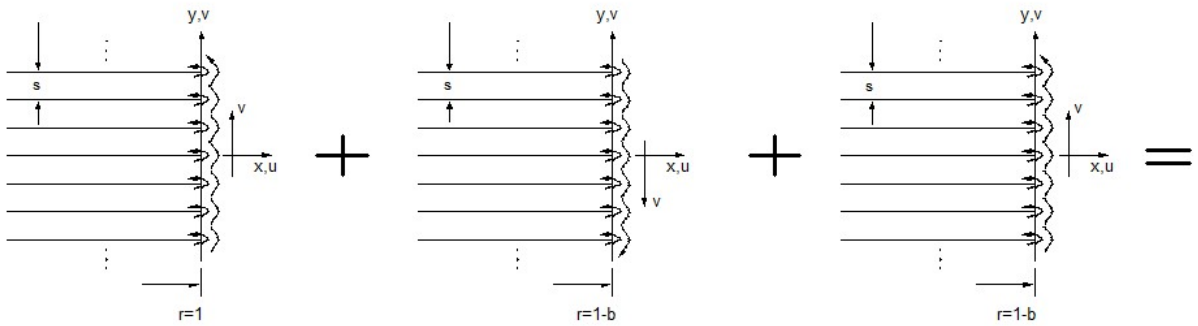
Figure 3. Extended Prandtl two-dimensional vortex sheet model.

The classic Prandtl finite-blade, lightly-loaded, rotor wake model is based on a set of semi-infinite vortex sheets that have the complex potential (e.g., Ref. 12) for the overall wake, Equation 1a-b. (The spacing between the vortex sheets, s, and the far-stream velocity, v_0, as $x \to \infty$.)

$$w = -v_0 \frac{s}{\pi} cos^{-1}\left(e^{\pi z/s}\right)$$

where

$$z = x + iy$$

(1a-b)

5

From the complex potential theory, the individual velocities can be derived from the expressions:

$$u = \frac{\partial w}{\partial x}$$

$$v = \frac{\partial w}{\partial y} = \frac{iv_0 e^{\pi(x+iy)/s}}{\sqrt{1 - e^{2\pi(x+iy)/s}}}$$

(2a-b)

Classic Prandtl analysis ends with considering the velocity/inflow within the rotor wake slipstream ($r \leq 1$ or $x \leq 0$). Further, the velocity/inflow within the rotor wake slipstream considered is the mean velocity across the vortex sheet-to-sheet spacing, s, which is given by Equation 3.

$$\bar{v} = \frac{1}{s} \int_0^s (v_0 + v) dy = v_0 \frac{s}{\pi} \cos^{-1}\left(e^{\pi x/s}\right)$$

(3)

Classic Prandtl rotor wake analysis is inadequate for indexed-tip proprotor analysis. First, the classic Prandtl analysis gives physically unrealistic results for the rotor wake beyond the classic rotor wake slipstream ($r > 1$ or $x > 0$). This is because the rotor upwash beyond $x > 0$ cannot be modeled from Equation 3. It is this rotor upwash that is critical to predicting the velocities across the tip region of indexed-tip proprotors. Arriving at a more physically realistic modeling of the tip region can be accomplished by extending the Prandtl analysis, instead of focusing on the mean inflow $\bar{v}$, consider the velocity, v, at the edge of one of the vortex sheets where $y = s$ and $x > 0$.

$$v = \frac{-ie^{\pi x/s}}{\sqrt{1 - e^{2\pi x/s}}}$$

(4)

There are some subtle considerations to be accounted for when interpreting Equation 4. The key reason why defining a mean value for the upwash is necessary is because Equation 4 has only real and physically realistic (producing an upwash) values for v for discrete integer values for y in terms of s, specifically, for $y \geq 0$, $y = 1s, 3s, 5s, \cdots$. For $y < 0$, only real and physically realistic values are obtained for $y = 2s, 4s, 6s, \cdots$. Alternatively, real, but unrealistic, values of v (where downwash instead upwash is predicted) result when half-integer values of y in terms of s are employed, i.e., $y = \pm\frac{1}{2}s, \pm\frac{3}{2}s, \pm\frac{5}{2}s, \cdots$.

Recognizing the above noted inherent analysis subtleties in Equation 4, for purposes of simplicity, a value of $y = s$ will be used to define a new extended-Prandtl inflow function (note that the Euler equation $e^{i\pi} + 1 = 0$ needs to be applied as a part of the following analysis). Finally, another issue with Equation 4 is that the result for v is singular at $x \to 0^+$. Accordingly,

a desingularization function ($\propto (x/(1 + x))^n$) needs to be incorporated into this expression. These modifications are incorporated in Equation 5.

$$\varphi(x, s, a, n) \equiv \frac{s}{\pi} \cos^{-1}\left(e^{\pi x/}\right) u(-x) + \left[1 - \frac{ie^{\pi(x+a)/s}}{\sqrt{1 - e^{2\pi(x+a)/s}}}\right] \left(\frac{x}{1 + x}\right)^n u(x)$$

(5)

In Equation 5, the Heaviside unit step function, $u(\cdots)$, is used. There is no a priori method to define the desingularization function constants, a and n. For this paper, the following ad hoc values are used: $a = 0.001$ and $n = 1/4$.

An inflow distribution for indexed-tip rotors/proprotors can be defined by superposition according to the Figure 3 framework.

$$\lambda = \mu + \lambda_i(C_T, C_{Tt}, \mu)\varphi(r - 1 + b, s_i, a, n) + r_{ac}\alpha_i\big(\varphi(r - 1, s_o, a, n) - \varphi(r - 1 + b, s_o, a, n)\big)$$

(6a)

where

$$s_i = \frac{2\pi}{N} \frac{r_{ac}(\alpha_i + \mu/r_{ac})}{\sqrt{1 + [r_{ac}(\alpha_i + \mu/r_{ac})]^2}}$$

(6b)

$$s_o = \frac{2\pi}{N} \frac{(\lambda_i + \mu)}{\sqrt{1 + (\lambda_i + \mu)^2}}$$

(6c)

$$\alpha_i = \frac{1}{2}\left[\frac{-\mu}{r_{ac}} + \sqrt{\left(\frac{\mu}{r_{ac}}\right)^2 + \frac{2C_{Tt}}{r_{ac}^2(2b - b^2)}}\right]$$

(6d)

$$\lambda_i(C_T, C_{Tt}, \mu) = \frac{1}{2}\left[-\mu + \sqrt{\mu^2 + \frac{2k^2(C_T - C_{Tt})}{(1-b)^2}}\right]$$

(6e)

Where k in Equation 6e is a semiempirical induced inflow constant.

An extended expression can also be derived to account for the inflow impact of the blade-root cutout that is typically seen for rotors and proprotors. This extended inflow expression is given below. Two induced flow constants, k and k_0, are used in this overall analysis. The induced flow constant k is used for the majority of the rotor, $r \geq {\sim}2r_c$. An induced flow constant k_0 for the blade root region of the rotor is also defined. The values used for subsequent results are $k = 1.38$ and $k_0 = 1$; the constant k was extracted for computational fluid dynamics results.

$$\lambda_{rc} = \lambda - \left(\frac{k_0}{k}\right)^2 \lambda_i(C_T, 0^+, \mu)\varphi(r - r_c, s_{rc}, a, n)$$

For $r < {\sim}2r_c$. Note that $s_{rc} = \frac{2\pi}{N}\frac{\mu}{\sqrt{1+\mu^2}}$.

$$\text{(7a)}$$

$$\lambda_{rc} = \lambda$$

For $r > 2r_c$

$$\text{(7b)}$$

EXTENDED PRANDTL INFLOW SUPERPOSITION MODEL FOR INDEXED-TIP PROPROTORS: ANALYTICAL RESULTS

Given the above analysis, a number of results are now presented and discussed. Figure 4 presents the results from Equations 5-7 for the inflow distribution for hover for a four-blade rotor operating at a thrust coefficient of CT=0.01 for a range of CTt (uniform loading between the inboard rotor and the tip is achieved is when CTt=0.0019 and CT=0.01, see Eq. 8).

$$CTt_{uniform} = (1 - (1 - b)^2)CT$$

$$\text{(8)}$$

If CTt is greater than $CTt_{uniform}$, then the indexed-tip is carrying more distributed lift than the (immediately) inboard-blade section; if CTt is less than $CTt_{uniform}$, then the tip is carrying less lift than the inboard-blade section.

(a)

(b)

9

(c)
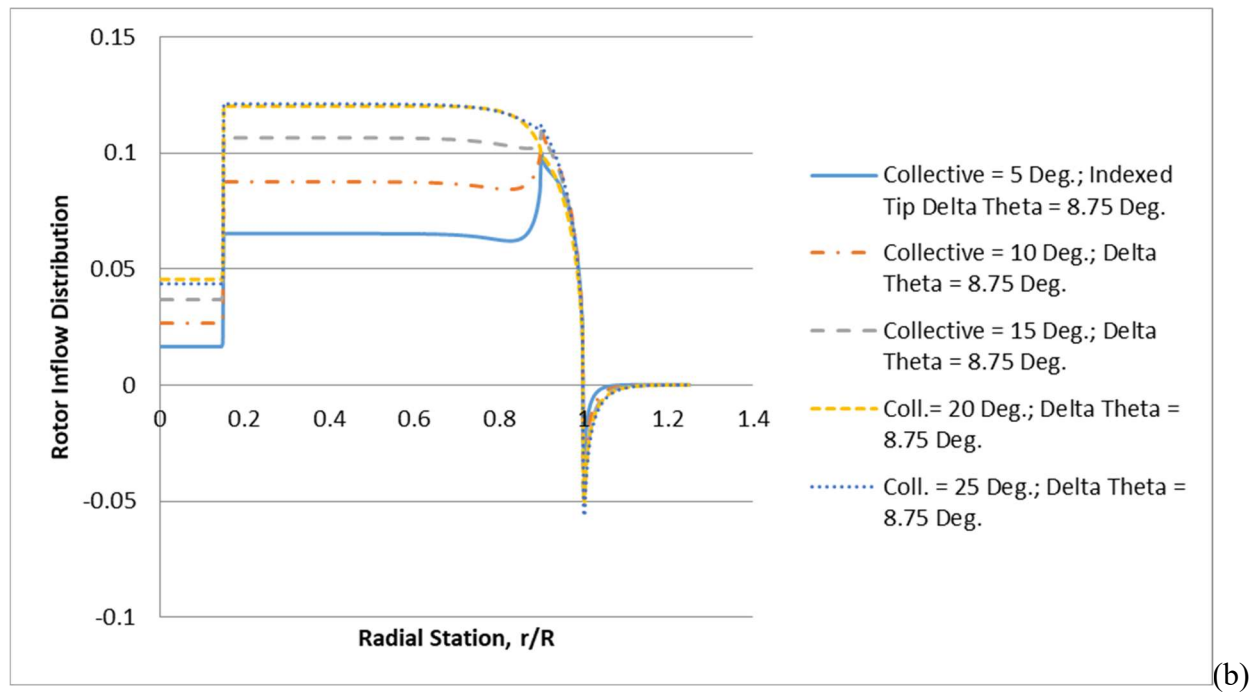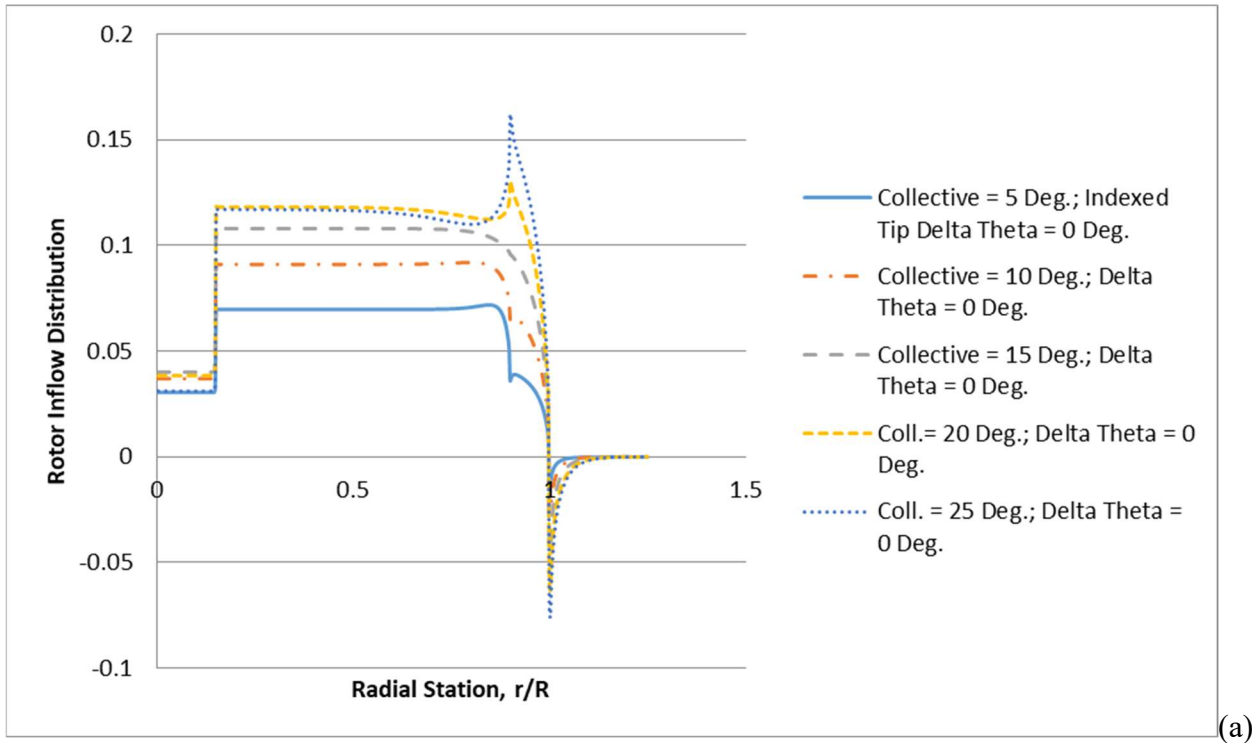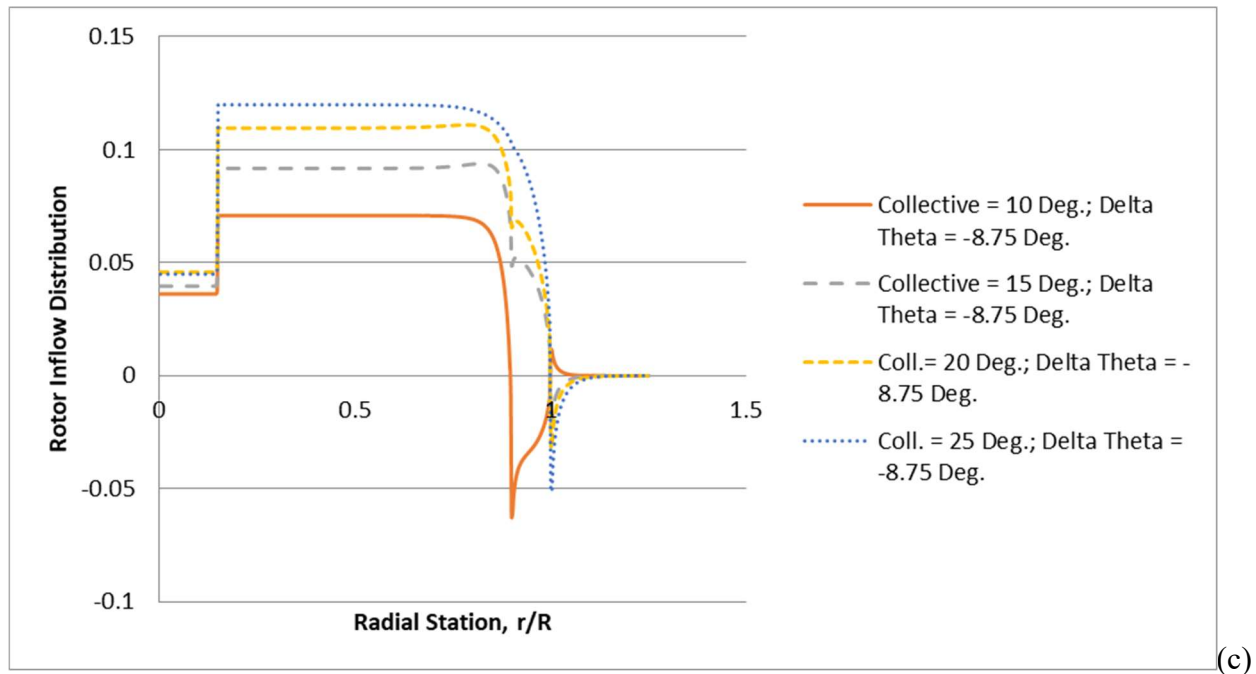
Figure 4. Inflow distributions for various indexed-tip $\Delta\theta$ and rotor collectives: (a) $\Delta\theta$= 0 degree, (b) $\Delta\theta$= 8.75 degrees, and (c) $\Delta\theta$= -8.75 degrees.

COMPUTATIONAL FLUID DYNAMICS RESULTS

The above analytical results provide valuable insights into the aeroperformance of indexed-tip proprotors but a deeper understanding of the problem requires the application of computational fluid dynamics (CFD). The computational fluid dynamics code RotCFD (Ref. 13) has been used to make extensive predictions as to rotor performance for hover and axial-flow forward-flight throughout this paper. The baseline rotor is based on the general characteristics of the NASA LCTR2 reference design (Ref. 14). Previous validation work for proprotors using RotCFD is detailed in Reference 15; note that stall limit corrections are not made in this paper as compared to Reference 21.

A considerable body of indexed-tip proprotor predictions are presented for both hover and various axial-flow conditions. Throughout this analysis, two different types of tips are examined: tips that continue the inboard twist rate of the proprotor outward across the tip span ("twisted tips") and those that do not have any twist across the tip span ("untwisted tips"). Finally, predictions are made for twisted and untwisted tips of varying lengths of tip span.

The objective of these CFD aeroperformance predictions is to identify the best performing indexed-tip configuration and $\Delta\theta$ settings for indexed-tip proprotors in hover and axial-flow

10

conditions, with the expectation that embedded actuators in the rotor blade will change the $\Delta\theta$ setting as needed as a function of rotor collective and axial-flow velocity. This includes determining the best length of tip span—and twisted versus untwisted tips—for both hover and axial-flow forward flight. All tips studied have chord distributions that are a continuation of the inboard-blade baseline rotor; tip sweep or anhedral are not incorporated into this CFD study. The aeroperformance focus will be on predicting rotor thrust and power coefficients and hover figure of merit or forward-flight propulsive efficiency. The CFD predictions will begin with 10-percent span indexed-tips that are untwisted. The other indexed-tip proprotor configurations will follow.

BASELINE ROTOR AND INDEXED-TIP PROPROTOR WITH UNTWISTED, 10-PERCENT SPAN INDEXED-TIPS

Figure 5 presents the twist distribution of the baseline rotor and a comparable indexed-tip rotor in the untwisted tip configurations, at 10-percent radial span increments.
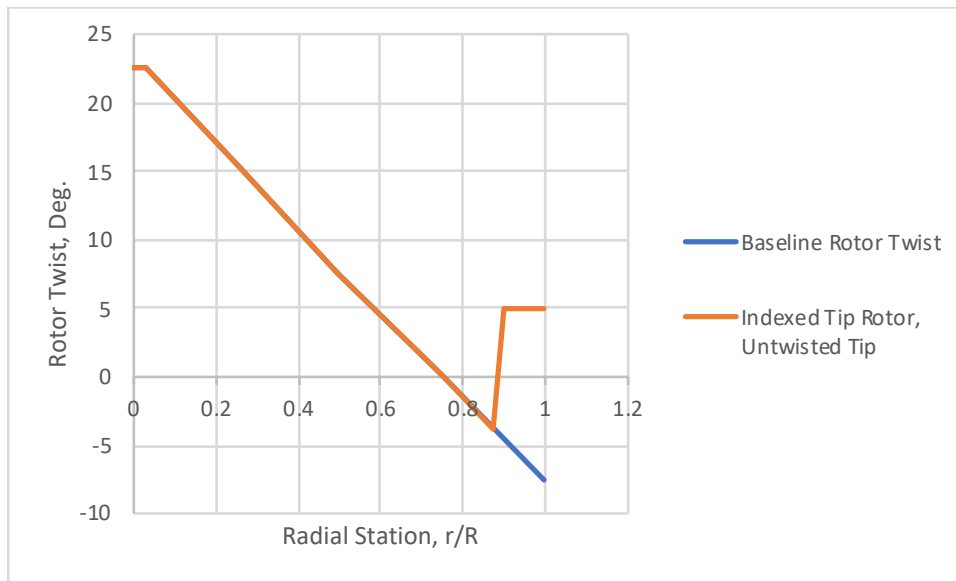
Figure 5. Representative rotor twist distribution: baseline rotor and 10-percent span indexed-tip set at 5 degrees tip-twist.

Figure 6a-b shows representative predicted rotor disk differential-pressure contours for the baseline rotor and the indexed-tip rotor for hover conditions. Figure 7a-b shows predicted rotor disk differential-pressure contours for the baseline rotor and indexed-tip rotor for an axial-flow cruise conditions of 500 feet per second (fps). The change in loading at the outer 10 percent of the rotor radius is a demarcation of the indexed-tip being setting set at a nonzero $\Delta\theta$.

11
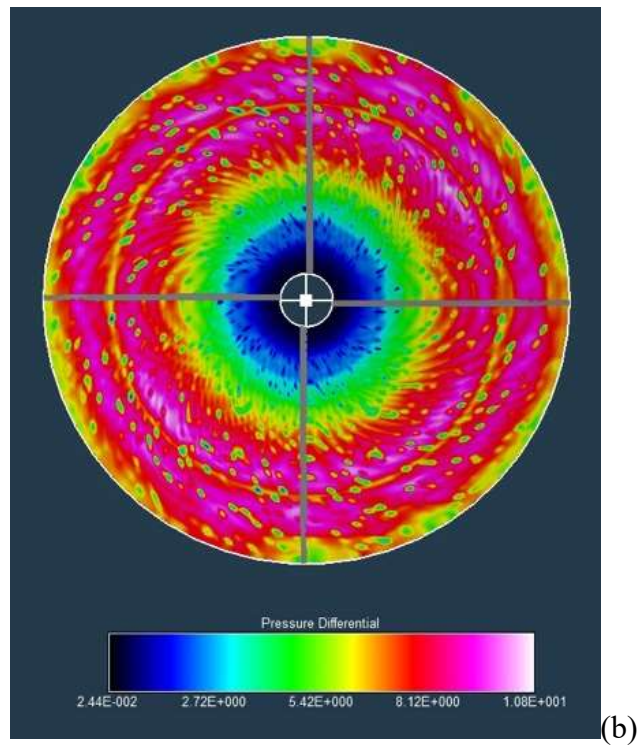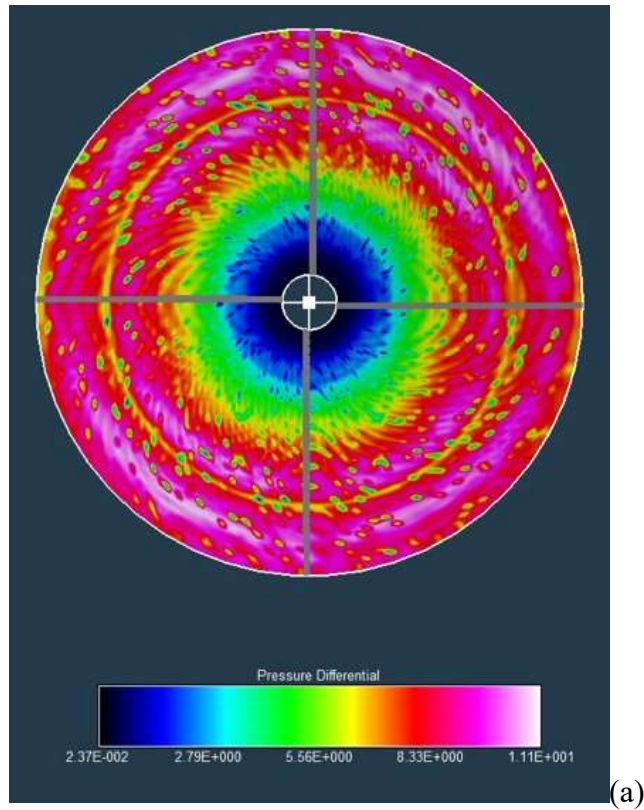
Figure 6. Representative hover results (differential-pressure across the rotor disk, collective = 20 degrees) for LCTR2 proprotor (Ref. 14): (a) baseline rotor and (b) 10-percent span indexed-tip set at 5 degrees tip-twist.
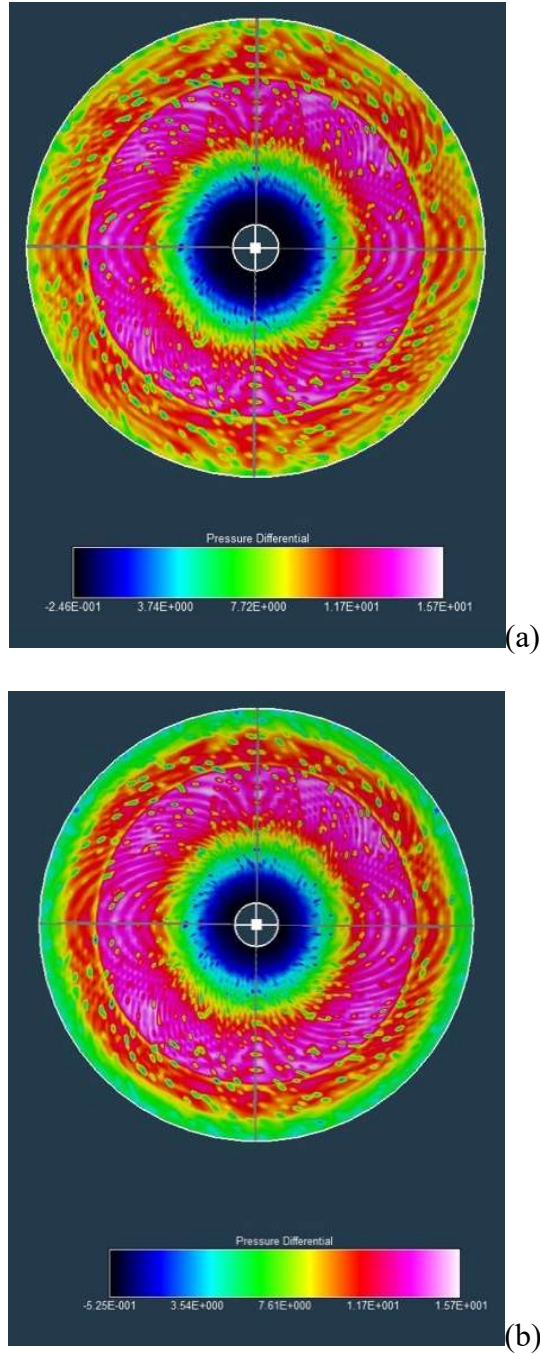
Figure 7. Representative cruise axial-flow results (differential-pressure across the rotor disk, collective = 60 degrees at V=500 fps) for LCTR2 proprotor (Ref. 14): (a) baseline rotor and (b) 10-percent span indexed-tip set at 5 degrees tip-twist.

13

1. Inflow Result Comparisons between Analysis and CFD

Figures 8-10 are predictions of the hover proprotor inflow distribution (at the rotor disk plane) for rotor collective sweeps and for different indexed-tip delta theta, $\Delta\theta$, angles.
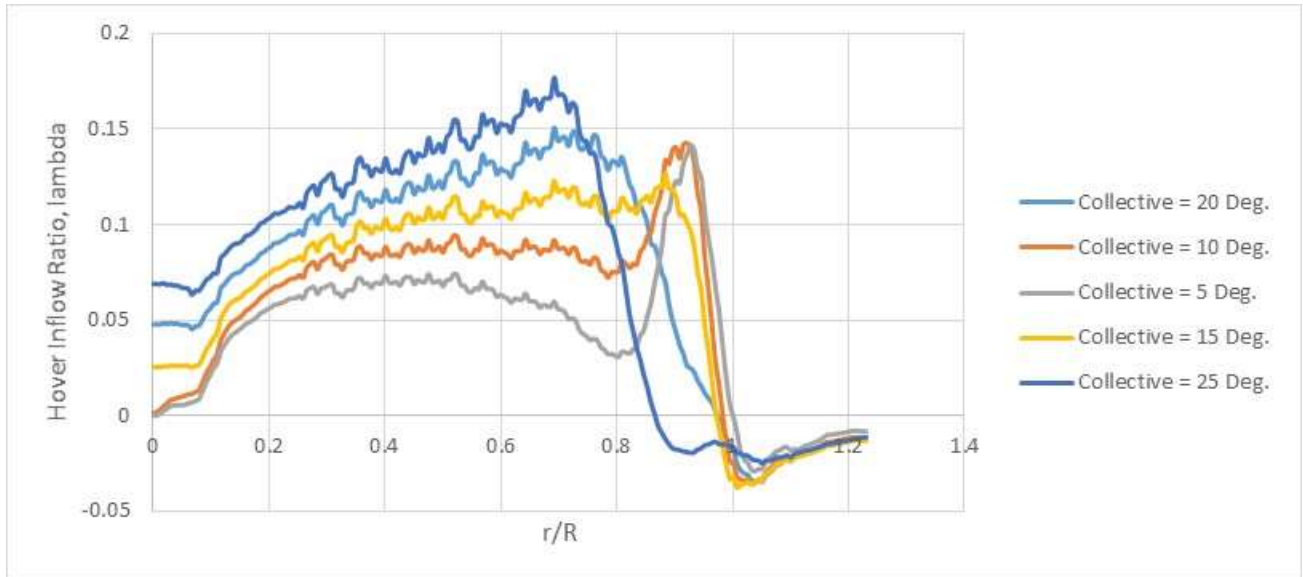
Figure 8. Collective sweep showing CFD rotor inflow results for $\Delta\theta$Tip= +8.75 degrees with untwisted tip outer-span.

Figure 8 clearly shows the influence of stall on the outboard indexed-tips for rotor collectives greater than 15 degrees. The stall results from the large positive $\Delta\theta$Tip angle used for the RotCFD results shown in Figure 8. Figures 9 and 10 present the inflow predictions for two additional $\Delta\theta$Tip, aka $\Delta\theta$, angles.
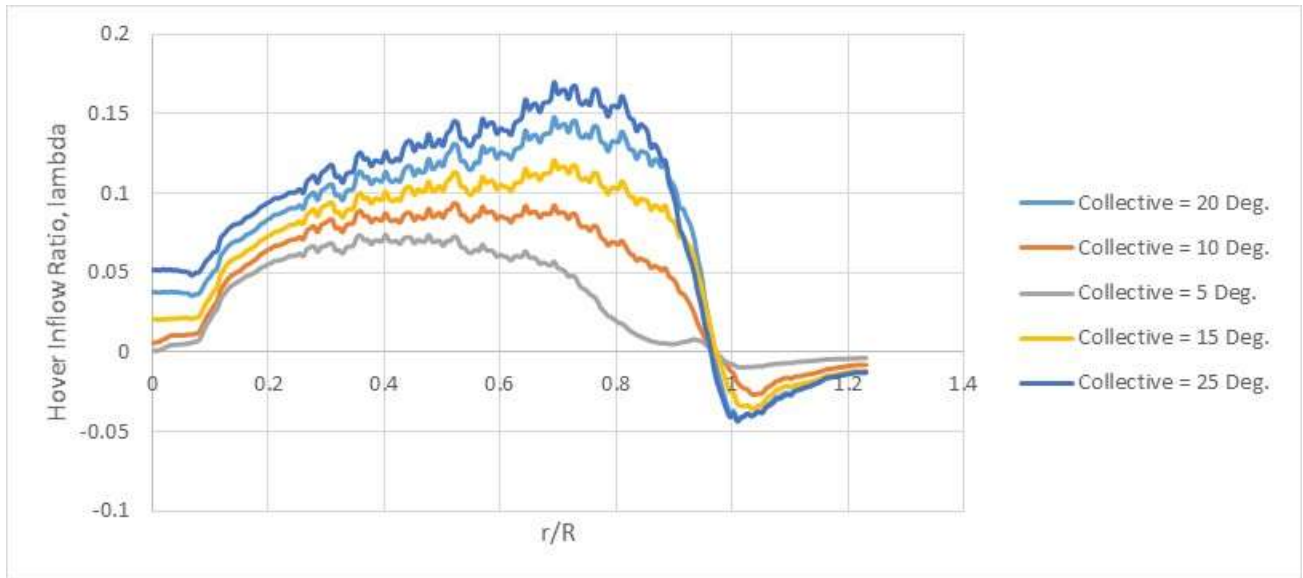
Figure 9. Collective sweep showing CFD rotor inflow results for ΔθTip= 0 degrees with untwisted tip outer-span.
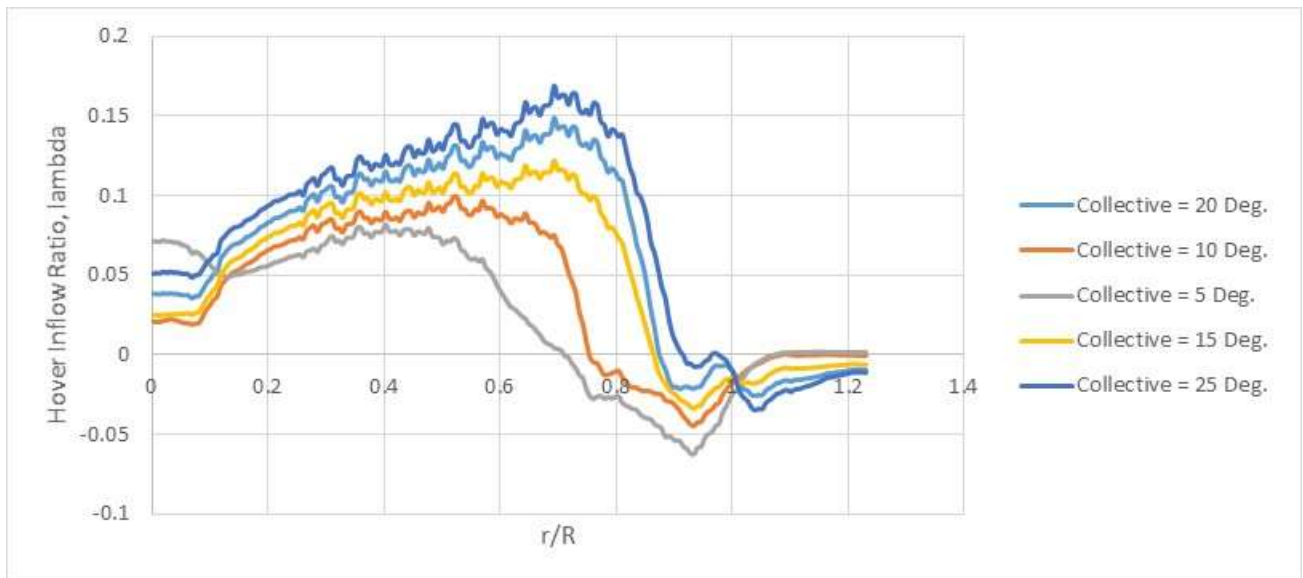
Figure 10. Collective sweep showing CFD rotor inflow results for ΔθTip= -8.75 degrees with untwisted tip outer-span.

15

Figures 11-13 are a series of hover inflow distribution predictions correlating the earlier introduced analytic Prandtl-type wake superposition results and the RotCFD predictions performed as a part of this study. The tip thrust coefficient contribution, C_{Tt}, is estimated from two sets of RotCFD predictions. The thrust predictions for the indexed-tip proprotor for various different $\Delta\theta_{Tip}$ values is subtracted by the thrust from a rotor having the same collective but truncated radius (minus the span of the indexed-tips). The difference between the two thrusts yields the tip thrust contribution used to estimate C_{Tt} and, thereby, used as input for the extended Prandtl analysis.
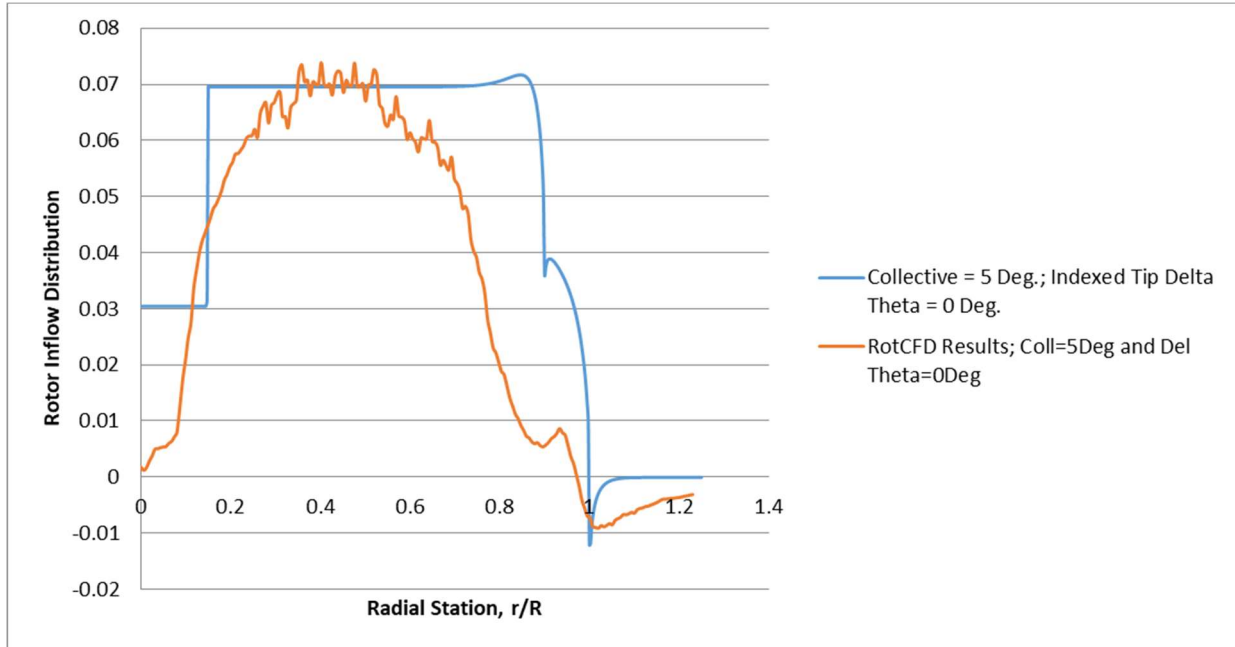
Figure 11. RotCFD and Prandtl-type superposition analysis for hover inflow radial distribution at θ=5 and ΔθTip=0.
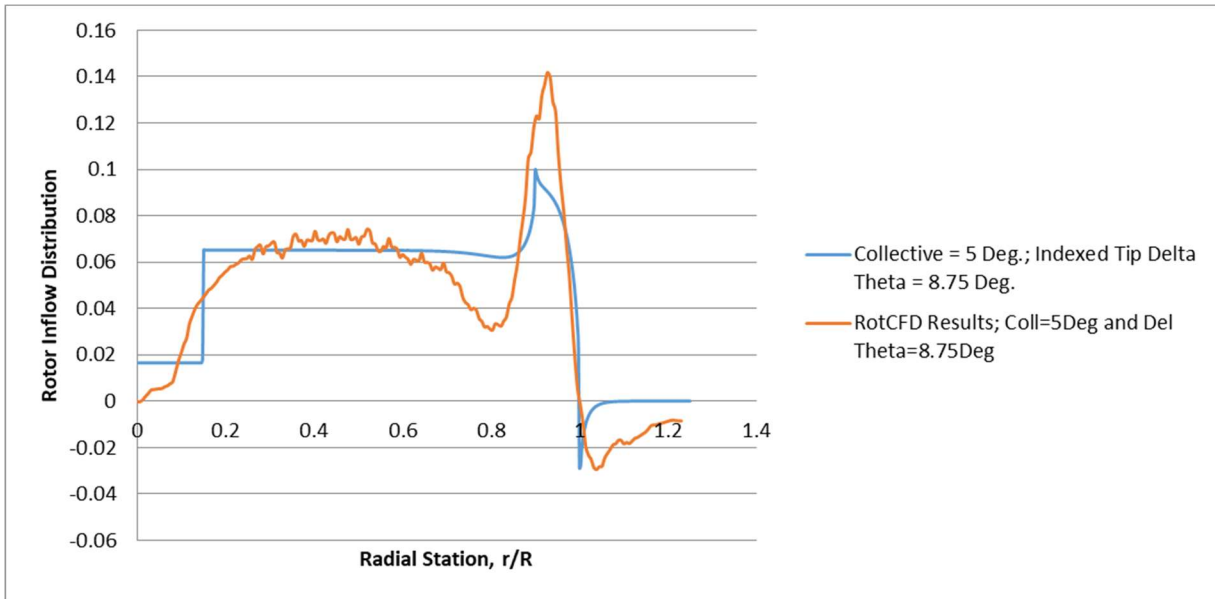
Figure 12. RotCFD and Prandtl-type superposition analysis for hover inflow radial distribution at θ=5 and ΔθTip = 8.75.
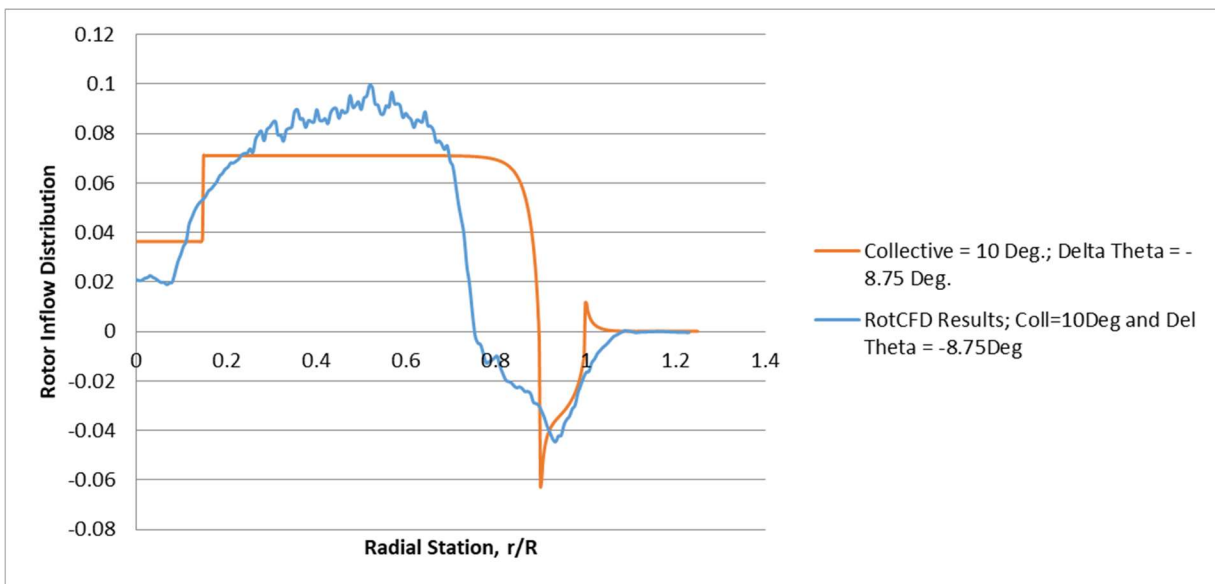
Figure 13. RotCFD and Prandtl-type superposition analysis for hover inflow radial distribution at θ=10 and Δθtip = -8.

17

2. Hover Performance CFD Results

The influence of indexed-tip angle, $\Delta\theta$, on rotor performance for hover is studied in Figures 14-16, which show the predicted hover rotor performance results for a nominal collective of 20 degrees (as compared to the baseline rotor that, by definition, has a $\Delta\theta=0$ and twist rate carried continuously across the rotor tips from the inboard-blade section). Interpretation of the hover thrust coefficient trends with respect to $\Delta\theta$ is explored. First, as $\Delta\theta$ becomes more negative, the less lift is carried by the rotor tips and, correspondingly, the lower the amount of thrust carried by the overall rotor. Second, as $\Delta\theta$ becomes more positive, the rotor tips begin to enter stall and the tip lift is therefore reduced leading to a corresponding reduction in overall rotor thrust. There does appear, though, a narrow band of indexed-tip approximately -1<$\Delta\theta$<3 degrees (for rotors with untwisted tips) that exceeds the thrust capability of the baseline rotor (that has a continuous twist rate carried from the inboard-blade section out across the blade tips).
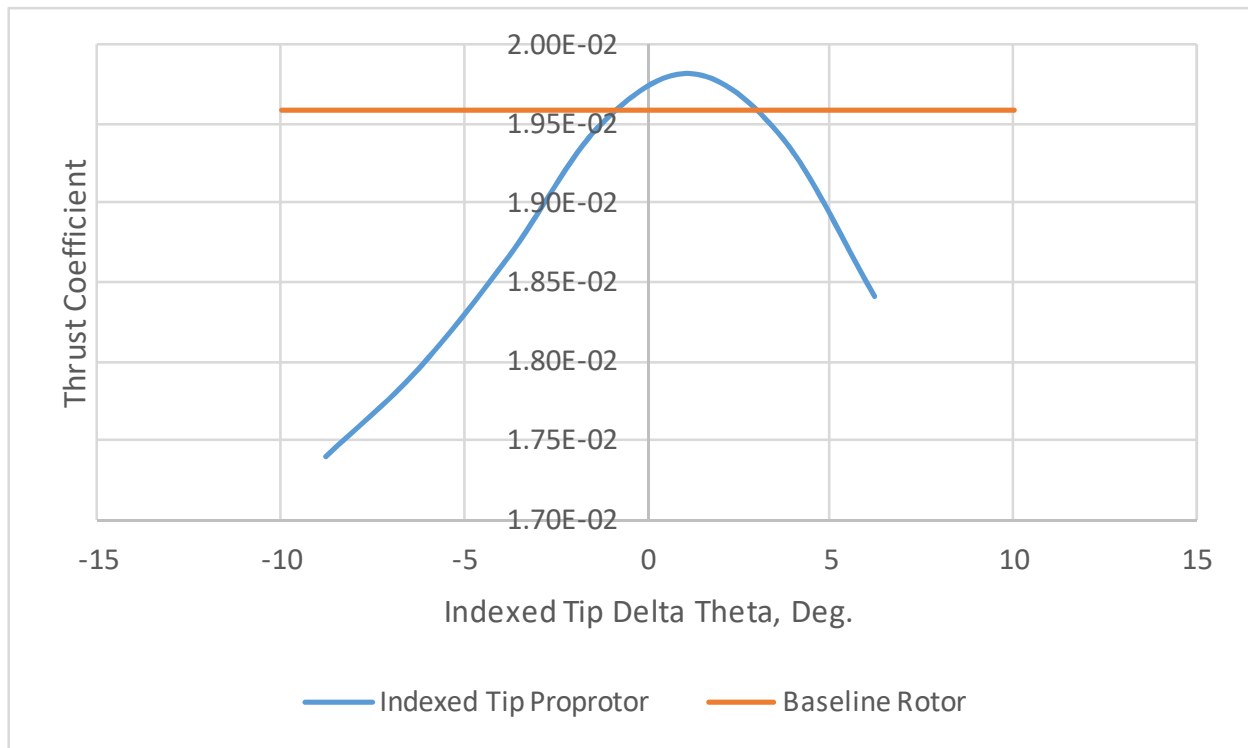
Figure 14. Thrust coefficient trend comparison between indexed tip proprotor as a function of indexed-tip $\Delta\theta$ and a baseline rotor.

Figure 15 hover torque coefficient trends with $\Delta\theta$ are also presented. First, as $\Delta\theta$ becomes more negative, the tip lift and the rotor thrust decrease; this means in turn that the induced-drag contribution to rotor torque decreases. Second, as the $\Delta\theta$ becomes more positive, as noted earlier, the tips stall and the profile-drag contribution increases significantly.

18
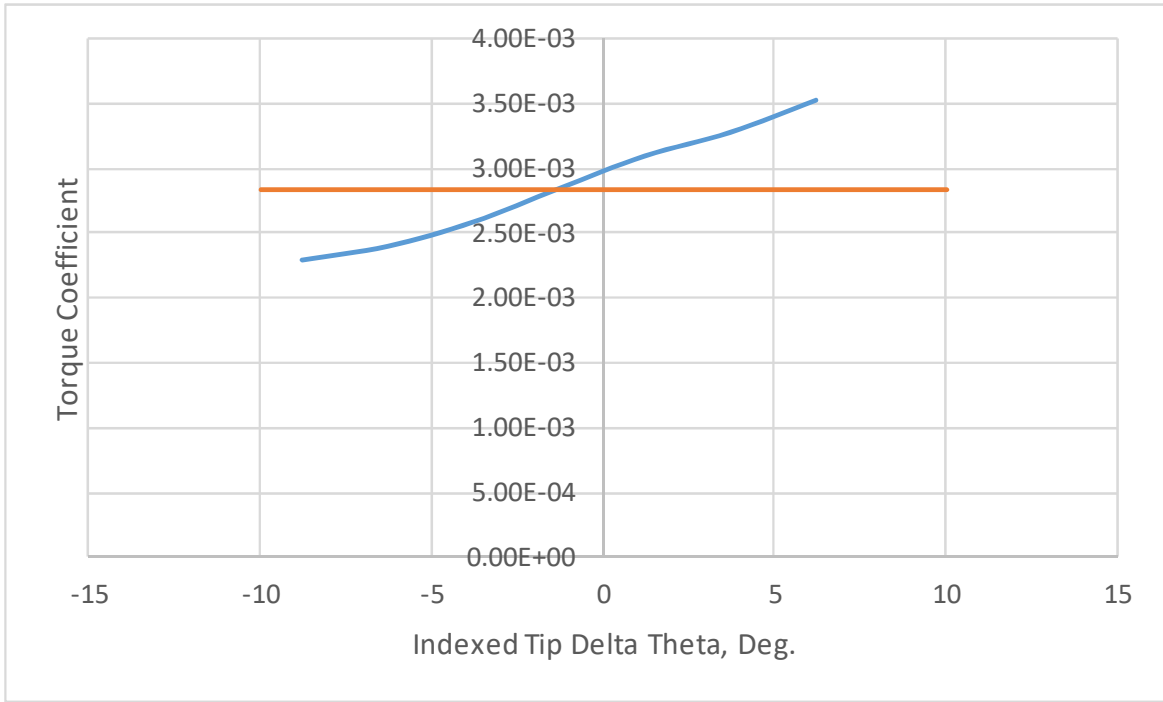
Figure 15. Torque coefficient trend (for an untwisted indexed-tip) as a function of indexed-tip Δθ.

Figure 16 hover figure-of-merit trend with Δθ is less intuitive than that of the thrust and torque coefficient trends. A small improvement in figure of merit over that of the baseline rotor is observed for Δθ < -2 degrees. This improvement appears to slowly reach an asymptotic limit as Δθ becomes more negative, for the range of Δθ computationally explored.
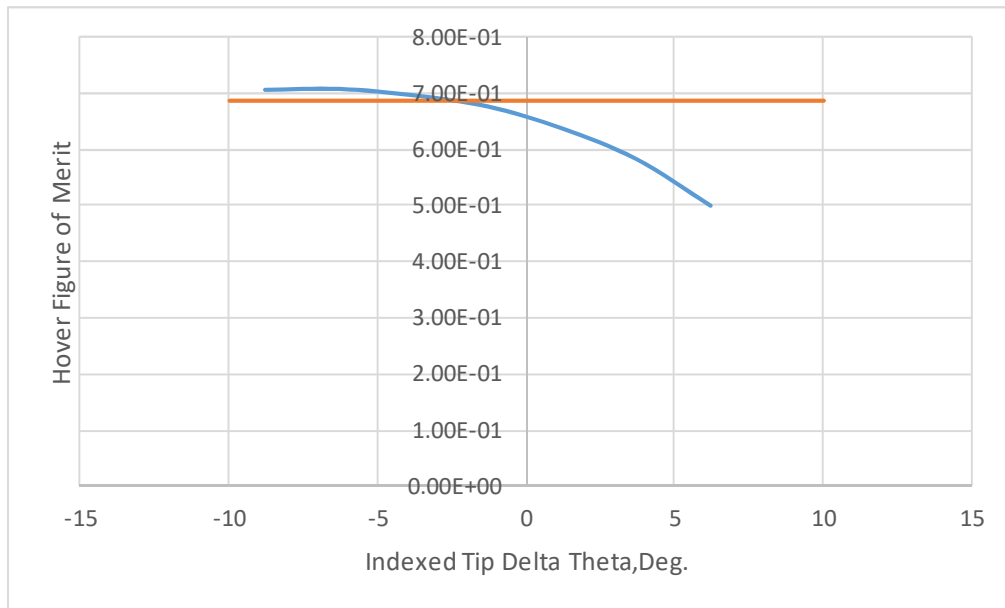
Figure 16. Figure of merit (for an untwisted indexed-tip) as a function of indexed-tip Δθ.

19

The previous hover aeroperformance trends in Figures 14-16 were at a fixed collective of 20 degrees for a range of $\Delta\theta$ values. The following hover trends are for a range of rotor collectives at two different $\Delta\theta$ values, i.e., $\Delta\theta = -8.75$ and $\Delta\theta = 8.75$. The below figures include the results of the baseline rotor with the twist rate from the inboard blade section carried across the outer tips. Note that an indexed-tip angle of $\Delta\theta = 0$ degrees (not shown in the figure) is not equivalent to the baseline rotor, as the indexed-tip is untwisted.
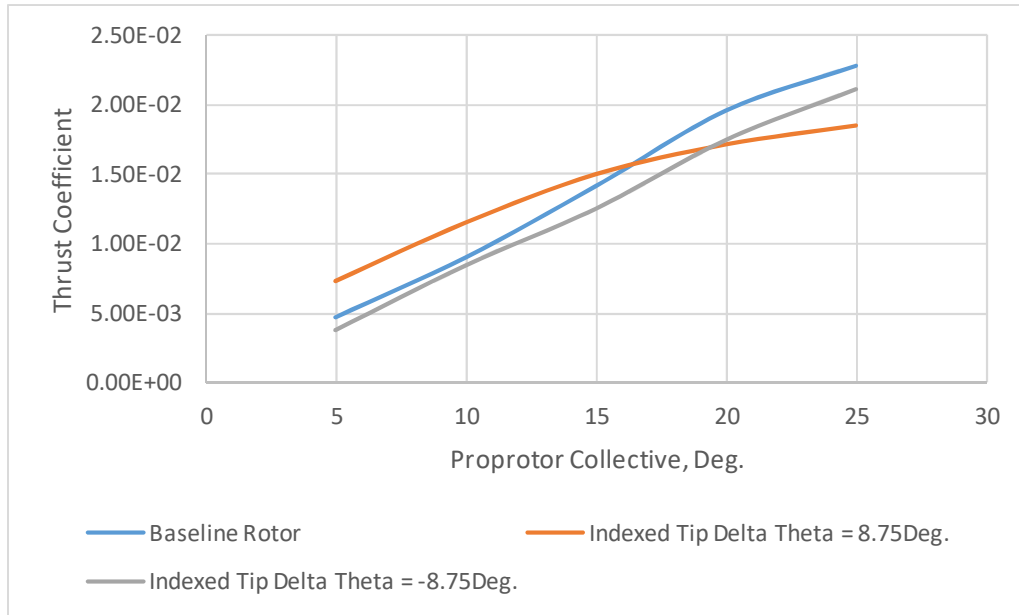
Figure 17. Thrust coefficient trends with collective at two different indexed-tip $\Delta\theta$ settings.
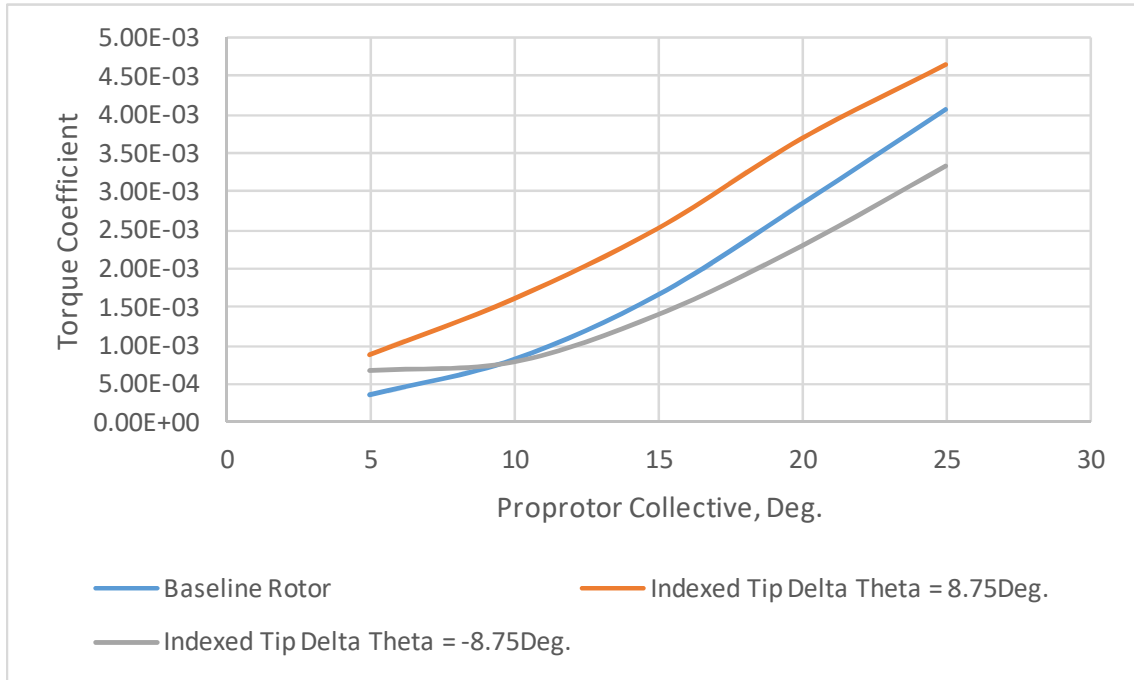
Figure 18. Hover power coefficient trends with collective at two different indexed-tip Δθ.
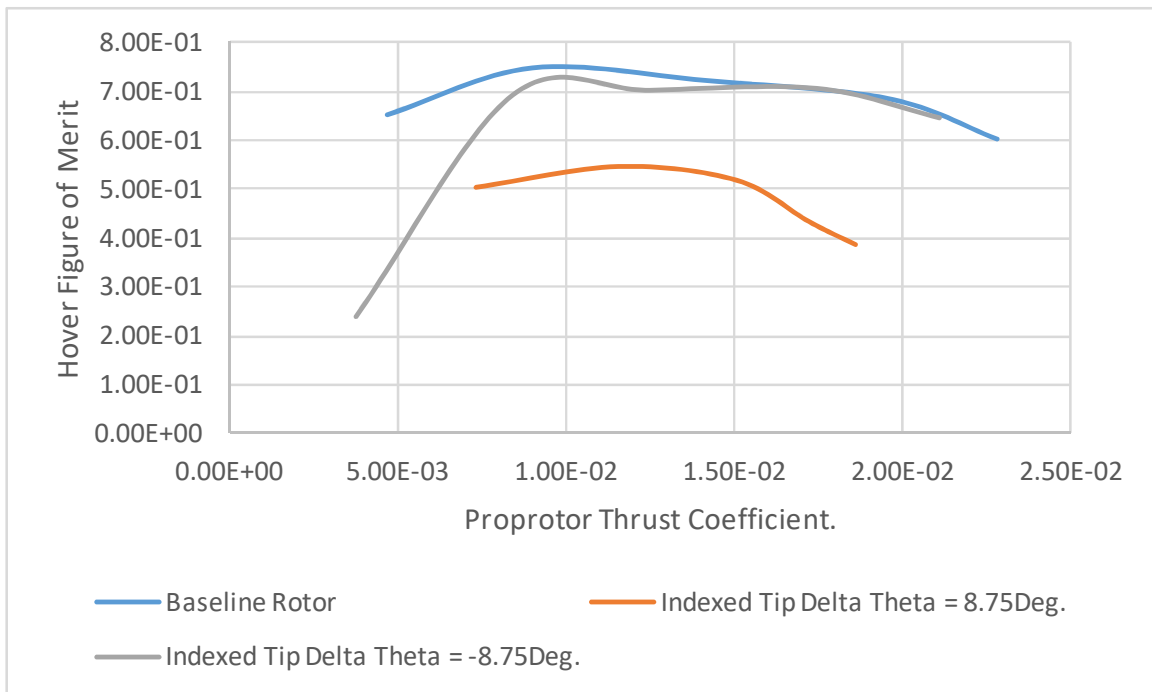
Figure 19. Hover figure-of-merit curves for various different indexed-tip Δθ angles against the baseline rotor.

21

Figure 19, for the two different Δθ values examined, did not show a clear figure-of-merit advantage as compared to the baseline rotor for the range of thrust coefficients predicted. Figure 16, with results at a fixed collective of 20 degrees for both the indexed-tip and baseline rotors, suggest that Δθ = -8.75 degrees should show small figure-of-merit improvements.

3. Cruise/Axial-Flow Performance CFD Results

Refer to Figure 5 where the rotor configuration has untwisted tips for the same indexed-tip configuration explored in Figures 14-19 for hover operating conditions. Figures 20-25 examine the aeroperformance characteristics under high-speed cruise/axial-flow conditions. Two different cruise speeds are examined: V=350 fps and V=500 fps. For each cruise speed, a different collective range is explored.
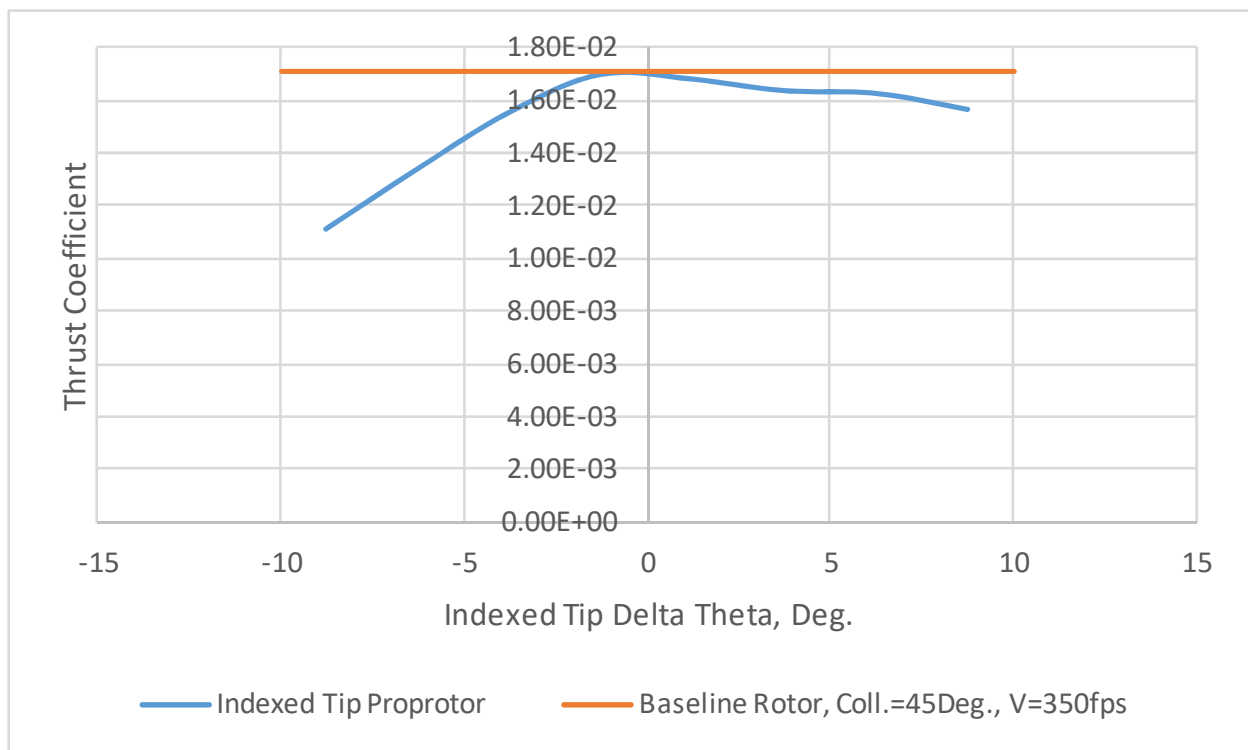
Figure 20. Cruise/axial flow thrust coefficient trend (for an untwisted indexed-tip) as a function of indexed-tip Δθ (Coll. = 45 degrees and V=350 fps).

22

Figure 21. Cruise/axial-flow power coefficient trend (for an untwisted indexed-tip) as a function of indexed-tip $\Delta\theta$ (Coll. = 45 degrees and V=350 fps).
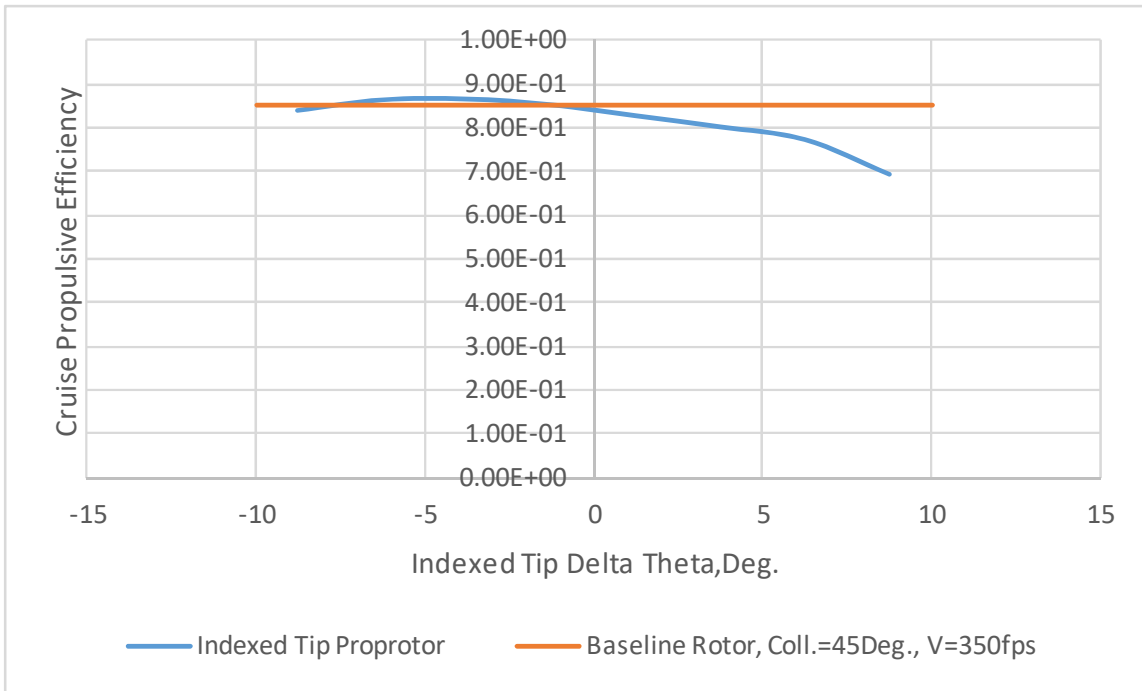
Figure 22. Cruise propulsive efficiency trends as a function of indexed-tip $\Delta\theta$ against the baseline rotor (V=350 fps).
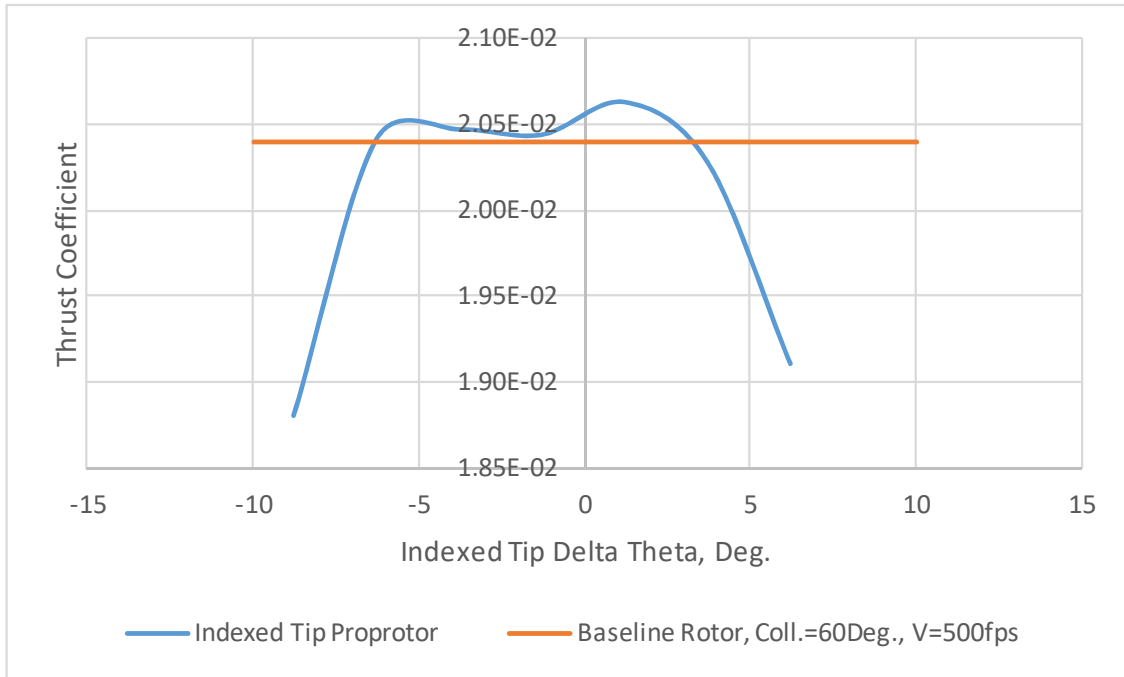
Figure 23. Cruise/axial-flow thrust coefficient trend (for an untwisted indexed-tip) as a function of indexed-tip $\Delta\theta$ (Coll. = 60 degrees and V=500 fps).
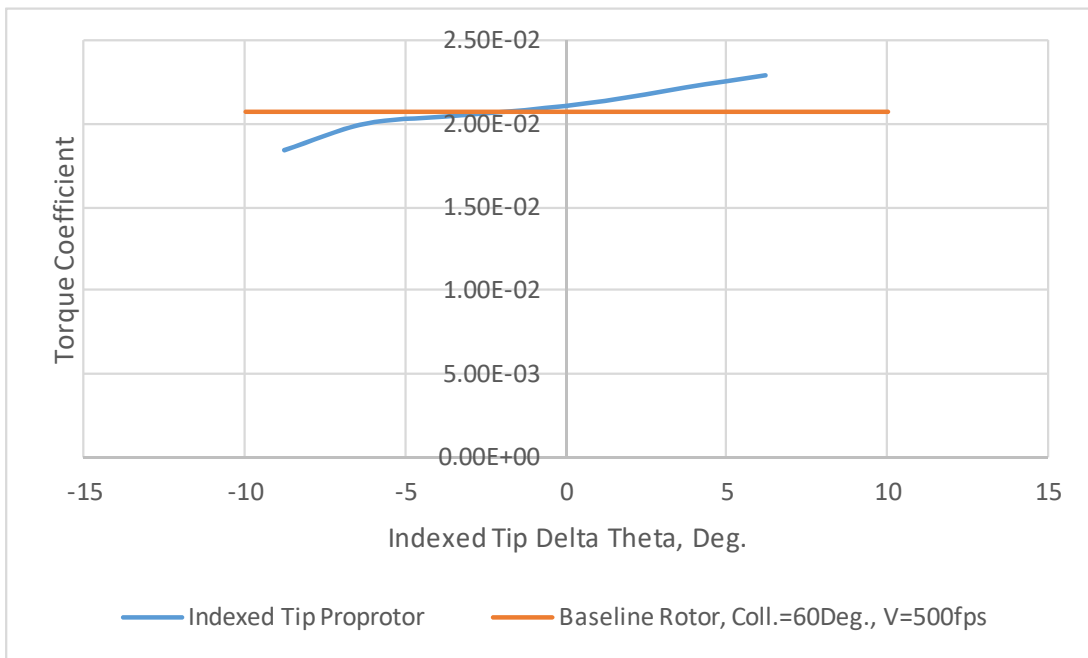
Figure 24. Cruise/axial-flow torque coefficient trend (for an untwisted indexed-tip) as a function of indexed-tip $\Delta\theta$ (Coll. = 60 degrees and V=500 fps).
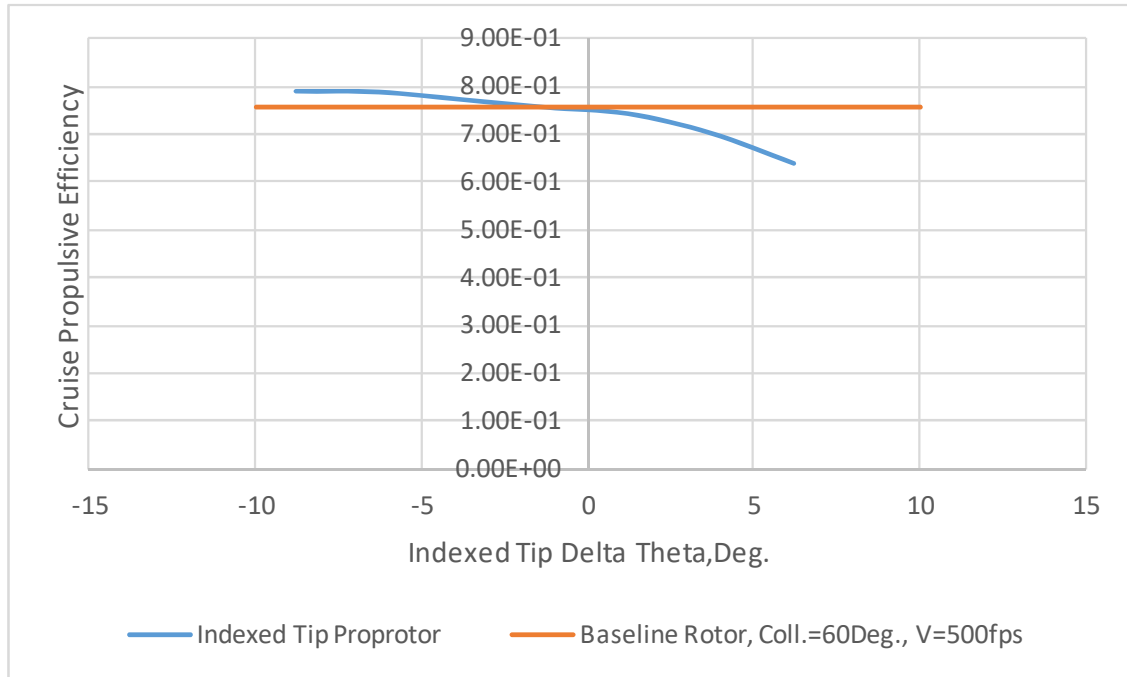
Figure 25. Cruise/axial-flow propulsive efficiency trend (for an untwisted indexed-tip) as a function of indexed-tip $\Delta\theta$ (Coll. = 60 degrees and V=500 fps).

Figures 26-28 reflect the cruise or axial-flow condition (at cruise speed of 500 fps) aeroperformance trends as a function of rotor collective for two different $\Delta\theta$ values. Figure 26 suggests that the $\Delta\theta$ = -8.75 degrees configuration shows improved thrust capability at higher collectives than the baseline rotor. Figure 27 suggests that the $\Delta\theta$ = -8.75 degrees configuration shows reduced torque requirements for all collectives as compared to the baseline rotor. It is unclear if these thrust and torque improvements lead to cruise propulsive efficiency improvements as shown in Figure 28 for the $\Delta\theta$ = -8.75 degrees and V=500 fps case.
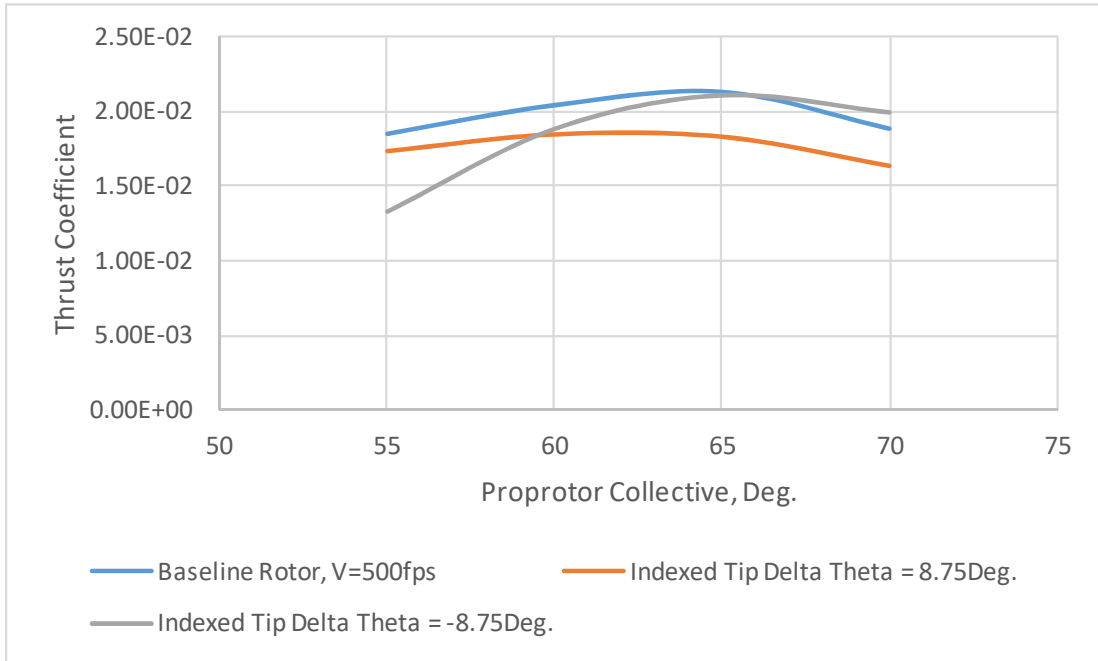
Figure 26. Cruise/axial-flow thrust coefficient trends for two different $\Delta\theta$ values as compared to baseline rotor results (V=500 fps).
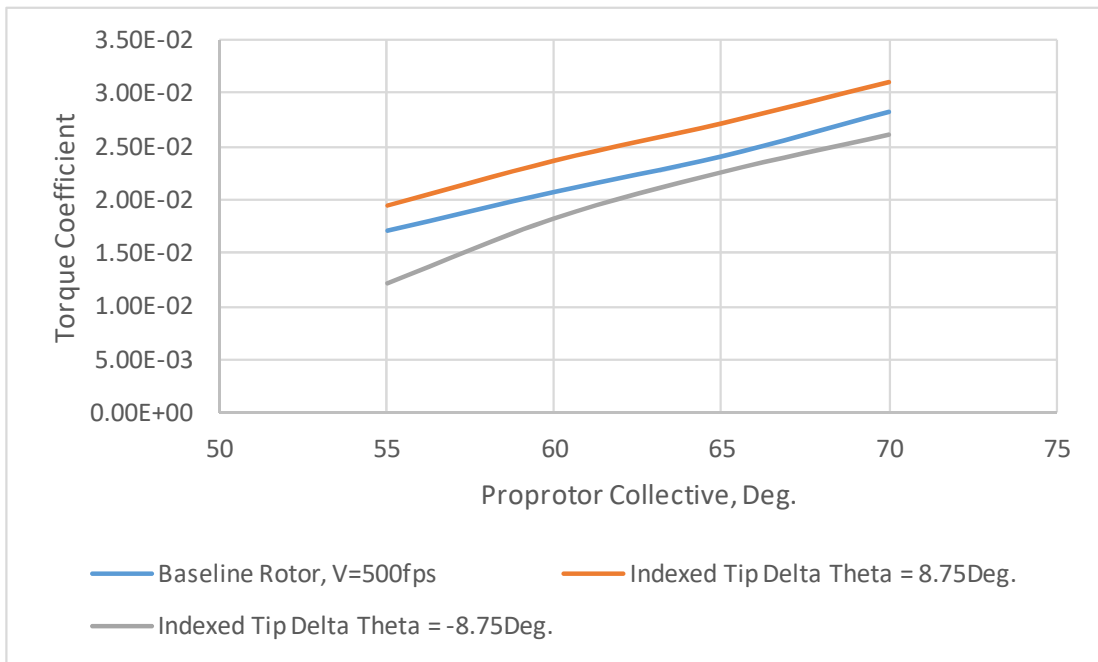
Figure 27. Cruise/axial-flow torque coefficient trends for two different $\Delta\theta$ values as compared to baseline rotor results (V=500 fps).
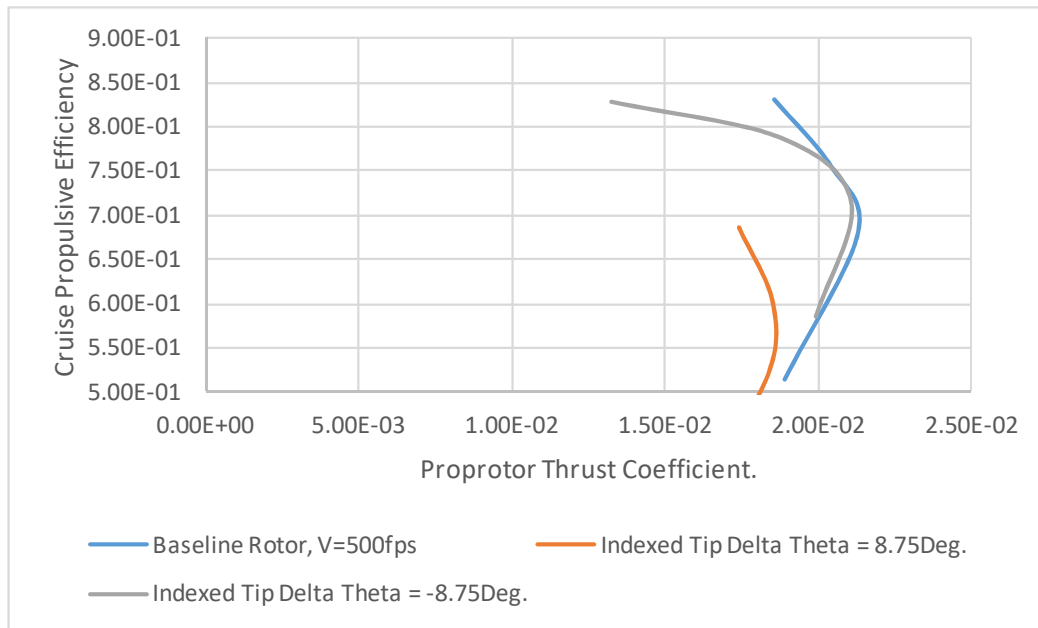
Figure 28. Cruise/axial-flow propulsive efficiency trends for two different Δθ values as compared to baseline rotor results (V=500 fps).

4. A Closer Look at Indexed-Tip Aerodynamics

The flow along a conventional rotor/proprotor blade is relatively two-dimensional. For that reason, mid-fidelity comprehensive analysis tools and mid-fidelity CFD tools such as RotCFD can use airfoil (two-dimensional aerodynamics) look-up tables for estimating the aerodynamic loading across rotor blades. Flow across the rotor blades is only highly three-dimensional near the blade root and out at the blade tips. Prior to the advent of high-fidelity rotorcraft computational fluid dynamics tools, it was relatively common to attempt experimentally to quantify the three-dimensional nature of the flow around rotor blades tips through wind tunnel testing of fixed or nonrotating semispan-wings with independently mounted wing tips. These wing tips would be of the same geometry as a nominal blade-tip and would be considered acceptable surrogates for the rotor blade-tips. The wing tip aerodynamic forces and moments would typically be measured with internal balances. The semispan-wing and wing-tip aerodynamic loads and flow characteristics would then be interpreted in terms of their potential influence on rotor performance and acoustics for rotors. This experimental approach was also taken during the 1980s and 1990s for semispan-wing wing tips simulating rotor indexed blade-tips, e.g., References 2-5 and 16.

As RotCFD uses two-dimensional airfoil look-up tables to partially model (in conjunction with a constant tip loss factor) the indexed blade-tips in this paper, it would be advantageous to compare the predicted RotCFD blade-tip aerodynamic forces against the some of the early experimental semispan-wing and indexed wing-tip data from References 2-5 and 16. The process by which RotCFD predictions are compared with experimental wind tunnel data is now described. By subtracting out the inboard rotor's performance characteristics from the indexed rotor performance, the incremental or delta performance influence of the indexed-tip is captured. The

inboard rotor performance is predicted by treating the inboard span of the indexed-tip proprotor as an equivalent "smaller" radii rotor in the CFD calculations (noting that the twist and chord distributions have to be scaled to the new/smaller rotor radii). This is captured in Equations 9a-b.

$$C_{Lt} = \frac{2\Delta T}{NS_t\rho V_{Ref}^2}$$

$$C_{Dt} = \frac{2\Delta P}{NS_t\rho V_{Ref}^3}$$

(9a-b)

Where C_{Lt} and C_{Dt} are the estimated three-dimensional indexed-tip lift and drag coefficients. The delta thrust, ΔT, and delta power, ΔP, are derived from subtracting out incremental thrust and power results from RotCFD for a (estimation artifice) smaller-radius "inboard-blade rotor" (rotor blade span is minus the indexed-tip tip span) incremental from the indexed-tip proprotor configuration total thrust and power. The reference velocity is the local radial station velocity at the midspan of the indexed-tip. N is the number of rotor blades and S_t is the tip planform area. Figures 29-31 provide estimates of C_{Lt} and C_{Dt} as a function of tip angle of attack or the inboard-blade reference angle of attack.
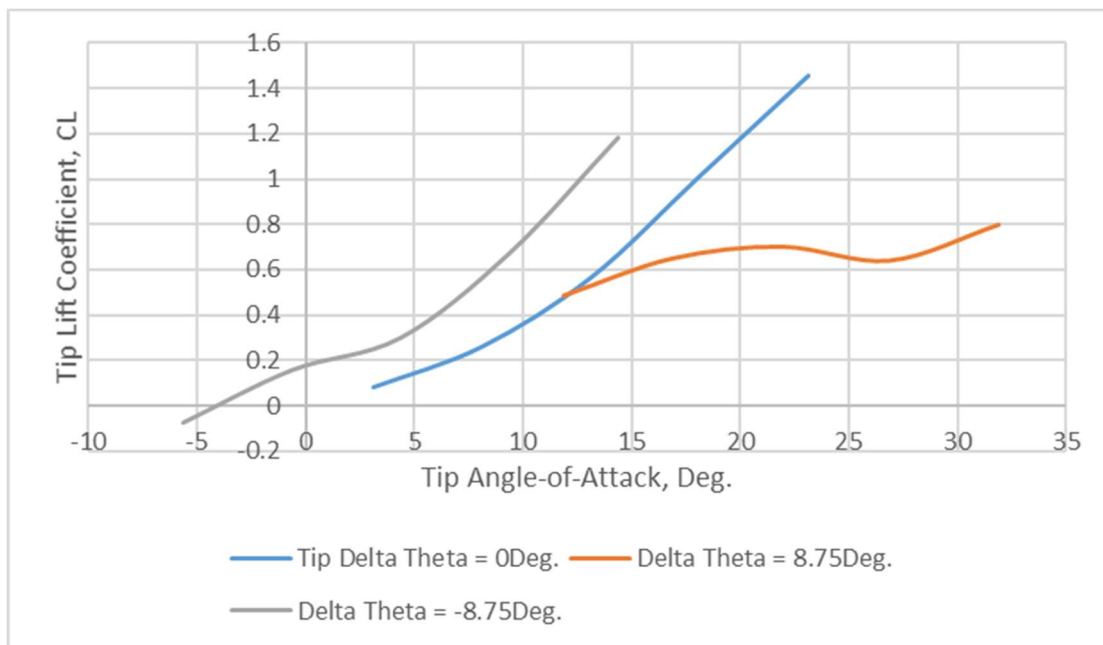
Figure 29. Tip lift coefficient curve as a function of tip angle of attack for three different indexed-tip Δθ.
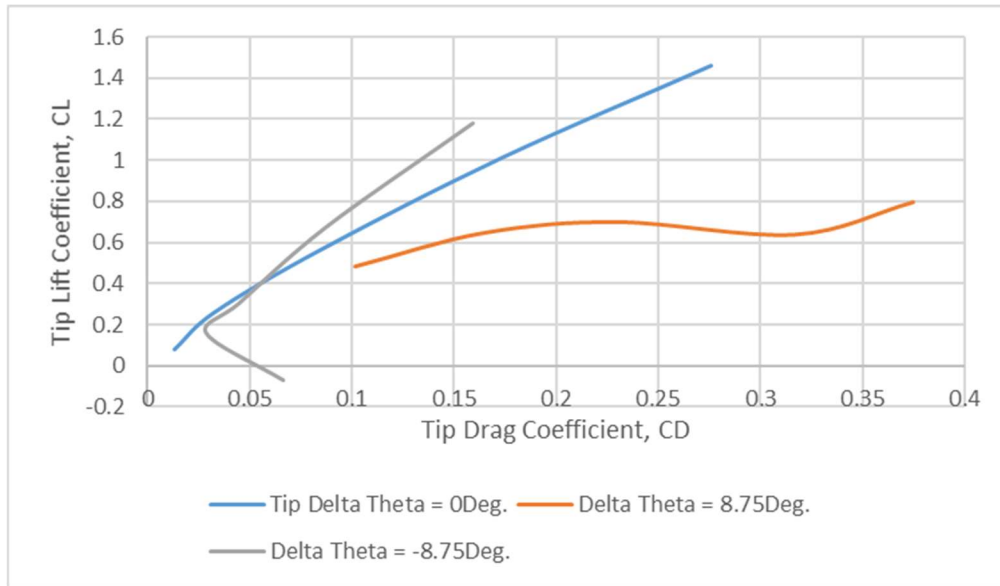
Figure 30. Tip lift-drag coefficient polar curves as a function of tip angle of attack for three different indexed-tip $\Delta\theta$.
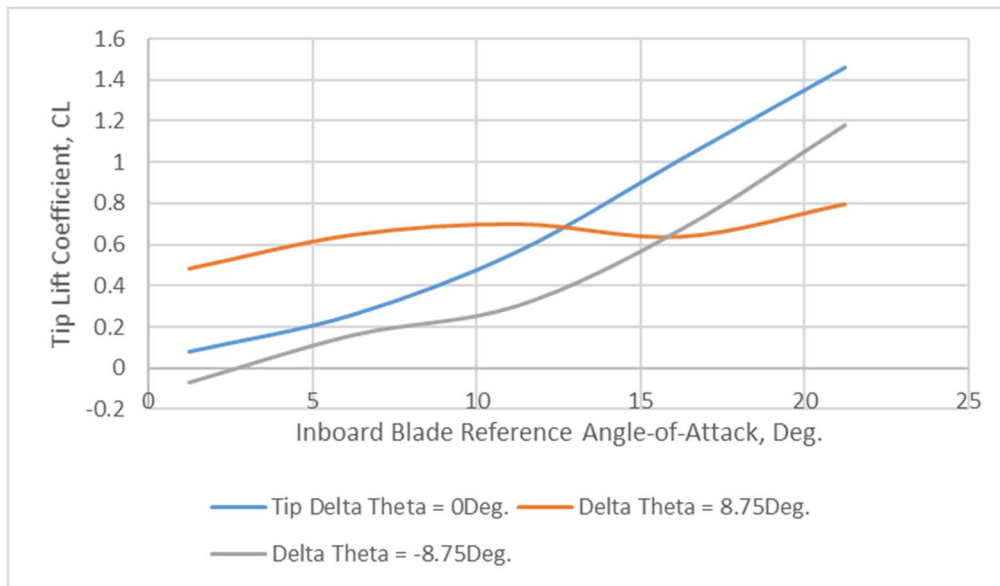
Figure 31. Indexed-tip effective lift and drag coefficient characteristics as a function of inboard-blade reference angle-of-attack hover conditions (Collective of 20 degrees).

The above derived indexed-tip effective lift and drag coefficients should be approximately equivalent to empirically derived indexed-tip lift and drag coefficients from Reference 15. A qualitative comparison between the RotCFD-derived indexed-tip lift and drag coefficients and experimental wind tunnel results reported in References 2, 3 and 16 (the specific semispan-wing and indexed-tip referenced in this report is "Configuration 3") are presented in Figures 32 and 33.

29

Overall, the agreement between the experimental data and the indexed-tip trends extracted from the RotCFD results are reasonable. In many regards, this lends credence to the experimental methodology of using semispan-wings and wing-tip extensions (with internal balances) to quantify the aerodynamic forces of wing tips and their extrapolation/interpolation to rotor blade-tip aerodynamic characteristics. The overall agreement also validates the RotCFD predictive capability—especially in the rotor blade tip region. Finally, it suggests that blade element momentum theory (BEMT), oftentimes used in rotor/rotorcraft conceptual design, can be extended/modified to incorporate simple semiempirical expressions for incremental rotor performance enhancement when accounting for exotic blade tips. This can be done recasting and solving for ΔP and ΔT, given experimental measurements (or high-fidelity computational predictions) of C_{Lt} and C_{Dt}.
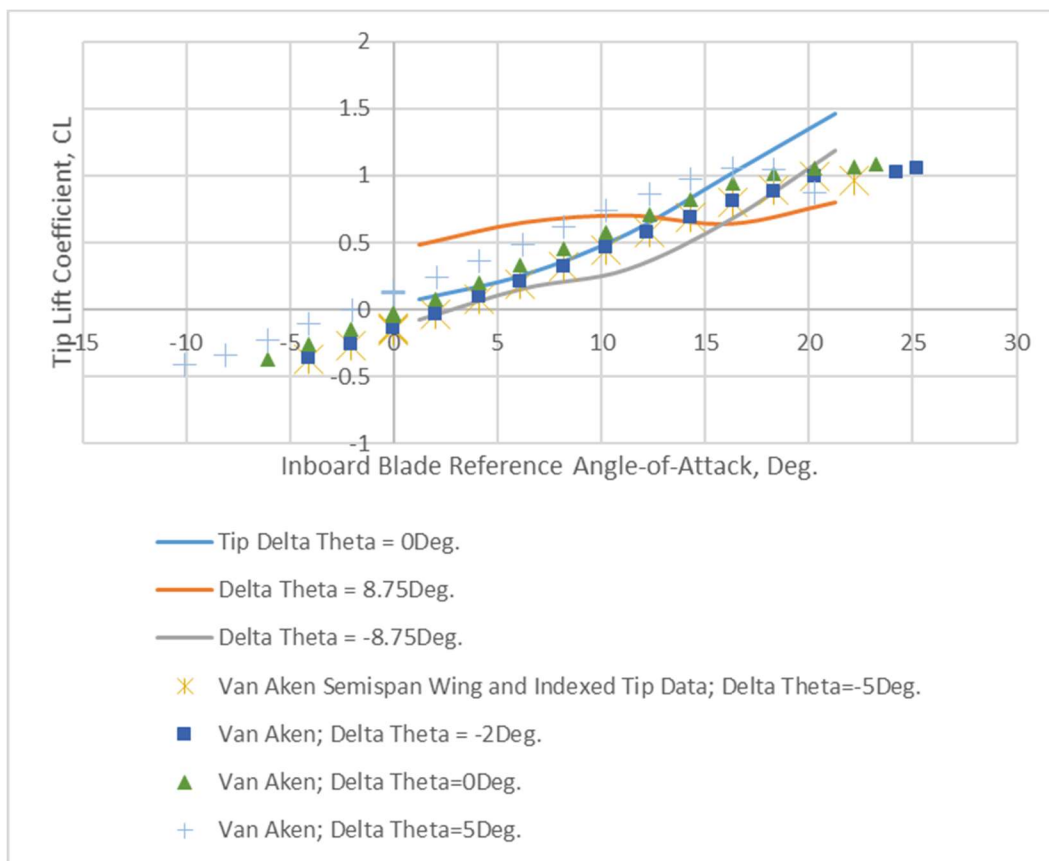
Figure 32. Tip lift curve qualitative comparison.
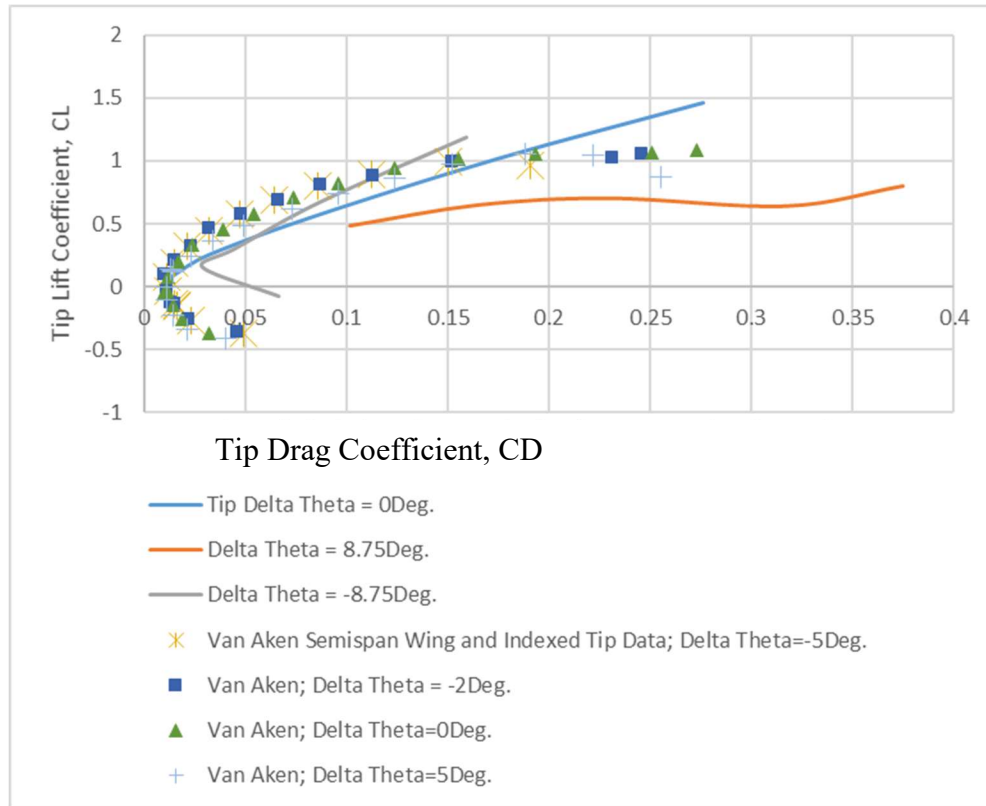
Figure 33. Tip lift-drag polar comparison.

ALTERNATE ROTOR WITH TWISTED, 10-PERCENT SPAN INDEXED-TIPS

Computational fluid dynamics results for an alternate indexed-tip proprotor configuration will now be presented. The proprotor reference twist distribution is shown in Figure. 34. The key difference between this new configuration and the earlier configuration is that indexed-tip in this new configuration has a twist rate identical to the baseline proprotor twist distribution. The first indexed-tip proprotor configuration studied in this paper had untwisted blade tips such that even with $\Delta\theta_{Tip} = 0$ the twist distribution of the indexed-tip proprotor deviated from the baseline proprotor in the outer tip region. With the second, alternate indexed-tip proprotor configuration twist distribution, when $\Delta\theta_{Tip} = 0$ the twist distributions between the baseline proprotor and the indexed-tip proprotor are identical. Accordingly, the predicted aeroperformance results for the new indexed-tip proprotor configuration at $\Delta\theta_{Tip} = 0$ are identical to the aeroperformance results for the baseline proprotor. This was not the case for the original indexed-tip proprotor configuration.

31

Figure 34. Alternative rotor twist distribution: baseline rotor and 10-percent span indexed-tip (with continuation of linear twist rate across tip) set at 4.16 degrees tip-twist ($\Delta\theta$ Tip = +8 degrees).
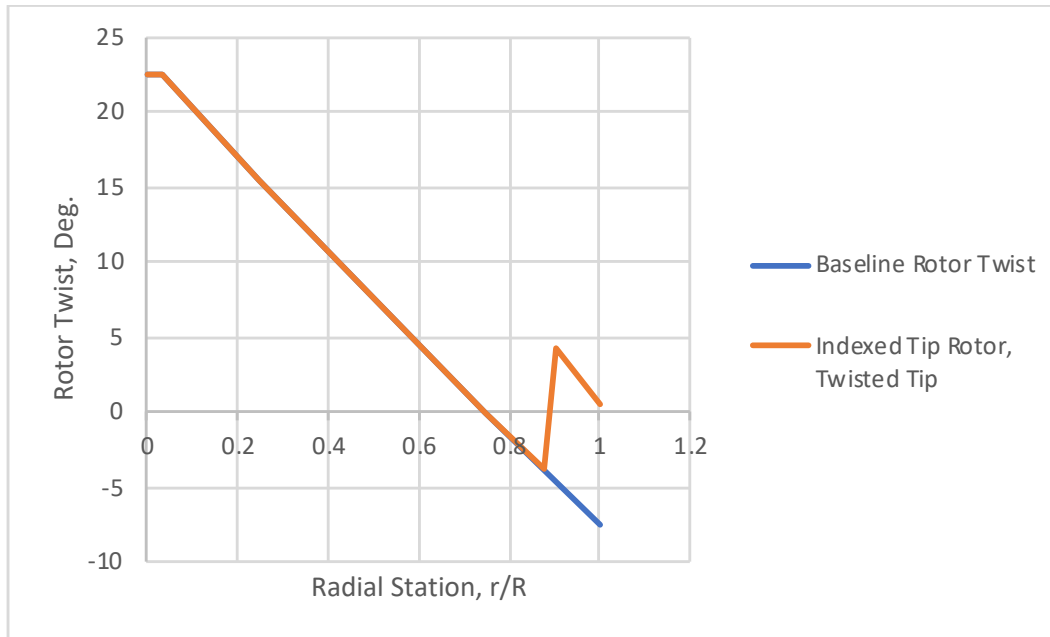
1. Hover Performance CFD Results

Figures 35a-c present hover performance results for the indexed-tip rotor with (linearly) twisted tips of 10-percent span. Note that in the case of $\Delta\theta = 0$ degrees, the indexed-tip rotor has the same twist distribution as the baseline rotor. Figure 35a presents hover thrust coefficient versus collective curves for several different $\Delta\theta$ for the 10-percent span linearly twisted tips; increasing $\Delta\theta$ results in an incremental increase/shift in thrust curves except when the rotor has clearly stalled. Figure 35b presents hover torque coefficient versus collective curves for several different $\Delta\theta$ for the 10-percent span linearly twisted tips; increasing $\Delta\theta$ results in an incremental increase/shift in torque curves. Figure 35c presents figure-of-merit curves as a function of thrust coefficient for various $\Delta\theta$; the only clear trend is that $\Delta\theta > 0$ degree results in general decreases in hover figure of merit.

(a)

(b)

(c)
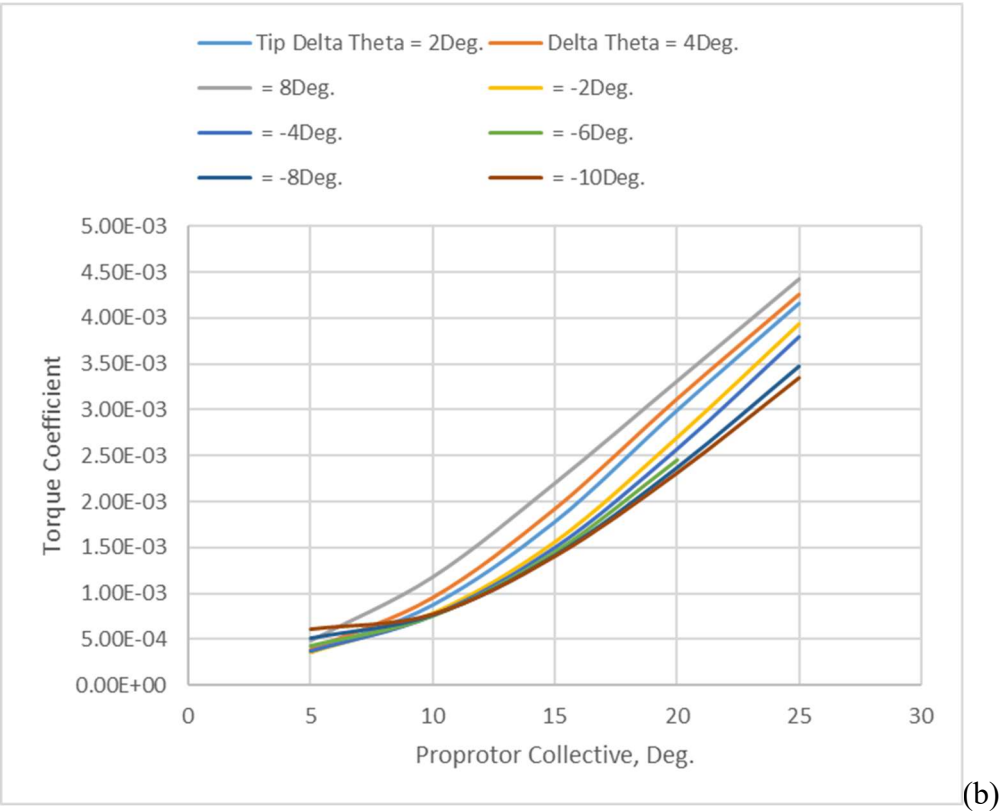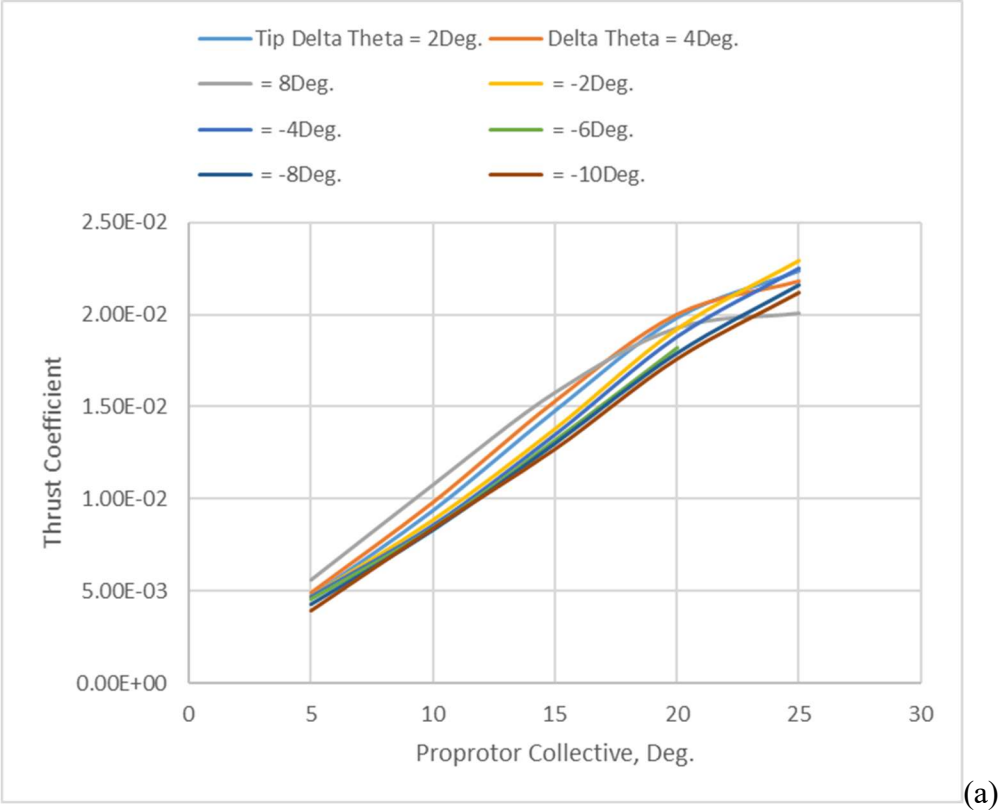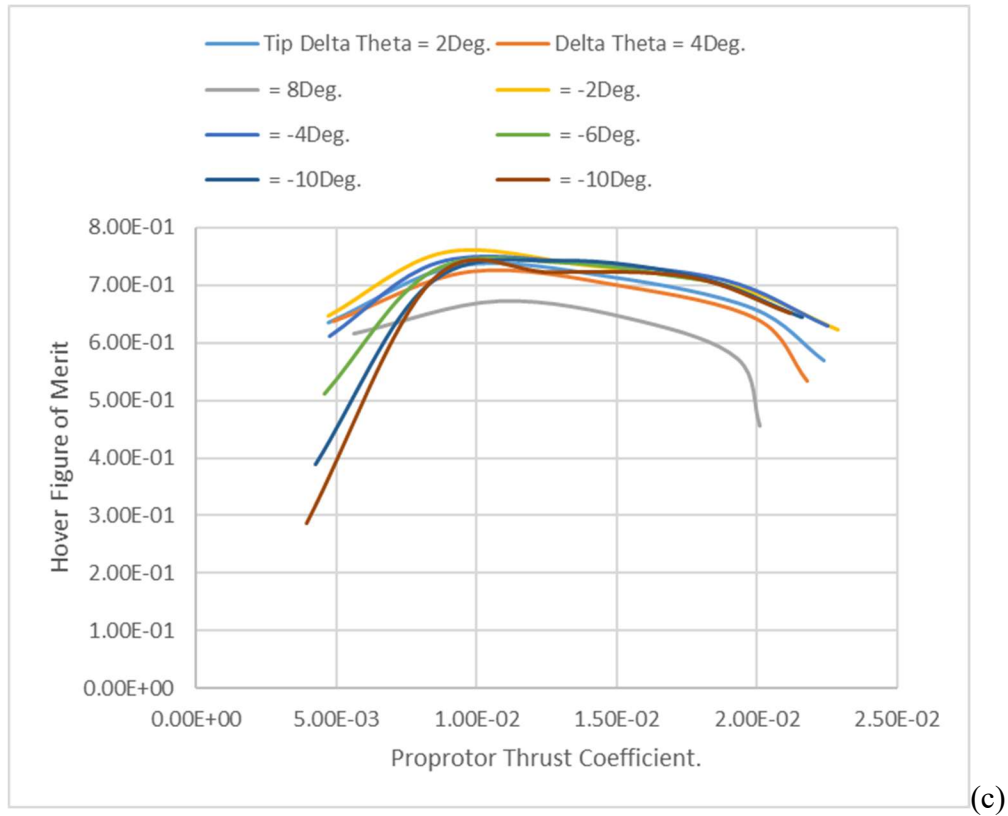
Figure 35. Hover performance curves for various indexed-tip Δθ angles (twisted tip): (a) thrust coefficient vs. rotor collective, (b) torque coefficient vs. collective, and (c) figure of merit vs. thrust coefficient.

A similar set of untwisted tips for various hover polar curves are presented (in addition to the results in Figs. 14-19) in Figures 36a-c. Figure 36c presents figure-of-merit curves as a function of thrust coefficient for various Δθ; there continues to be a clear trend where Δθ > 0 degrees results in general decreases in hover figure of merit. Results suggest that Δθ = −5 degrees appear to give the best overall figure of merit over the greatest thrust range. The twisted tip versus the untwisted tip comparisons are presented to show which type of indexed-tip yields the best performance.

(a)

(b)

35

(c)
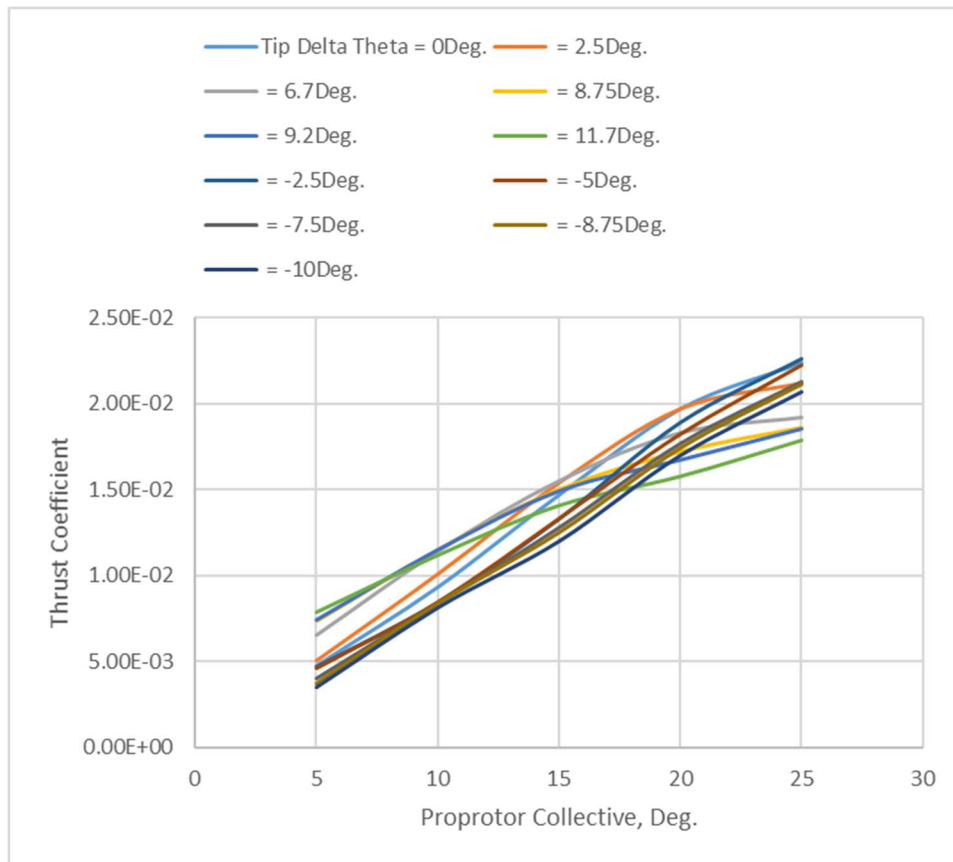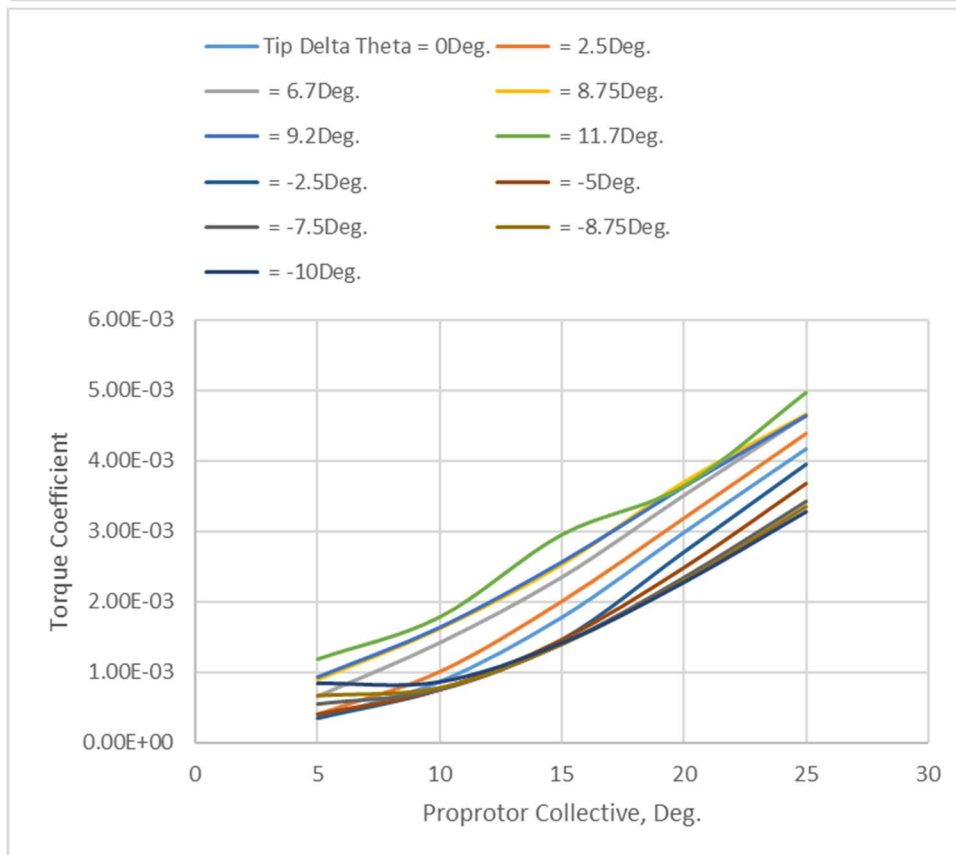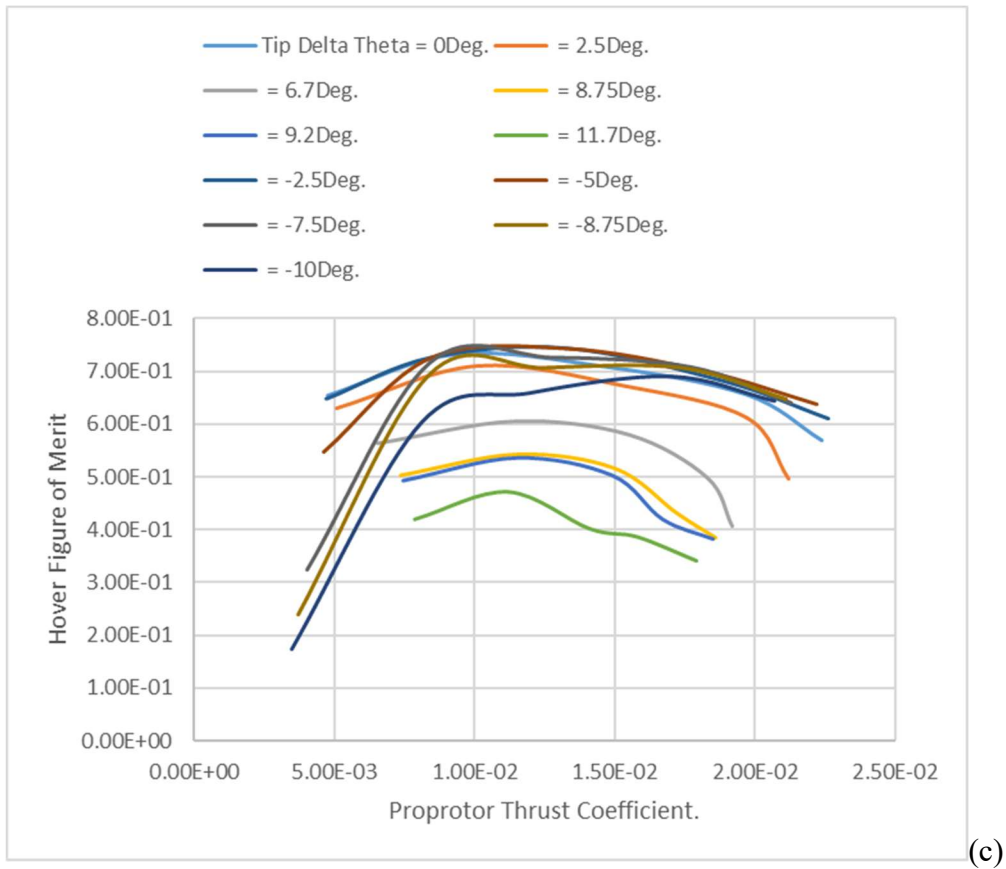
Figure 36. Hover performance curves for various different indexed-tip Δθ angles (untwisted tip) against the baseline rotor: (a) thrust coefficient vs. rotor collective, (b) torque coefficient vs. collective, and (c) figure of merit vs. thrust coefficient.

Figures 37a-c present direct comparisons between hover performance results for indexed-tip rotors with twisted and untwisted tips at Δθ ~ -2 to -2.5 degrees (nominally the same Δθ) respectively. The results for twisted and untwisted tips are very similar. Small gains, though, are seen in the hover figure of merit curves for the twisted tip versus the untwisted tip configuration.

(a)

(b)

(c)
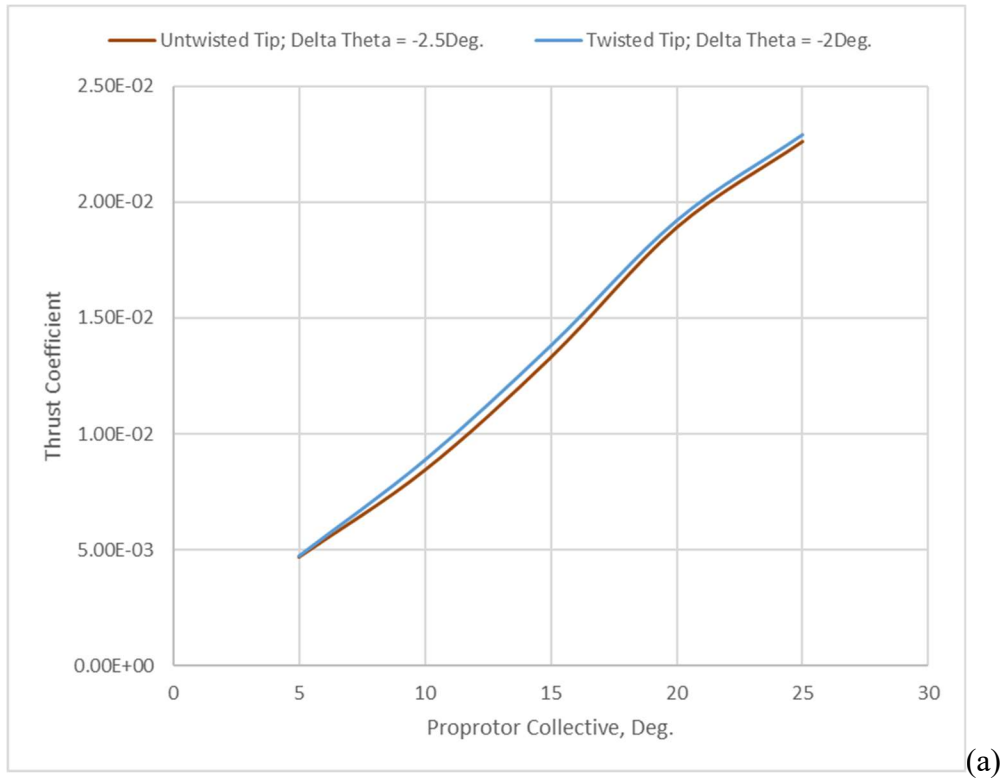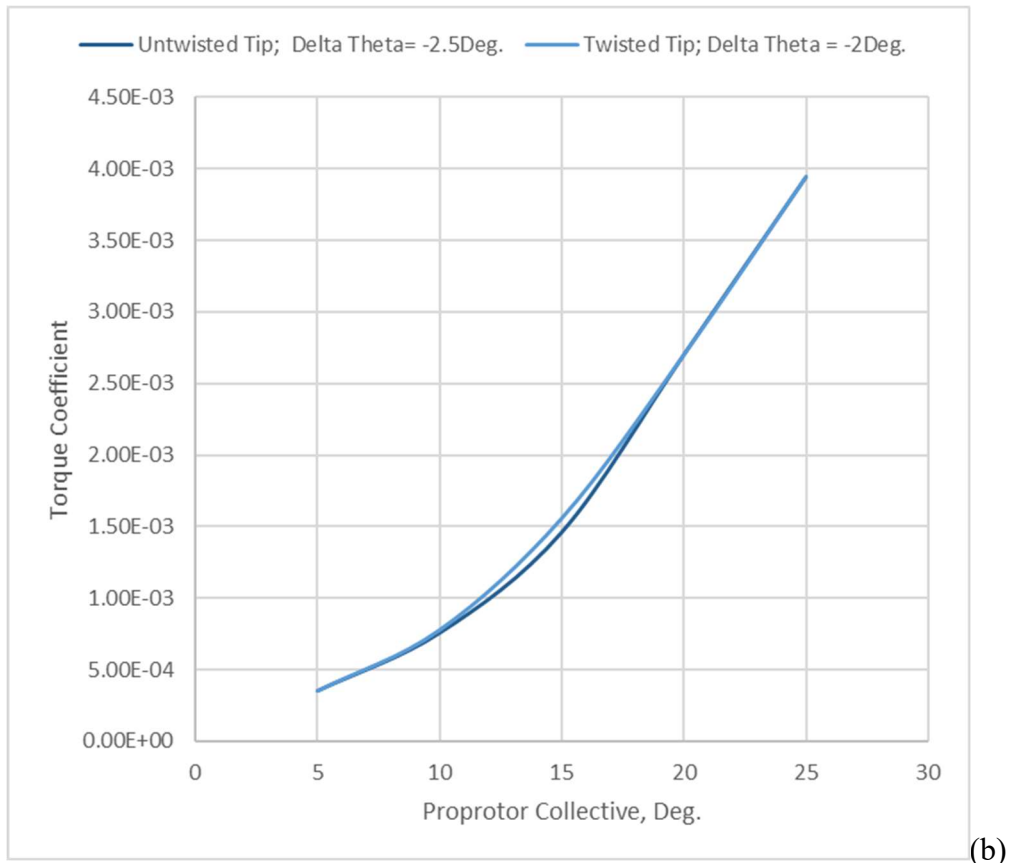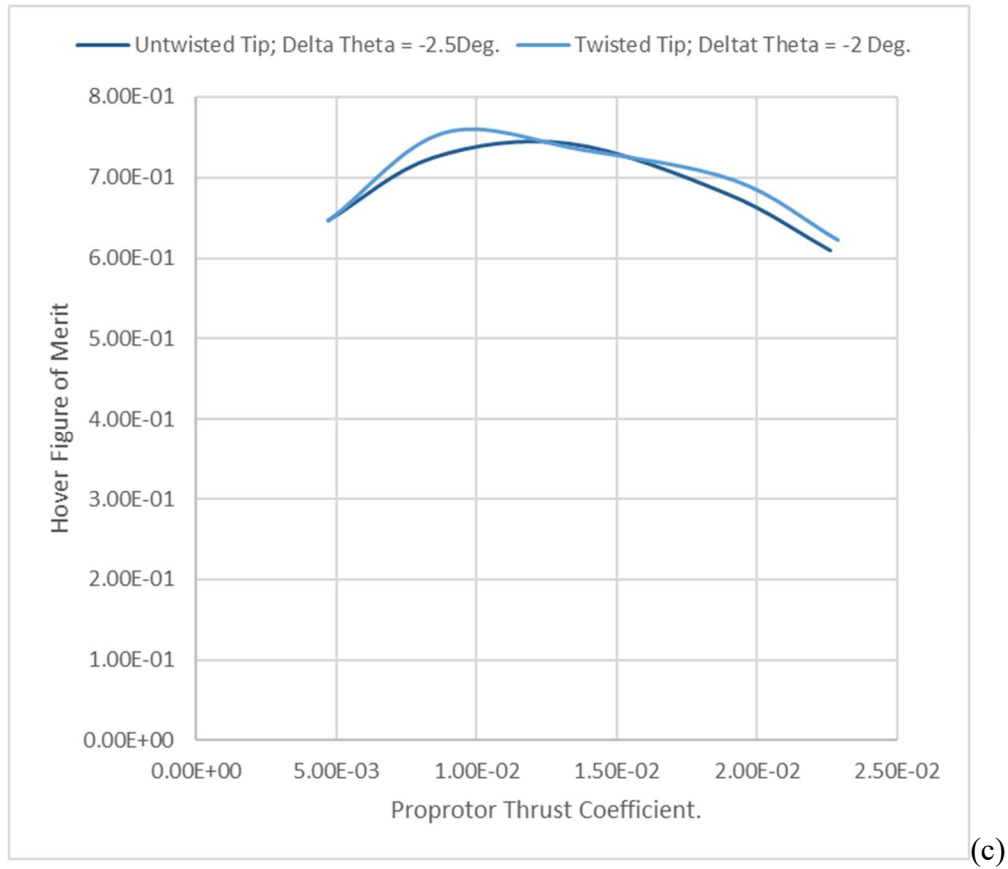
Figure 37. Hover performance comparison between twisted versus untwisted indexed-tips (at Δθ ~ -2 to -2.5 degrees): (a) thrust coefficient vs. collective, (b) torque coefficient vs. collective, and (c) figure of merit vs. thrust coefficient.

Figures 38a-c present direct comparisons between hover performance results for indexed-tip rotors with twisted and untwisted tips at Δθ ~ -7.5 to -8 degrees respectively (again nominally the same Δθ). The results for twisted and untwisted tips are also very similar. Small gains are shown in the figure-of-merit curves for the twisted tip versus the untwisted-tip configuration.

(a)

(b)

(c)
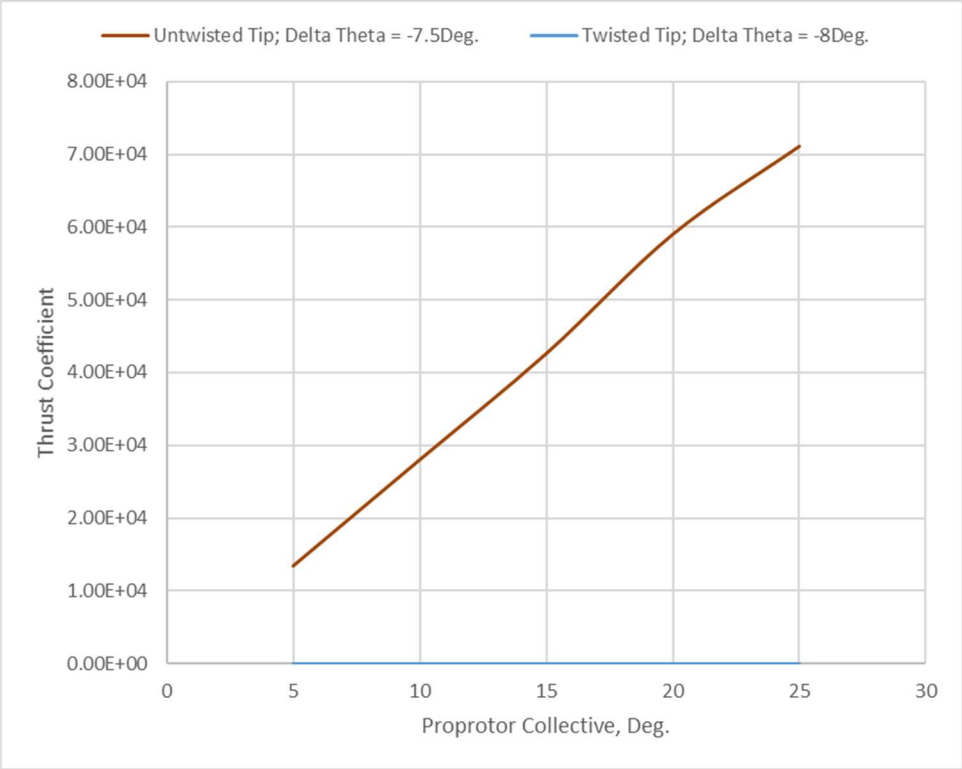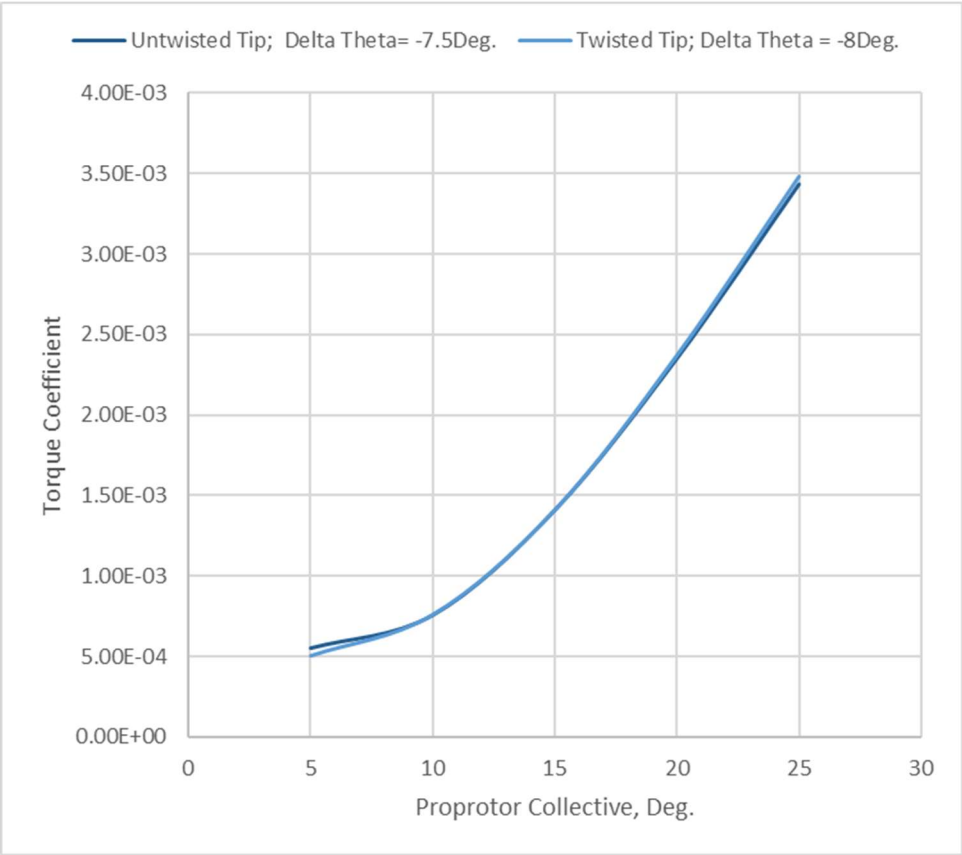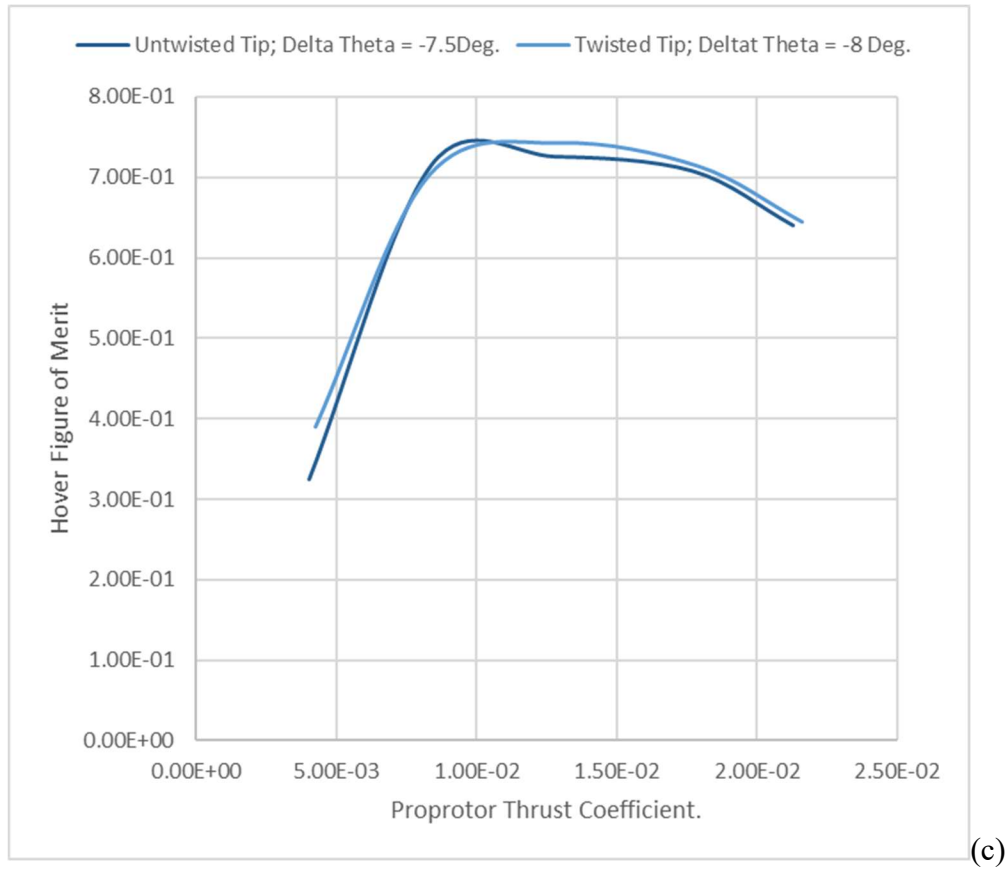
Figure 38. Hover performance comparison between twisted versus untwisted indexed-tips (at Δθ ~ -7.5 to -8 degrees): (a) thrust coefficient vs. collective, (b) torque coefficient vs. collective, and (c) figure of merit vs. thrust coefficient.

Figures 39 and 40 are even more detailed assessments of the effect of Δθ on rotor hover figure of merit for twisted- and untwisted-tip indexed-tip rotors. The best performing Δθ for twisted tips for maximum figure of merit seems to be lower (more nose down) than the Δθ for untwisted tips. Further, as rotor collective is increased, the indexed-tips require more nose down/negative Δθ. Finally, the maximum value of figure of merit is higher for the twisted tips than for the untwisted tips.
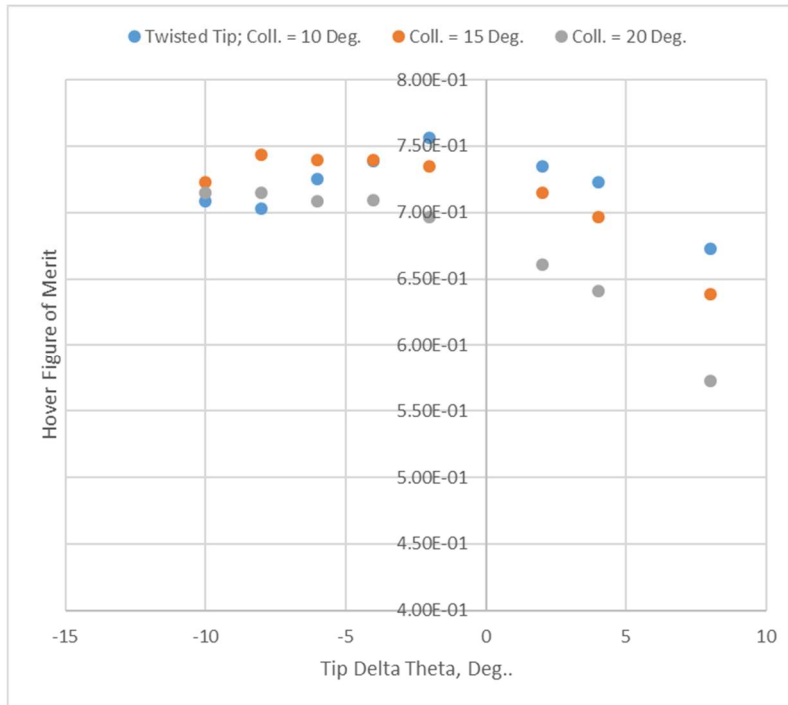
Figure 39. Influence of Δθ on indexed-tip proprotor hover figure of merit for various rotor collectives (for twisted indexed-tips).
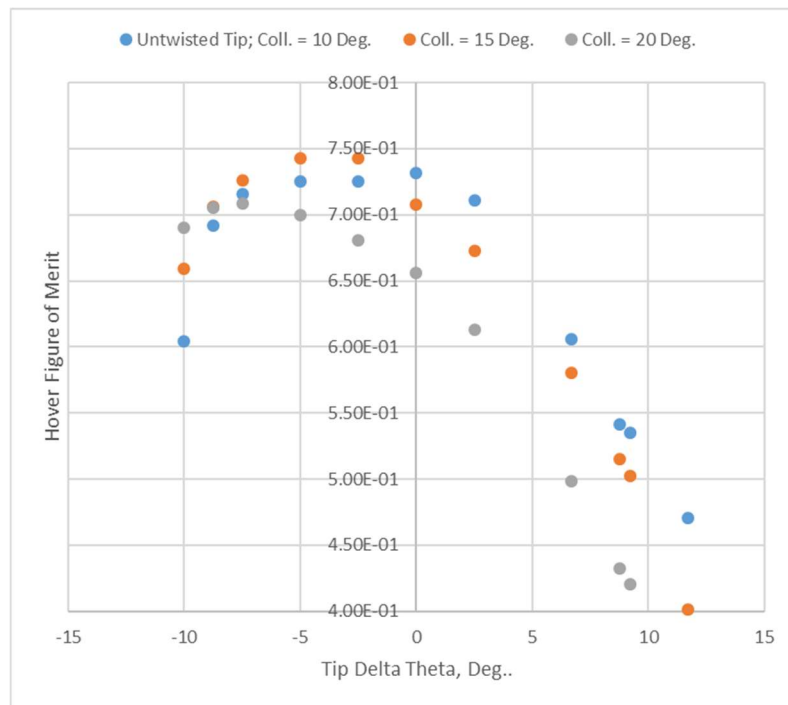
Figure 40. Influence of Δθ on indexed-tip proprotor hover figure of merit for various rotor collectives (for untwisted indexed-tips).

41

2. Cruise/Axial-Flow Performance CFD Results

Figures 41-43 are a series of performance trends for axial-flow conditions for twisted indexed-tips. Figure 41 (V=350 fps cruise speed) presents thrust coefficient as a function of collective; similar to the earlier hover results, the rotor thrust curves increase/shift upward as $\Delta\theta$ increase, until the rotor overall stalls. Figure 42 demonstrates that the rotor power coefficient curves also increase/shift upwards as $\Delta\theta$ increases. Figure 43 shows that as $\Delta\theta$ decreases, the rotor power coefficient decreases for a given thrust to an asymptotic limit.
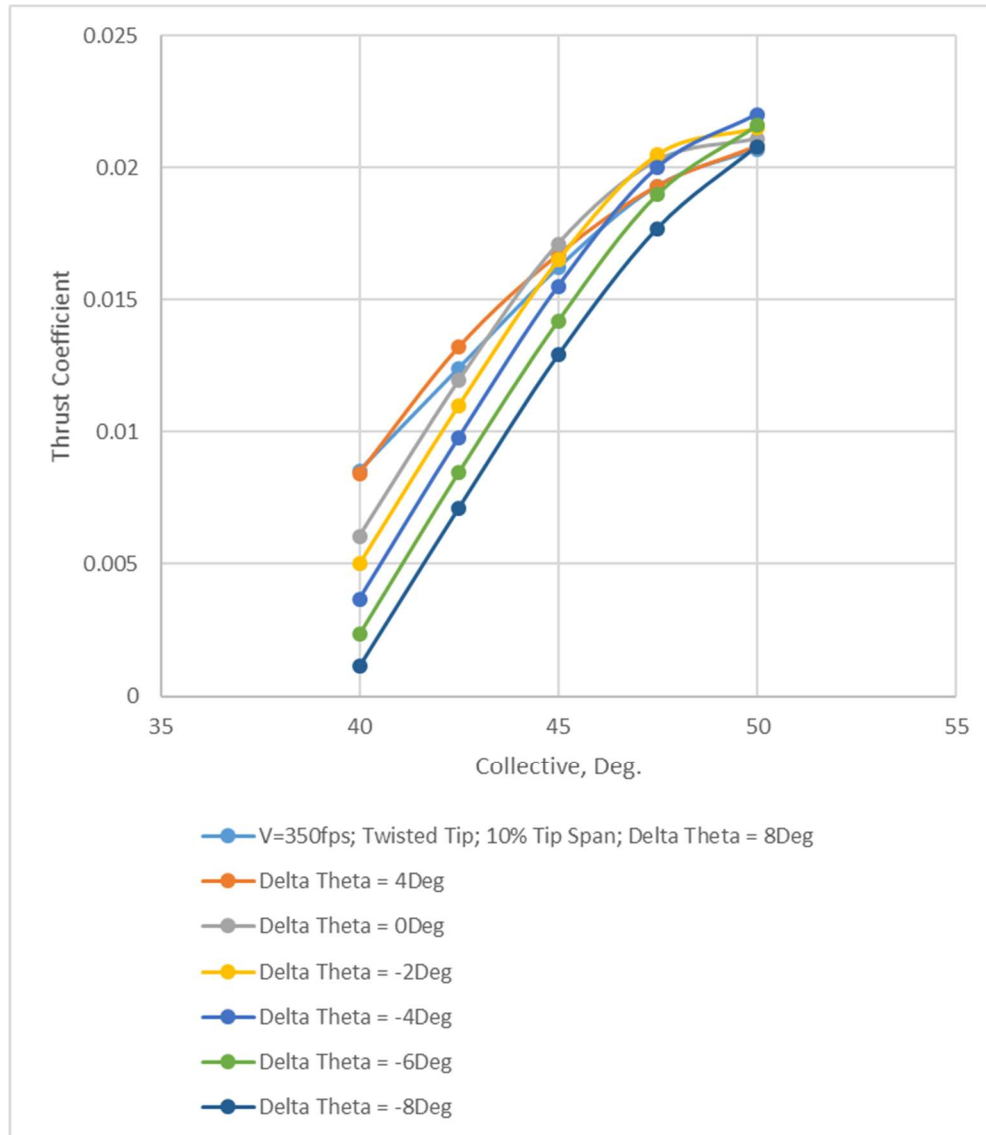
Figure 41. Thrust coefficient versus rotor collective at an axial-flow cruise speed of 350 fps for different values of $\Delta\theta$.
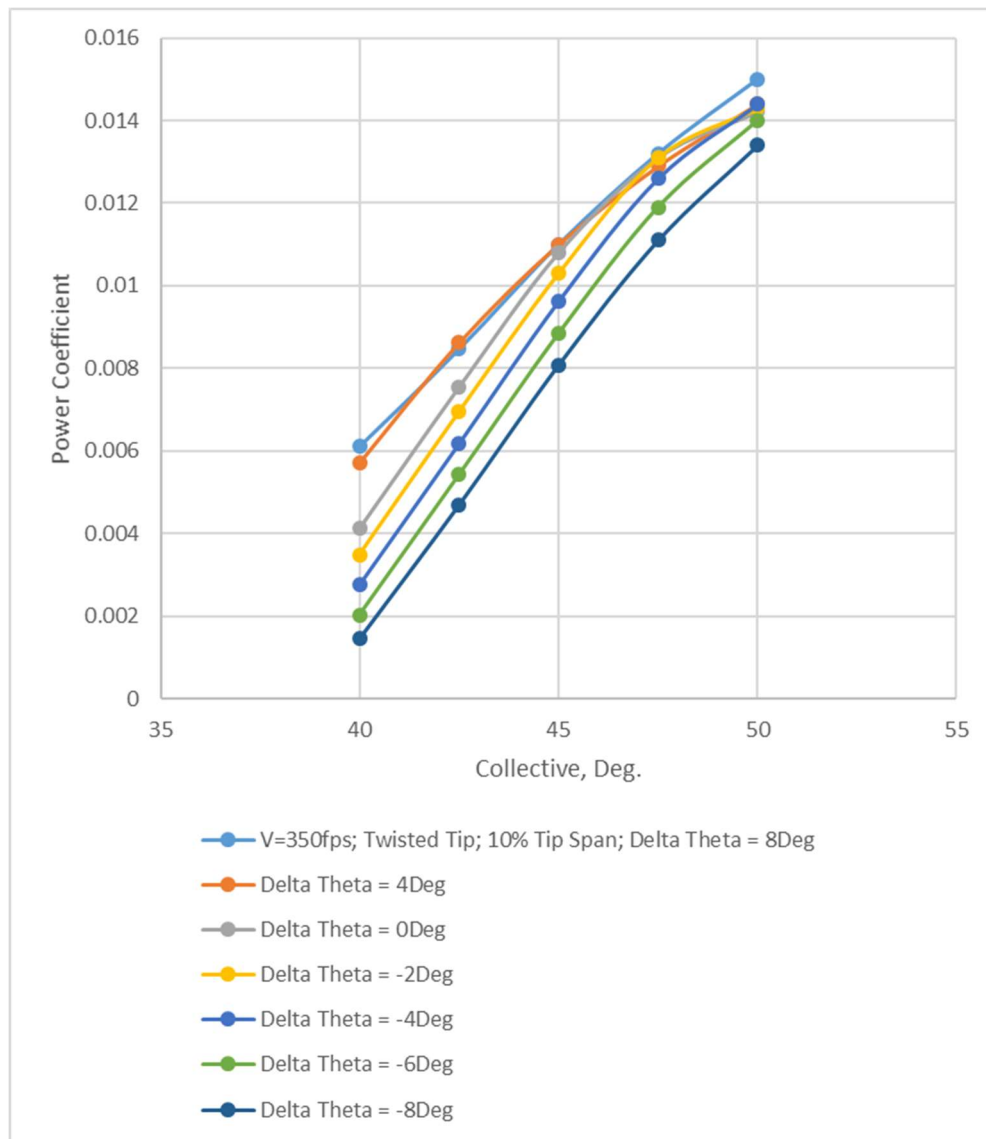
Figure 42. Power coefficient versus rotor collective at an axial-flow cruise speed of 350 fps for different values of $\Delta\theta$.
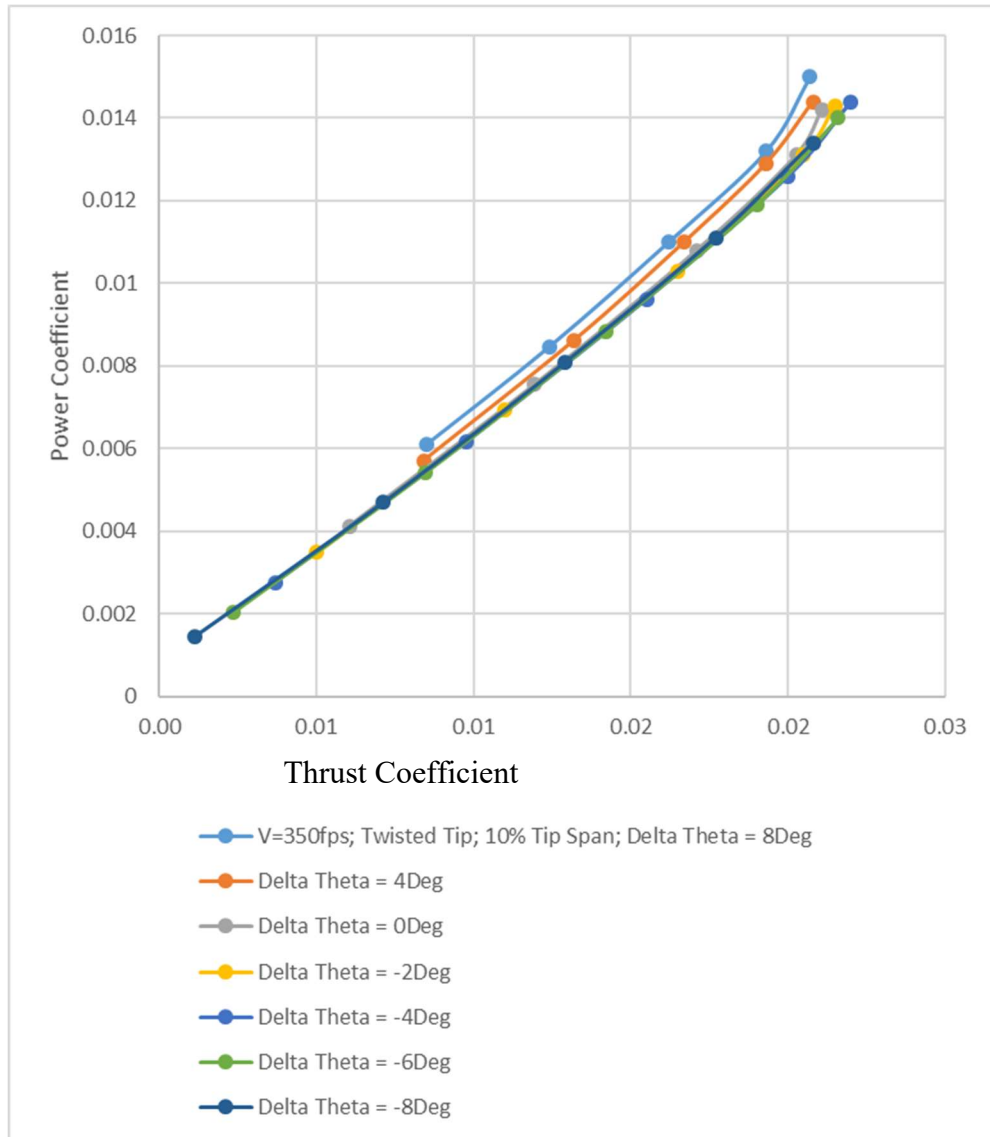
Figure 43. Power coefficient versus rotor thrust coefficient at an axial-flow cruise speed of 350 fps for different values of Δθ.

Figures 44-46 show the performance trends for a twisted tip at a cruise axial-flow velocity of 500 fps. The rotor collectives presented in these figures are more centered around the rotor stall angle as compared to the 350 fps results.
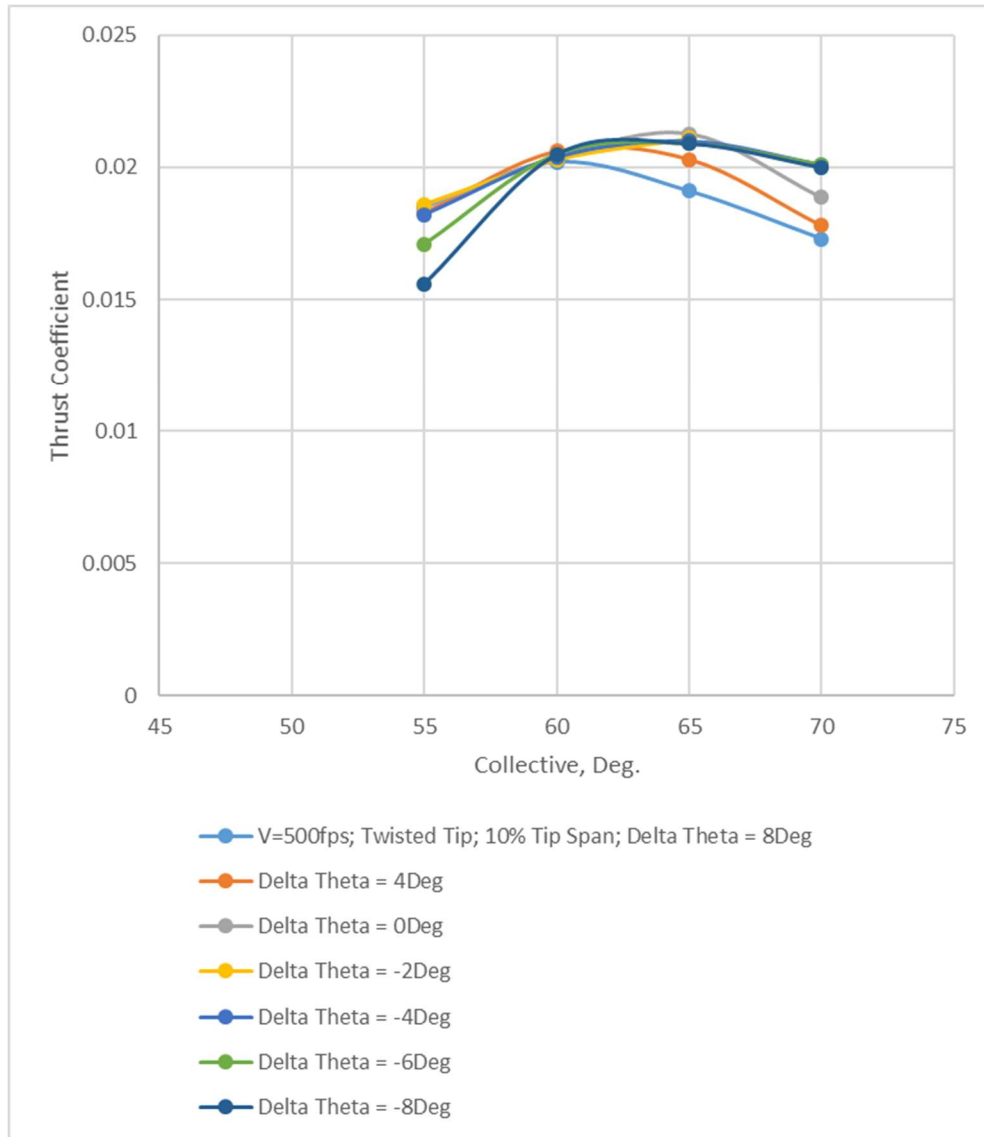
Figure 44. Thrust coefficient versus rotor collective at an axial-flow cruise speed of 500 fps for different values of Δθ.
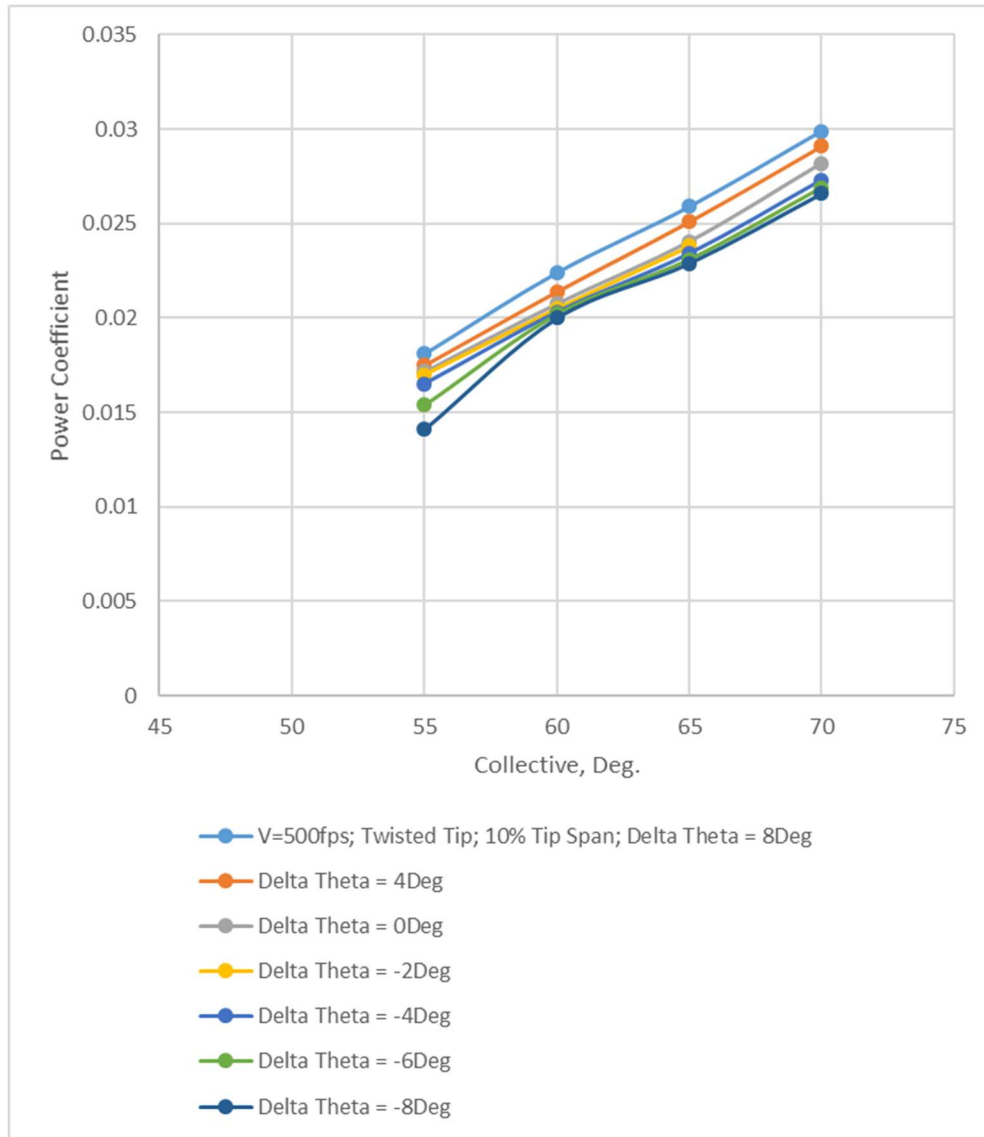
Figure 45. Power coefficient versus rotor collective at an axial-flow cruise speed of 500 fps for different values of Δθ.
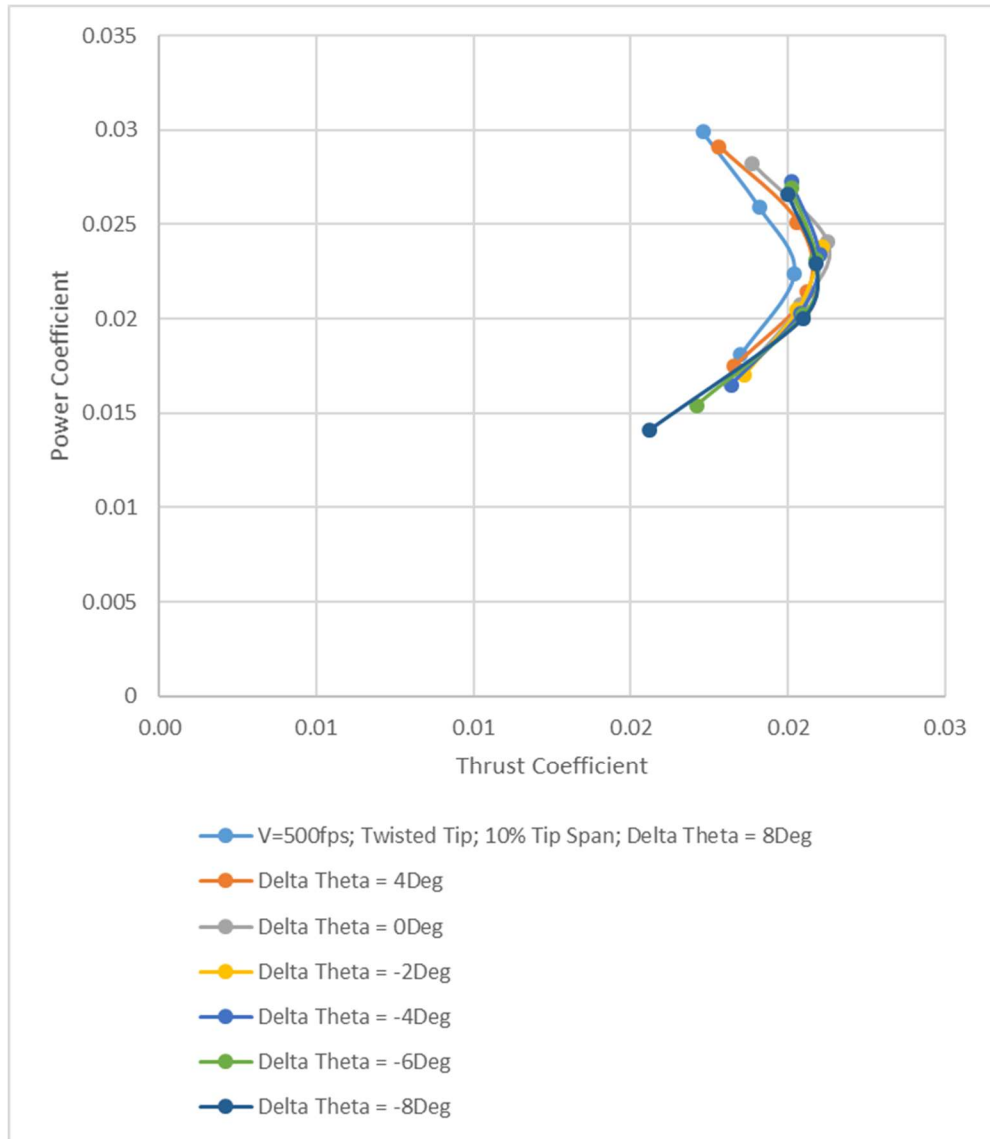
Figure 46. Power coefficient versus rotor thrust coefficient at an axial-flow cruise speed of 500 fps for different values of Δθ.

Figures 47 and 48 show the cruise propulsive efficiency trends for a twisted tip at a cruise axial-flow velocity of 350 fps. Figure 48 suggests for most of the collective range studied that decreasing Δθ (where Δθ<0) increases (to some asymptotic level) the cruise propulsive efficiency for a cruise speed of 350 fps.
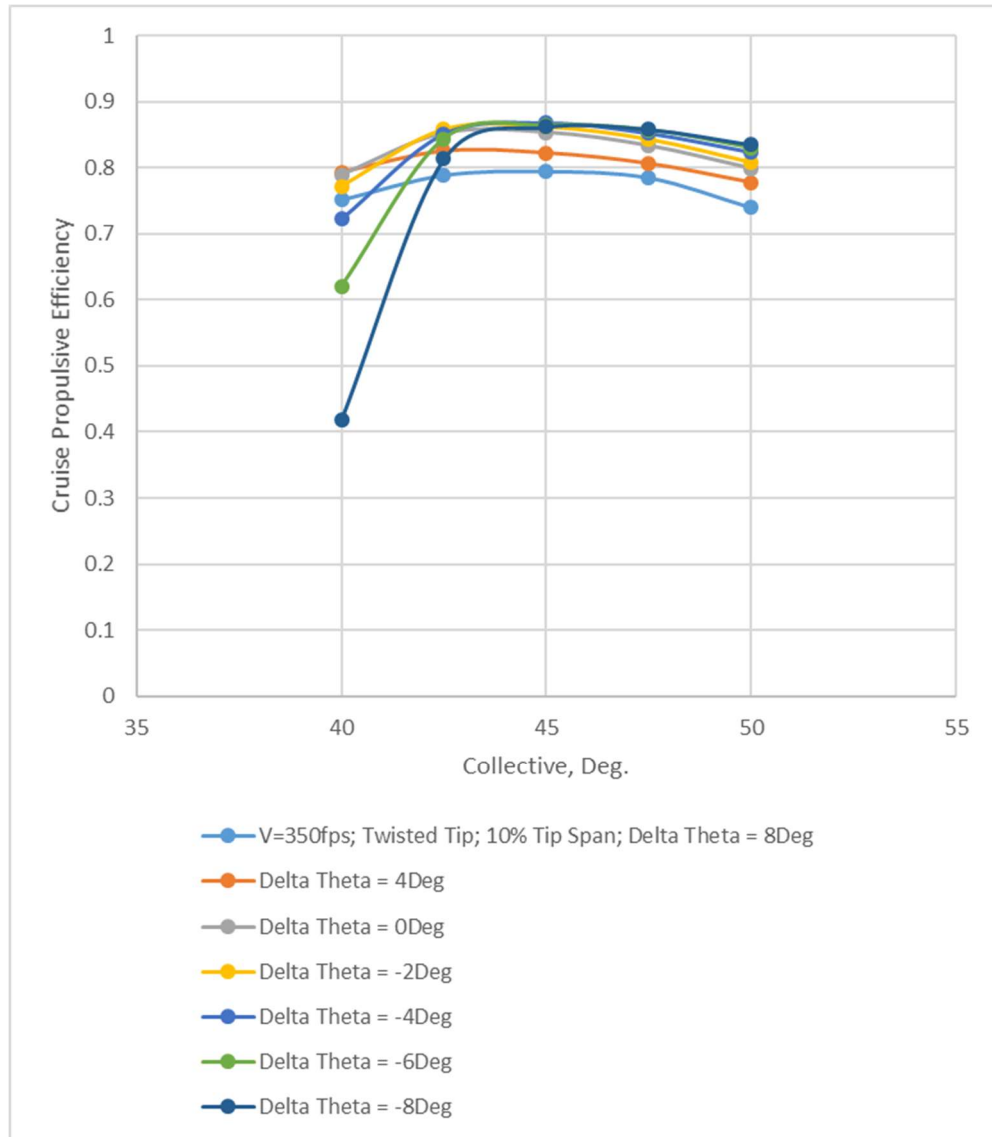
Figure 47. Cruise propulsive efficiency as a function of rotor collective, for axial-flow cruise speed of 350 fps, for twisted indexed-tips (for 10-percent span) for different Δθ.
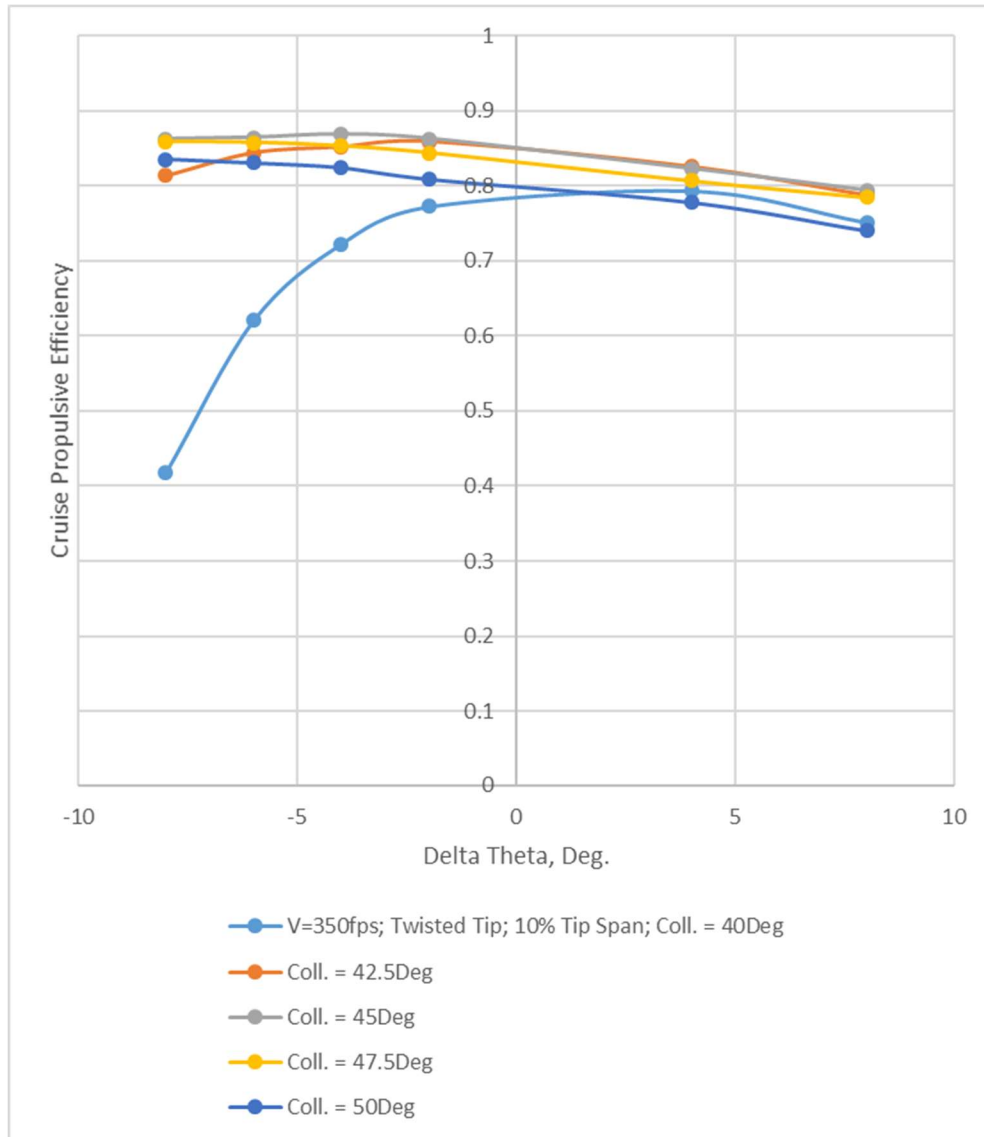
Figure 48. Cruise propulsive efficiency as a function of Δθ for twisted indexed-tips (10-percent span) for axial-flow cruise speed of 350 fps for different rotor collectives.

Figures 49 and 50 show the performance trends for a twisted tip at a cruise axial-flow velocity of 500 fps. Figures 49 and 50 also support the same observation made for the V=350 fps, that decreasing Δθ (where Δθ<0) increases (to some asymptotic level) the cruise propulsive efficiency for a cruise speed of 500 fps. Future work should present predictions for Δθ < −10 degrees to see if there is a maximum reached in propulsive efficiencies as Δθ becomes more negative.
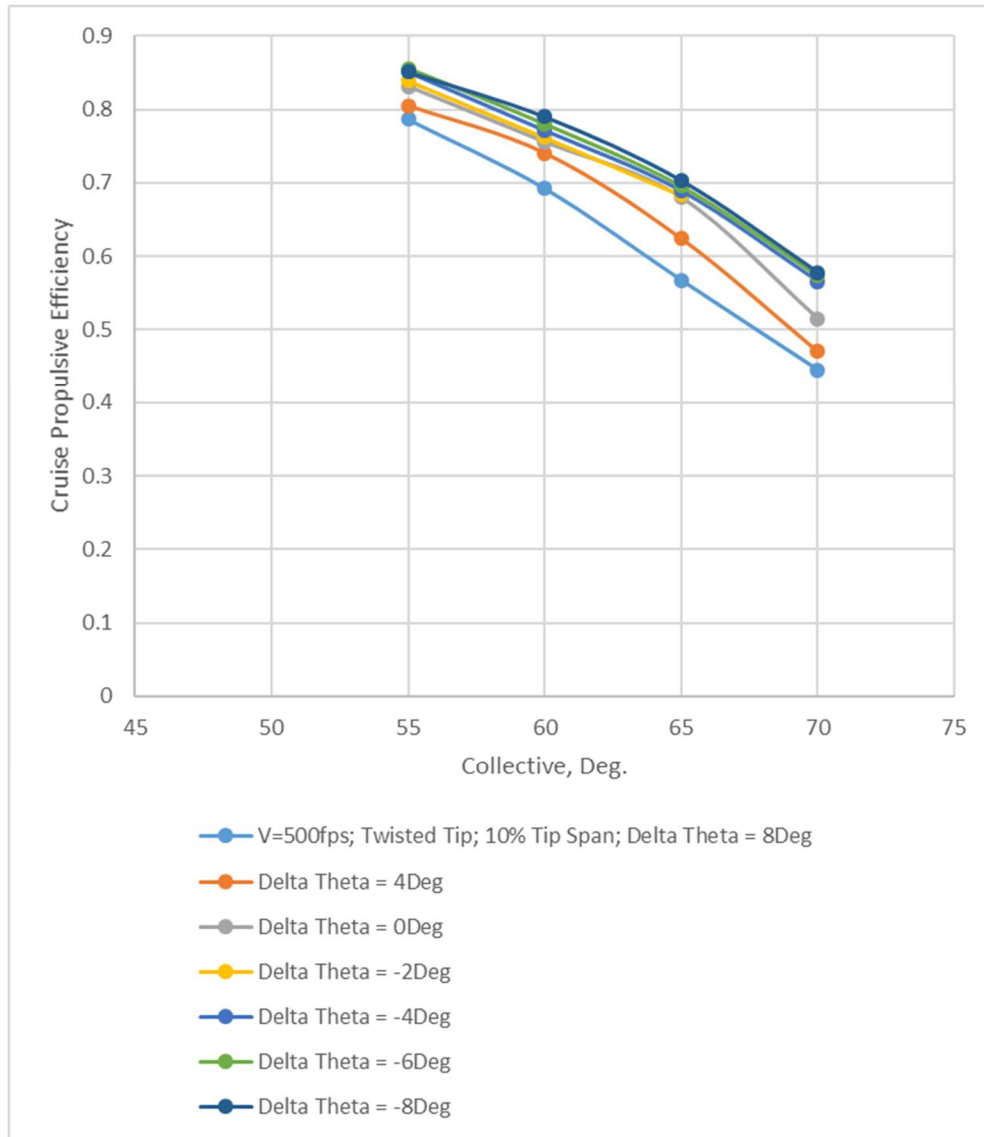
Figure 49. Cruise propulsive efficiency as a function of rotor collective for twisted indexed-tips (10-percent span) for axial-flow cruise speed of 500 fps for different Δθ.
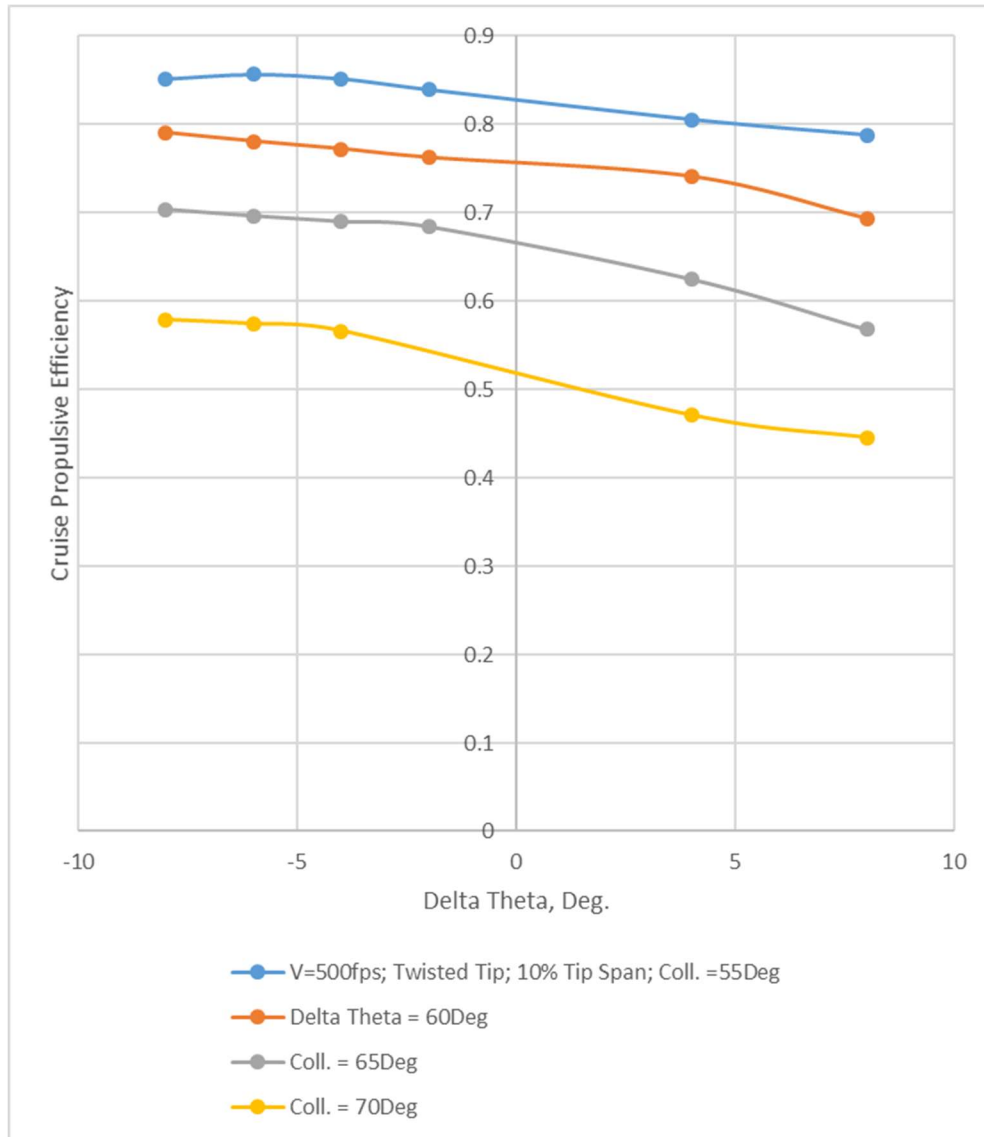
Figure 50. Cruise propulsive efficiency as a function of Δθ for twisted indexed-tips (10-percent span) for axial-flow cruise speed of 500 fps for different rotor collectives.

THE INFLUENCE OF (UNTWISTED INDEXED-TIPS) TIP SPAN ON ROTOR AEROPERFORMANCE

All of the CFD results presented so far in this paper have been for a tip span of 10-percent rotor radii. The next set of results (first for hover and then for cruise/axial-flow conditions) explore the influence of tip span on indexed-tip (untwisted tip) rotor aeroperformance trends. Figure 51 presents a representative set of twist distributions for various (untwisted-tip) tip spans. Future work should consider a similar study of twisted tip span influence on rotor aeroperformance.

51
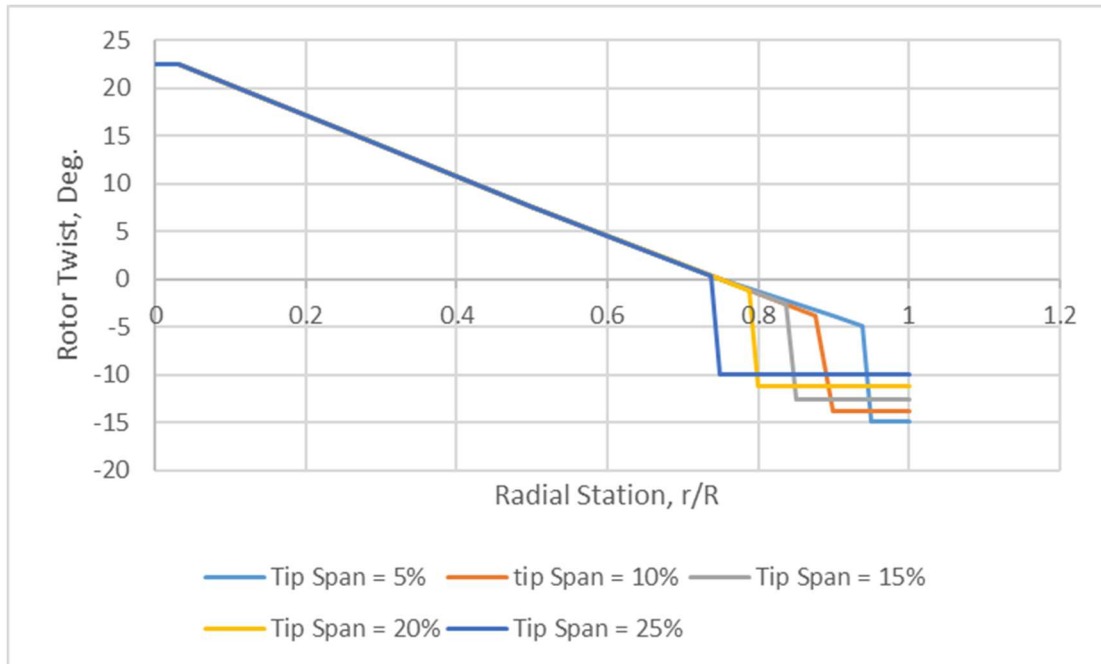
Figure 51. Rotor twist distributions for various (untwisted) indexed-tip tip-spans (constant $\Delta\theta$ = -10 degrees for all twist distributions).

1. Hover Performance CFD Results

The direct effect of tip span for a set of untwisted indexed-tips on rotor hover figure of merit is shown in Figures 52 and 53. As seen in Figure 52, tip span of 10-percent rotor radius appears to yield the best hover figure of merit for the rotor collectives studied and for untwisted indexed tips with a $\Delta\theta$ = -5 degrees. Also, as seen in Figure 53, the best tip span seems to be split between 10 and 15 percent depending on the rotor collective.
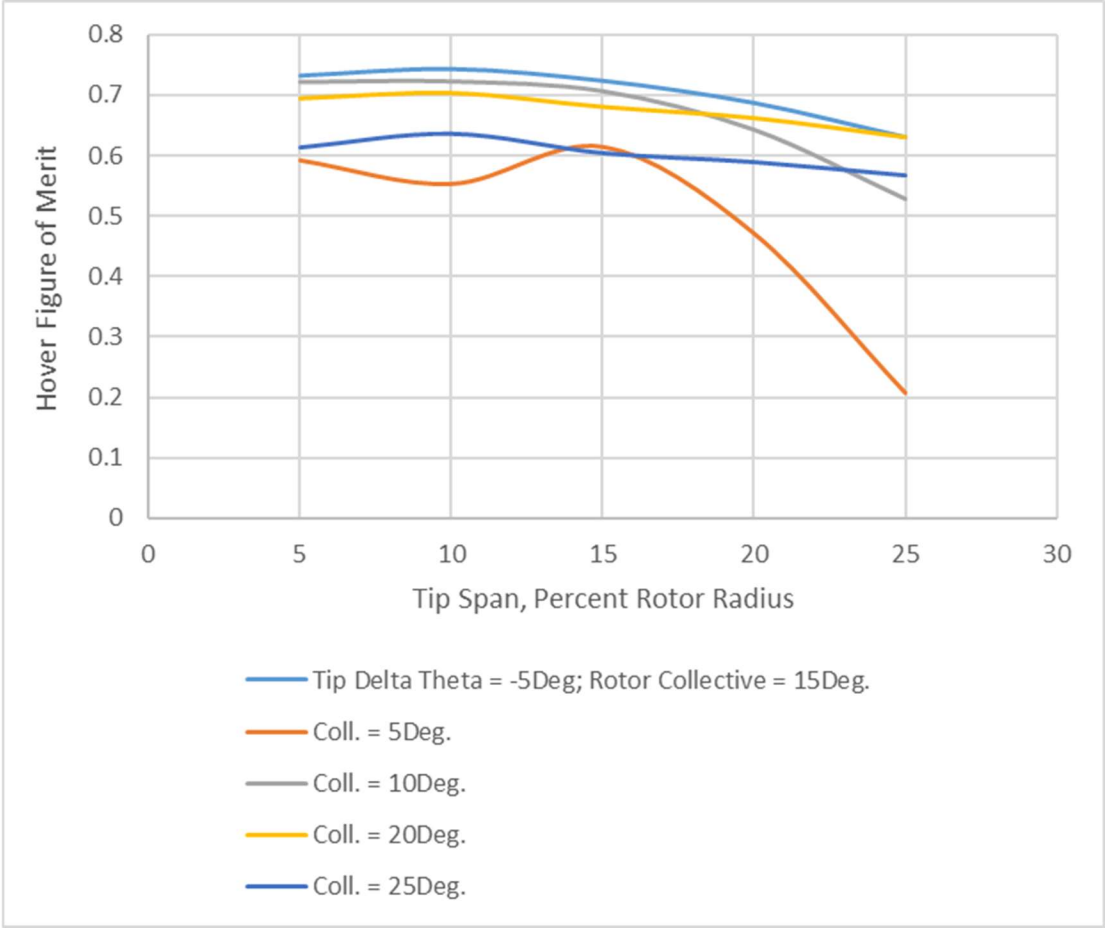
Figure 52. Effect of untwisted tip span for a Δθ = -5 degrees for different rotor collectives for hover.
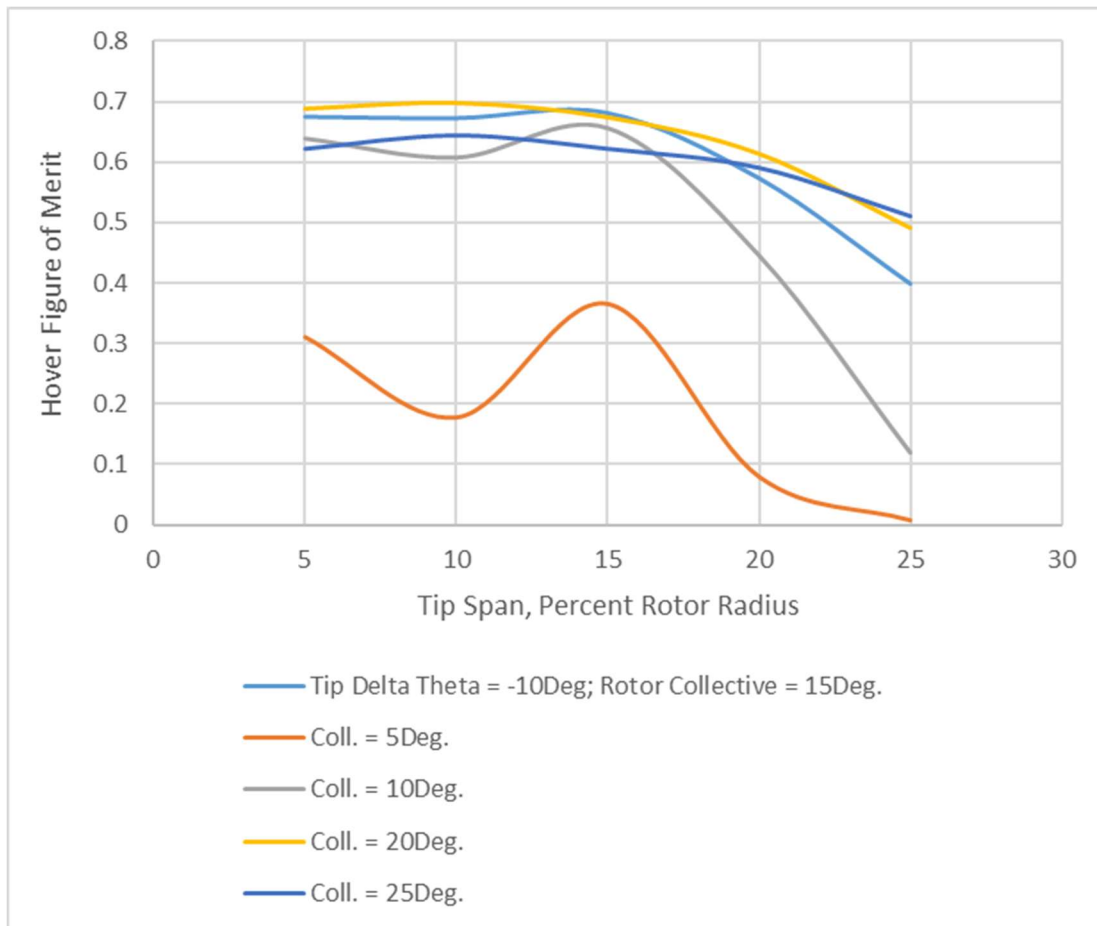
Figure 53. Effect of untwisted tip span for a Δθ = -10 degrees for different rotor collectives for hover.

Figures 54-56 show a more detailed set of rotor performance curves for hover for Δθ = -5 degrees. Figure 54 reveals thrust coefficient as a function of collective for various tip spans (all tips set at Δθ = -5 degrees). Figure 55 shows rotor torque coefficient as a function of collective for various tips spans. Figure 56 is figure of merit as function of thrust coefficient for various tip spans. Figure 56 supports the early observation that 10-percent tip span seems to yield the best result, though still only matching the baseline rotor hover performance.

Figure 54. Thrust coefficient as a function of rotor collective, for $\Delta\theta$ = -5 degrees, for different tip spans (percent of rotor radius).

Figure 55. Rotor torque coefficient as a function of rotor collective, for $\Delta\theta$ = -5 degrees, for different tip spans (percent of rotor radius).

Figure 56. Hover figure of merit as a function of rotor thrust coefficient, for Δθ = -5 degrees, for different tip spans (percent of rotor radius).

Figures 57-59 show a set of rotor performance curves for hover for a Δθ = -10 degrees. These results complement the Figures 54-56 results for Δθ = -5 degrees. Figure 59 suggests the best tip span is between 5- and 10-percent span. This also suggests, for untwisted tips, that it is hard to match or exceed the hover figure of merit of the baseline rotor (which would be functionally equivalent to asymptotically approaching zero tip span).

Figure 57. Thrust coefficient as a function of rotor collective, for Δθ = -10 degrees, for different tip spans (percent of rotor radius).

Figure 58. Rotor torque coefficient as a function of rotor collective, for Δθ = -10 degrees, for different tip spans (percent of rotor radius).

57

Figure 59. Hover figure of merit as a function of rotor thrust coefficient, for Δθ = -10 degrees., for different tip spans (percent of rotor radius).

2. Cruise/Axial-Flow Performance CFD Results

Figures 60-62 are a set of rotor performance curves for an axial-flow cruise speed of 500 fps for a Δθ = -5 degrees for a range of different (untwisted) tip spans. Note that a tip span of 10 percent is not shown in this figure. Figure 60 shows that the larger tip spans will have more of a (small) increase in thrust capability at the higher rotor collectives. Figure 62 shows a cruise efficiency benefit of the 20-percent tip span over the baseline rotor for high thrust conditions. It is important to note that the 15-percent tip span case deviates from the general efficiency trends observed the other tip spans, including the baseline rotor, for 500 fps cruise condition. This will have to be examined more closely in future work.
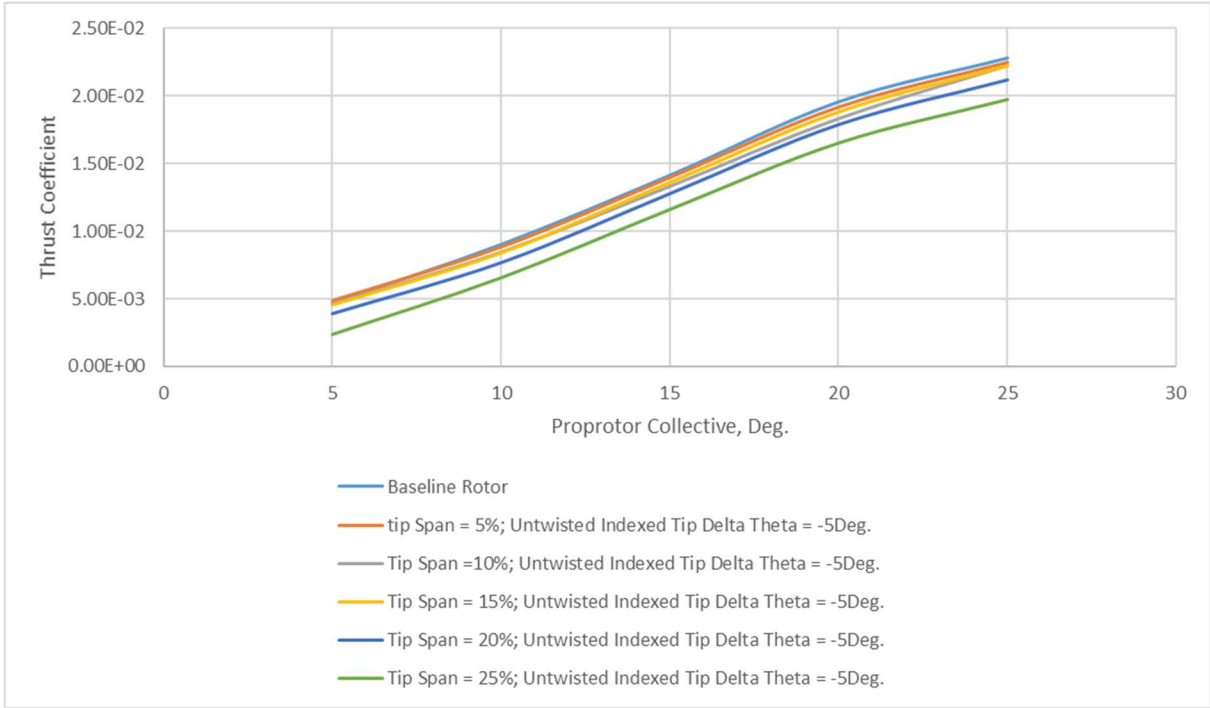
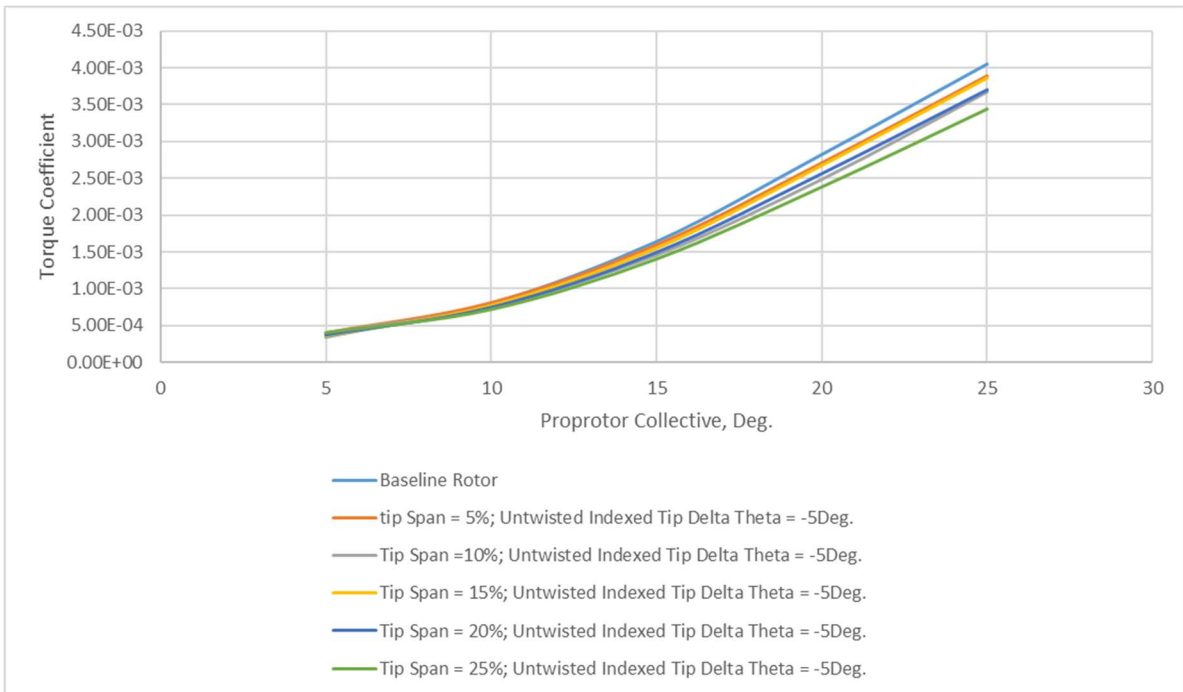Figure 60. Thrust coefficient as a function of rotor collective, for Δθ = -5 degrees, for different tip spans (percent of rotor radius) for an axial-flow cruise speed of 500 fps.

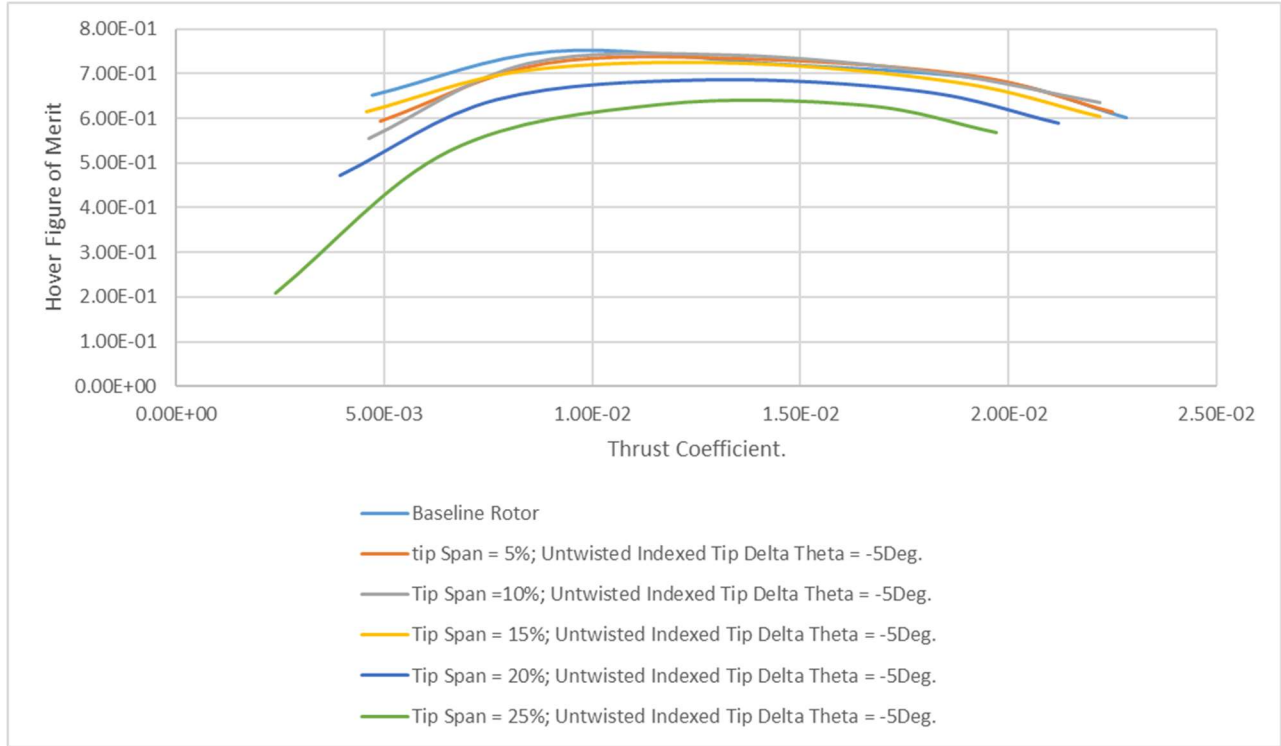Figure 61. Torque coefficient as a function of rotor collective, for Δθ = -5 degrees, for different tip spans (percent of rotor radius) for an axial-flow cruise speed of 500 fps.

59

Figure 62. Cruise propulsive efficiency as a function of thrust coefficient, for Δθ = -5 degrees, for different tip spans (percent of rotor radius) for an axial-flow cruise speed of 500 fps.

Figures 63-65 are a set of rotor performance curves for an axial-flow cruise speed of 500 fps for a Δθ = -10 degrees. Note that a tip span of 10 percent is not shown in these figures. Figure 63 shows increased thrust capability for the 15- and 20-percent tip spans over that of the baseline rotor for high collectives. Figure 65 shows that a 15-percent tip span is the closest of tip spans to approach matching the baseline rotor cruise propulsive efficiency.
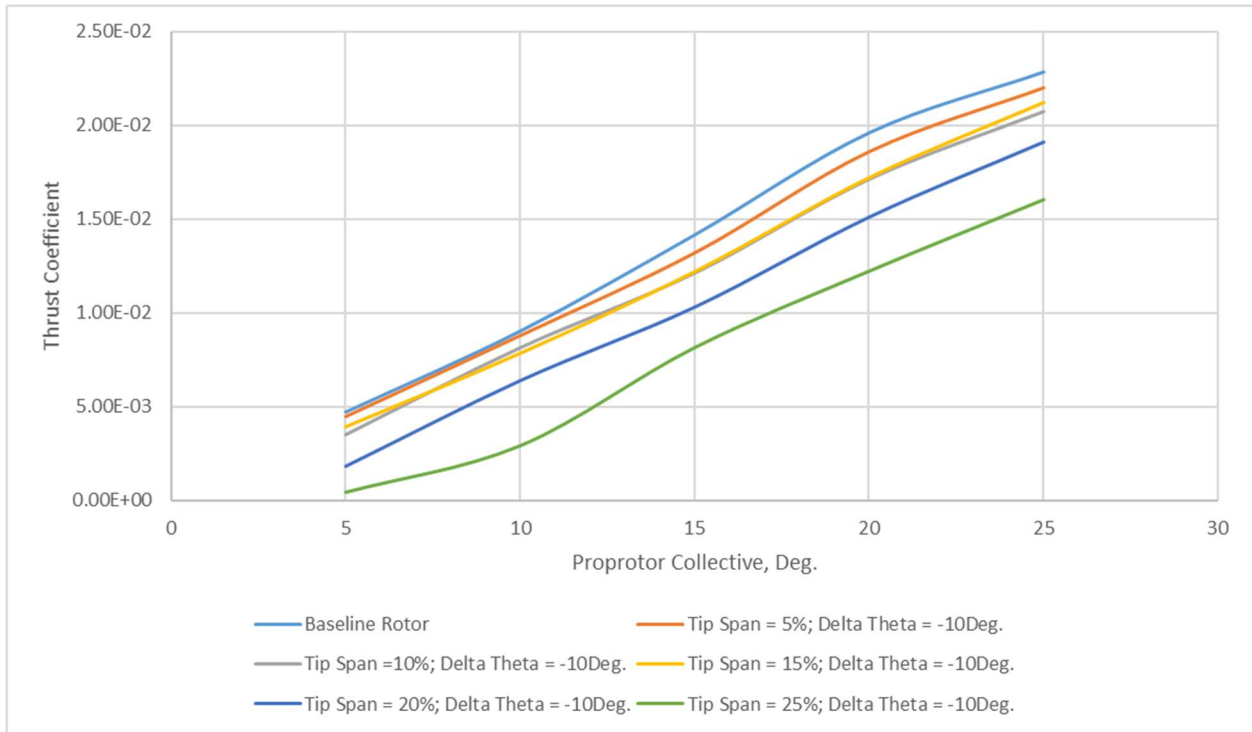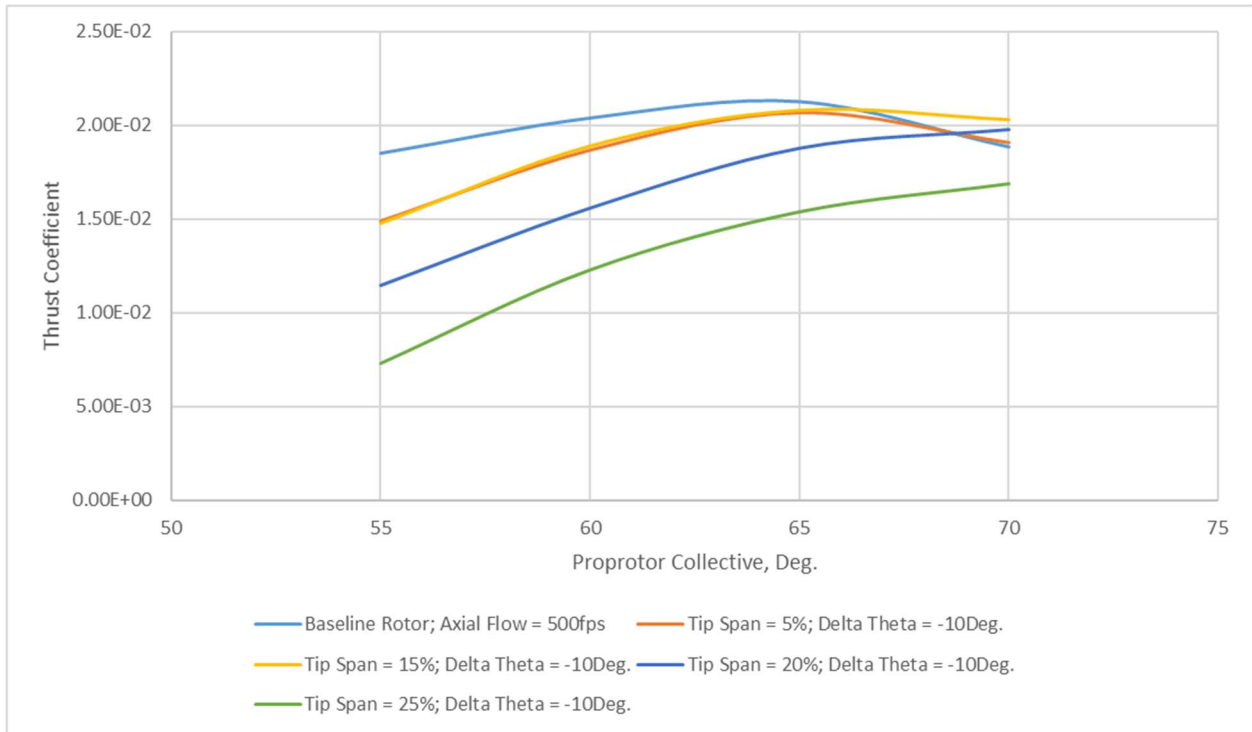
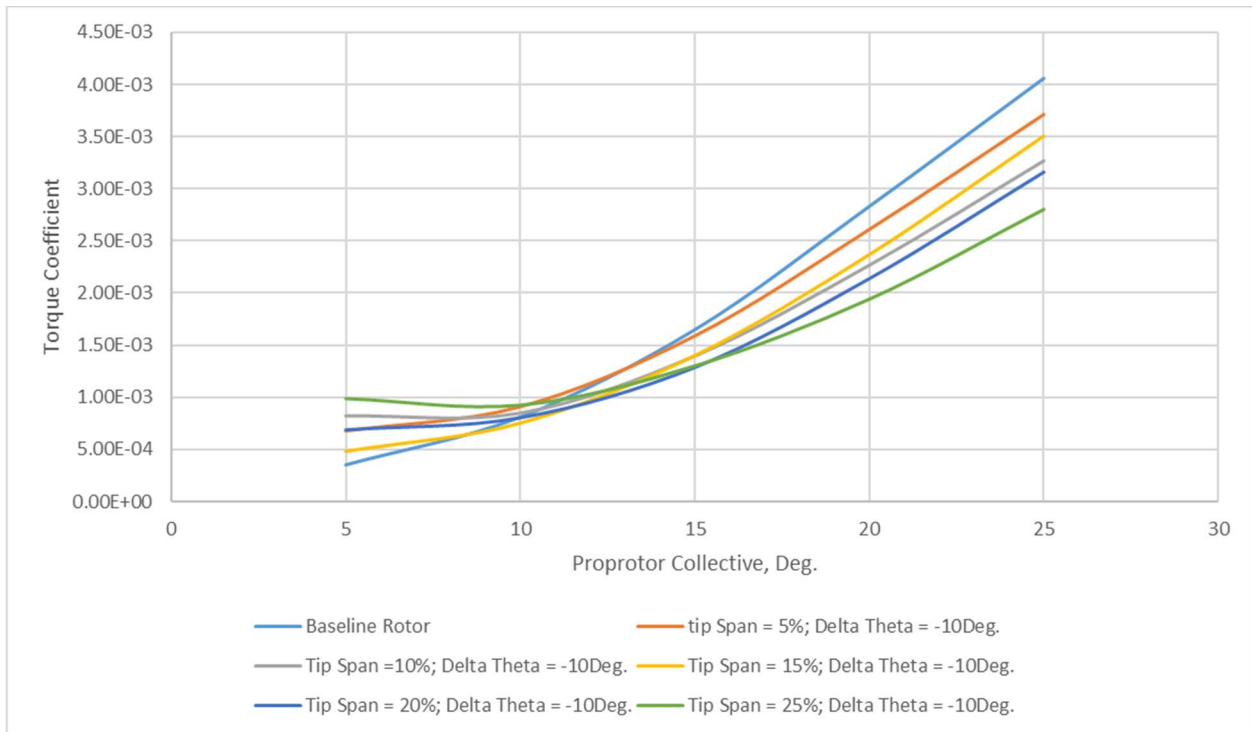Figure 63. Thrust coefficient as a function of rotor collective, for $\Delta\theta$ = -10 degrees, for different tip spans (percent of rotor radius) for an axial-flow cruise speed of 500 fps.
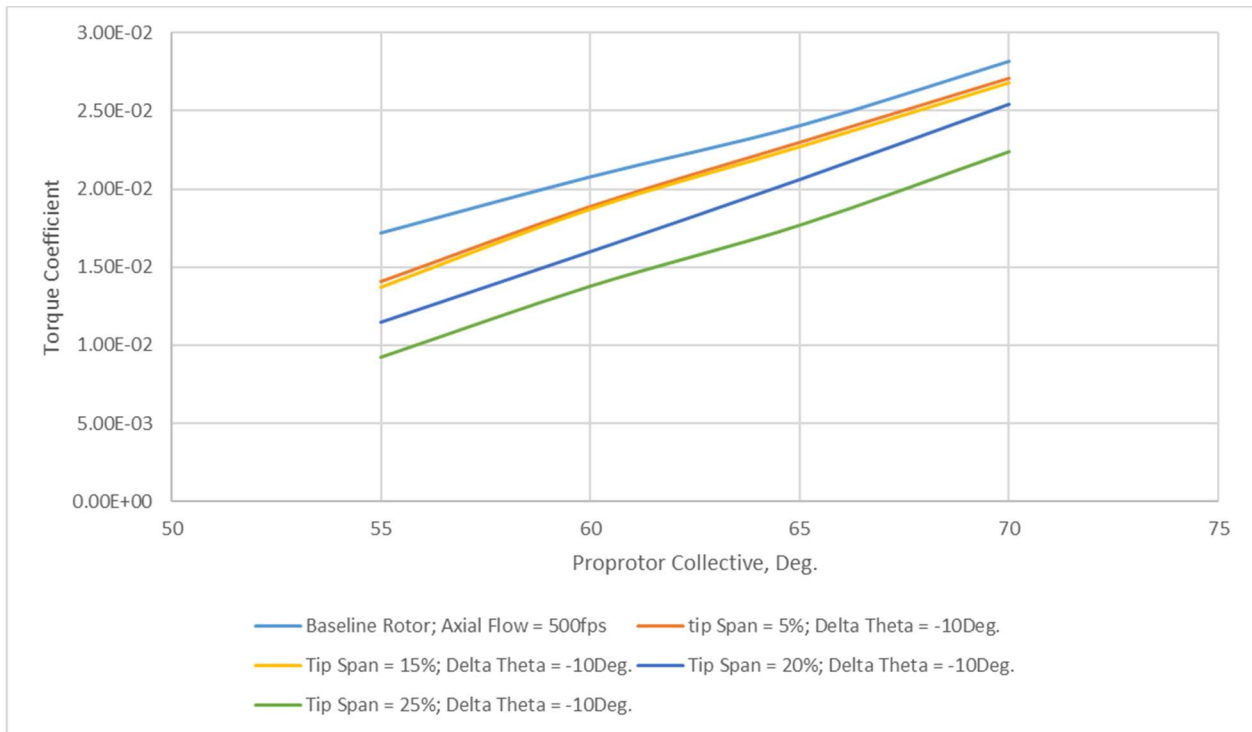
Figure 64. Torque coefficient as a function of rotor collective, for $\Delta\theta$ = -10 degrees, for different tip spans (percent of rotor radius) for an axial-flow cruise speed of 500 fps.
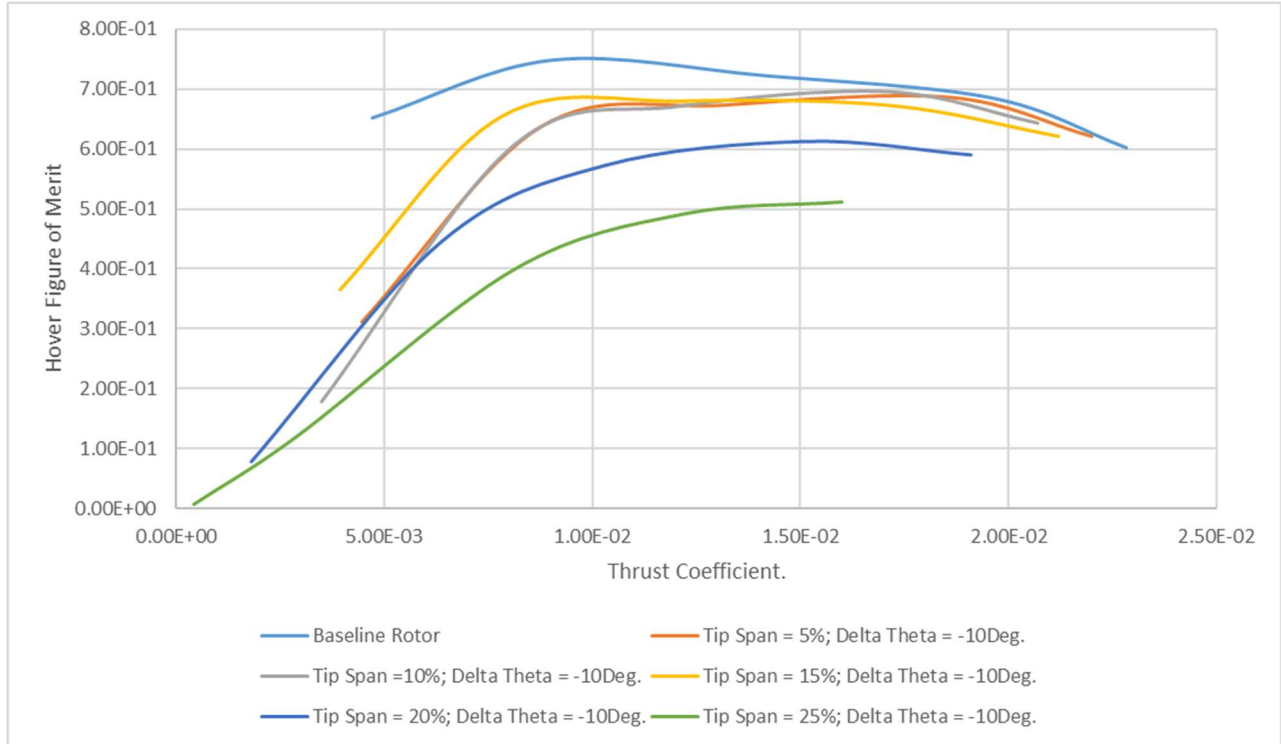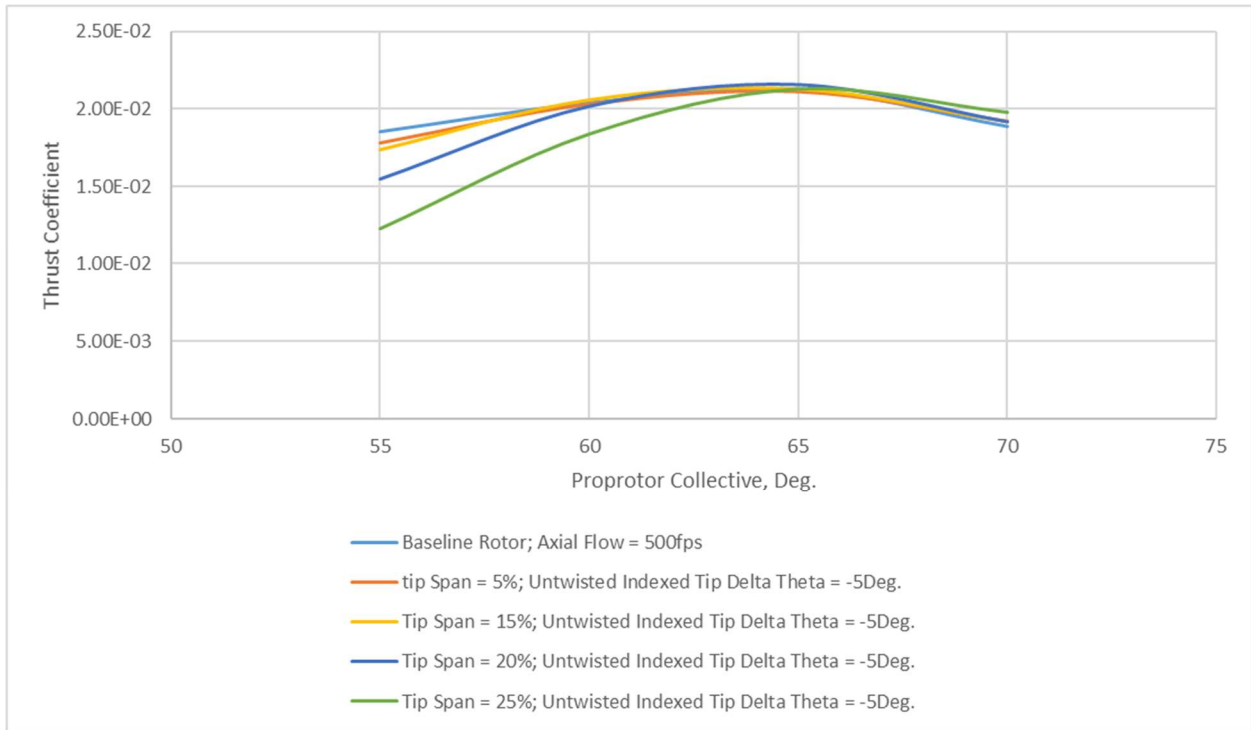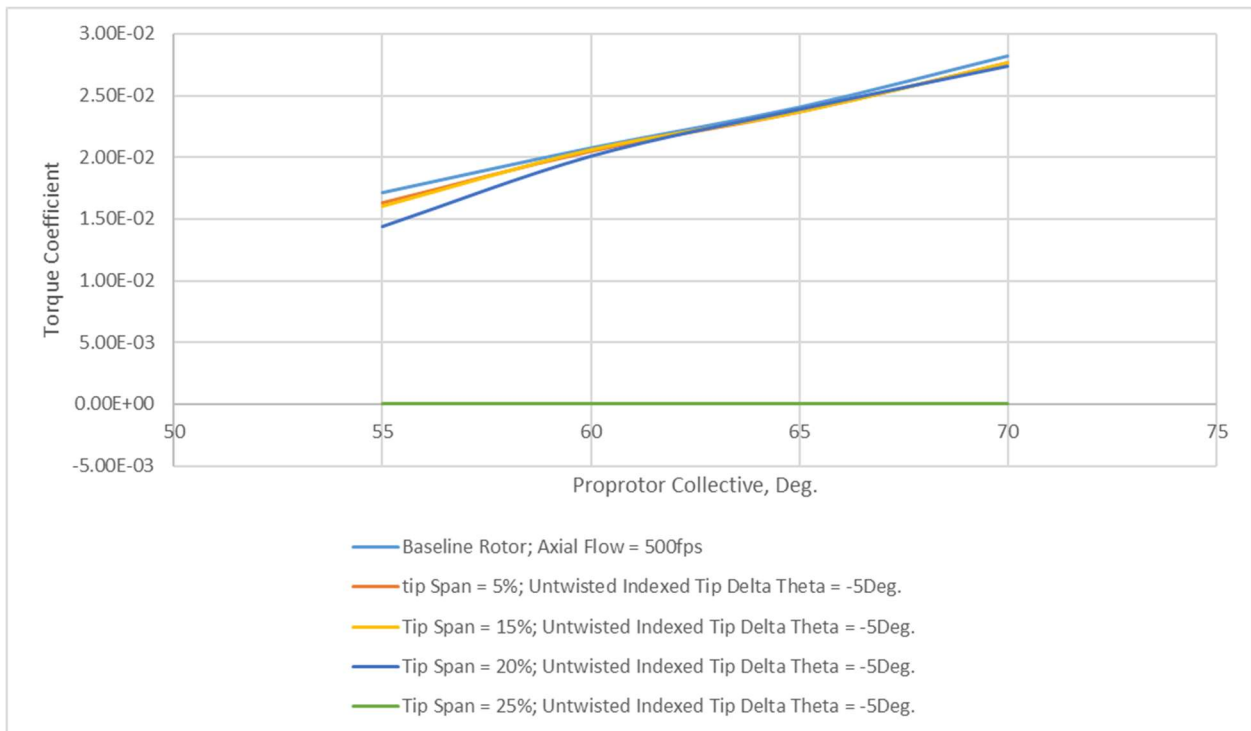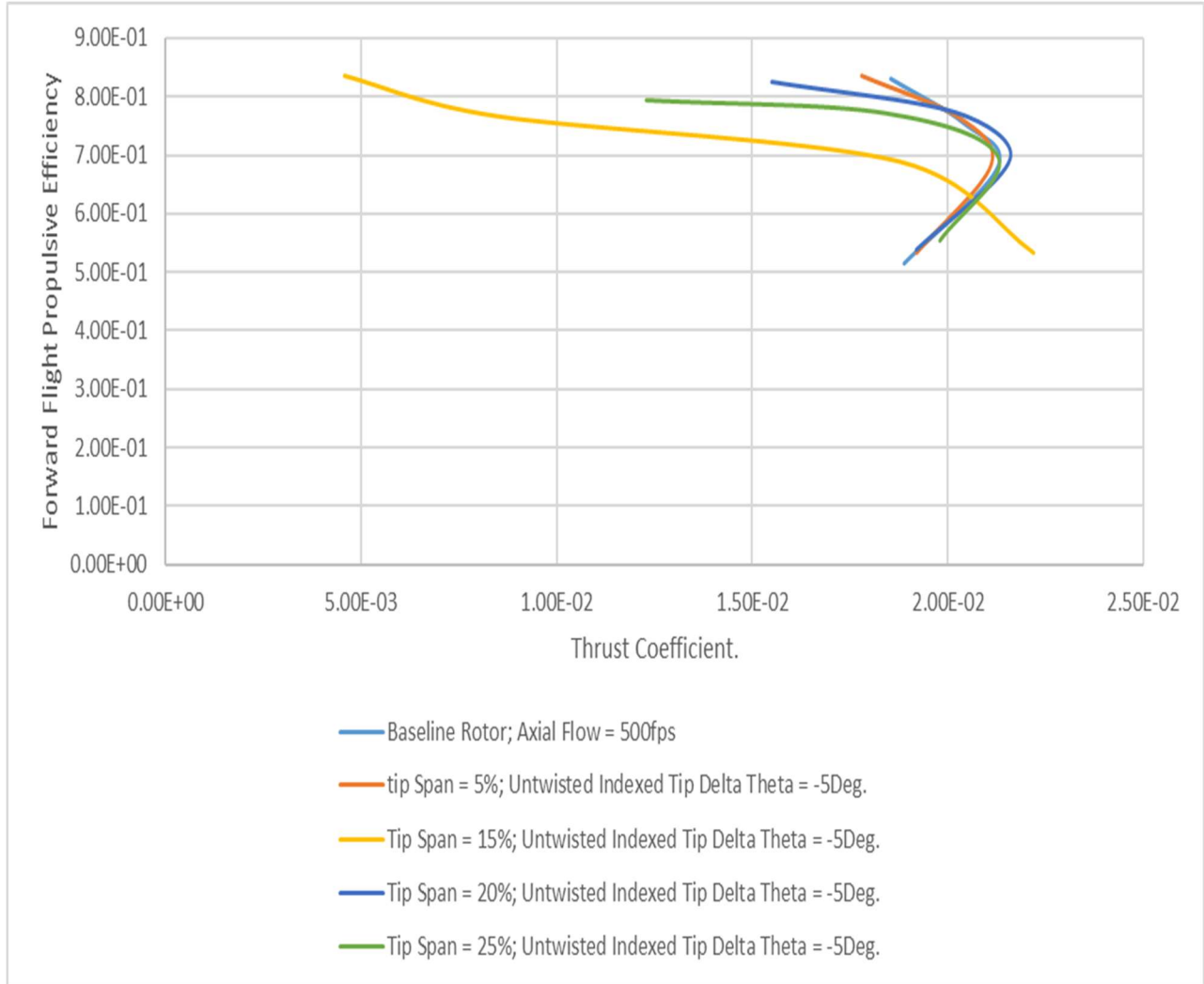
61
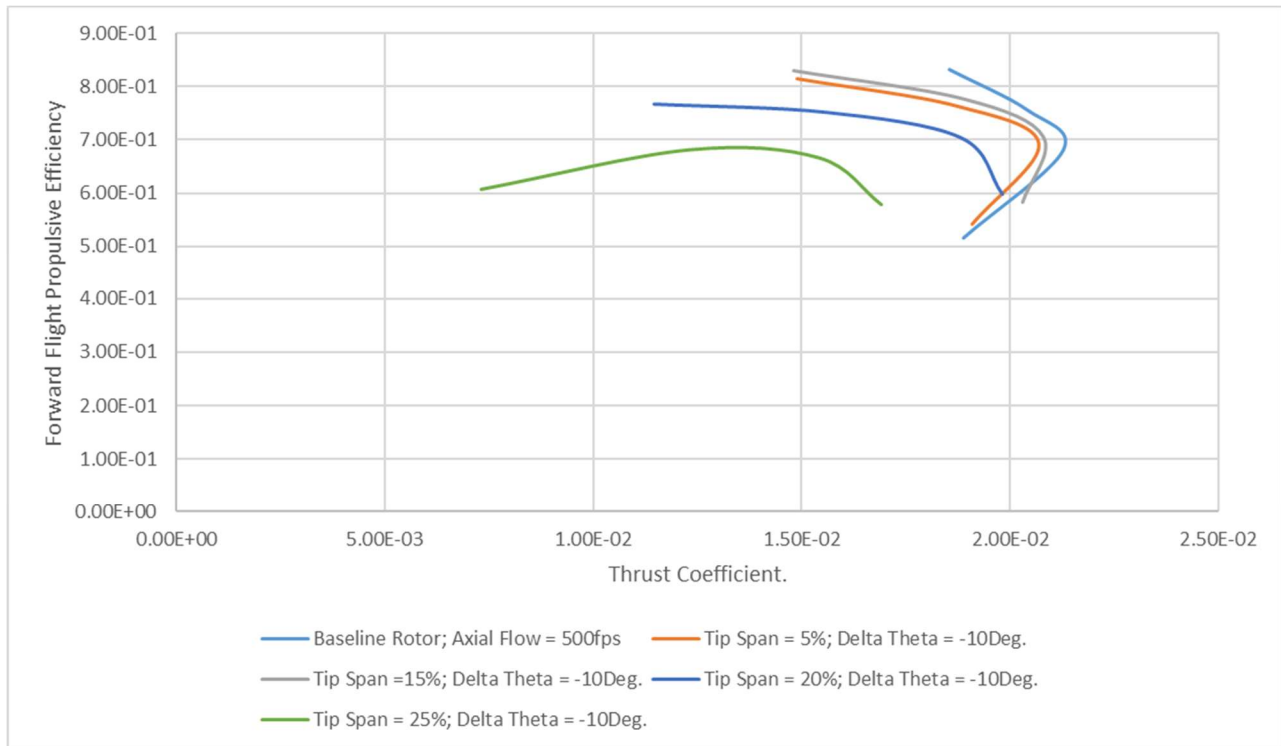
Figure 65. Cruise propulsive efficiency as a function of rotor thrust coefficient, for Δθ = -10 degrees, for different tip spans (percent rotor radius) for axial-flow cruise speed of 500 fps.

CONCLUDING REMARKS

Tiltrotor proprotor design is by definition a compromise between arriving at an efficient hover twist distribution and an efficient distribution for axial-flow forward-flight cruise. The potential incorporation of actively controlled indexed-tips to proprotor blades perhaps provides a better compromise solution for achieving efficient aeroperformance for proprotors for all tiltrotor aircraft flight regimes. The work presented is a combination of analytical treatment of the problem and CFD modeling. For example, the interactional aerodynamics analytical expressions derived in this paper have been shown to correctly model several key features of the proprotor inflow distribution.

The key observations from this work are as follows:

1. An extension of classic Prandtl finite-blade rotor wake analysis appears to model the rotor wakes of indexed-tip proprotors. This was generally confirmed through comparison of the extended-Prandtl analysis results and the computational fluid dynamics predictions.

2. Small improvements in hover figure of merit and axial-flow cruise propulsive efficiency appear to be feasible for both twisted- and untwisted-tips for various

indexed-tip $\Delta\theta$ angles. Indexed-tip angles ranging $\Delta\theta = \pm 10$ degrees were studied in this paper.

3. The optimum indexed-tip $\Delta\theta$ angles are thrust coefficient and axial-flow cruise speed dependent; optimum angles are also dependent on both the indexed-tip type (twisted or untwisted) or tip span in terms of percent radius.

4. The best tip spans, in terms of making small improvements to figure of merit or cruise propulsive efficiency, are relatively short spans, e.g., $tip\ span \leq 15\ percent$.

5. Twisted indexed-tips appear to be slightly better than untwisted tips for the axial-flow cruise cases studied, i.e., 350 fps and 500 fps. Untwisted indexed-tips seem to be slightly better for hover conditions.

6. There is a secondary benefit for indexed-tip rotors on fixed-pitch propellers. The benefit is that the indexed-tips could be commanded/deflected to positive $\Delta\theta$ angles to increase rotor thrust above that of a baseline fixed-pitch propeller.

7. Another secondary benefit is that the current work partially validates the utility of the often-tried approach of using semi-span wing/tip wind tunnel experimental data to factor into, or refine, rotor performance estimates of rotors with novel/advanced tips (fixed or pitching).

The work performed in this paper has solely focused on analytical and computational fluid dynamics hover and axial-flow cruise aeroperformance assessments of indexed-tip proprotors and propellers. Accordingly, considerable future research and development work would be necessary to develop such rotor systems for aircraft. For example, future work is needed to study the aerodynamic and structural loads of indexed-tip proprotors in edgewise forward-flight helicopter-mode and transition/conversion. In helicopter-mode and transition/conversion, indexed-tips could be used to reduce the overall net twist rate of the rotors to reduce blade aerodynamic and structural loading.

REFERENCES

1. Stroub, R., Young, L., Keys, C., and Cawthorne, M., "Free-Tip Rotor Wind Tunnel Test Results," American Helicopter Society 41st Annual Forum, Ft. Worth, TX, May 1985.

2. Martin, D. and Stroub, R., "VSAERO Analysis of Structurally Decoupled Tip Planforms for a Semispan Wing," AIAA 87-2416, 5th Applied Aerodynamics Conference, Monterey, CA, August 17-19, 1987.

3. Kumagai, H., "Spanwise Lift Distributions and Wake Velocity Surveys of a Semi-Span Wing with a Discontinuous Twist," NASA CR 177532, May 1989.

4. Van Aken, J., "An Investigation of Tip Planform Influence on the Aerodynamic Load Characteristics of a Semi-Span, Unswept Wing and Wing-Tip," NASA CR 177428, Dec. 1986.

5. Young, L.A. and Martin, D.M., "Aerodynamic Spring and Damping of Free-Pitching Tips on a Semispan Wing," AIAA CP 92-2111, AIAA Dynamics Specialist Conference, Dallas, TX, April 16-17, 1992.

6. Nixon, M., "Improvements to Tilt Rotor Performance Through Passive Blade Twist Control," NASA TM 100583, Apr. 1988.

7. Fulton, M. and Hodges, D., "Application of Composite Rotor Blade Stability Analysis to Extension-Twist Coupled Blades," AIAA CP 92-2254, 33rd AIAA/ASME/ASCE/AHS/ASC Structures, Structural Dynamics, and Materials Conference, Dallas, TX, Apr. 1992.

8. Bernhard, A.P.F. and Chopra, I., "Development of a Smart-Moving-Blade-Tip and an Active-Twist Rotor Blade Driven by a Piezo-Induced Bending-Torsion Coupled Beam," AHS Annual Forum, Virginia Beach, VA, April 1997.

9. Shen, J., Chopra, I., and Johnson, W., "Performance of Swashplate Ultralight Helicopter Rotor with Trailing-Edge Flaps for Primary Flight Control," AHS 59th Annual Forum, Phoenix, AZ, May 6-8, 2003.

10. Straub, F.K., Anand, V.R., Birchette, T.S., and Lau, B.H., "SMART Rotor Development and Wind Tunnel Test," 35th European Rotorcraft Forum, Hamburg, Germany, Sept. 22-25, 2009.

11. Stroub, R.H., "CONSTANT LIFT ROTOR FOR A HEAVIER THAN AIR CRAFT," US Patent No. 4137010, Jan. 30, 1979.

12. Johnson, W., "Helicopter Theory," Princeton University Press, Princeton, NJ, 1980.

13.   Rajagopalan, G., "RotCFD a Tool for Aerodynamic Interference of Rotors: Validation and Capabilities," Future Vertical Lift Aircraft Design Conference, San Francisco, CA, Jan. 18-20, 2012.

14.   Acree, C.W., Yeo, H., and Sinsay, J., "Performance Optimization of the NASA Large Civil Tiltrotor," International Powered Lift Conference, London, United Kingdom, July 22-24, 2008.

15.   Koning, W., Acree, C.W., and Rajagopalan, R.G., "XV-15 Tilt Rotor Performance Validation Using Computational Fluid Dynamics," AHS Technical Meeting on Aeromechanics Design for Vertical Lift, Holiday Inn at Fisherman's Wharf, San Francisco, CA, Jan. 20-22, 2016.

16.   Martin, D.M. and Young, L.A., "Experimental Study of an Independently Deflected Wingtip Mounted on a Semispan Wing," NASA TM 102842, Sept. 1991.

17.   Paisley, D., "Rotor Aerodynamic Optimization for High Speed Tiltrotors," AHS 43rd Annual Forum, St. Louis, MO, May 1987.

18.   Liu, J. and McVeigh, M., "Design of Swept Blade Rotors for High-Speed Tiltrotor Application," AIAA Aircraft Design Systems and Operations Meeting, AIAA 91-3147, Baltimore, MD, September 23-25, 1991.

19.   Felker, F., Signor, D., Young, L., and Betzina, M., "Performance and Loads Data from a Hover Test of a 0.658-Scale V-22 Rotor and Wing," NASA TM 89419, Apr. 1987.

20.   Felker, F., "Results from a Test of a 2/3-Scale V-22 Rotor and Wing in the 40- by 80-Foot Wind Tunnel," AHS 47th Annual Forum, Phoenix, AZ, May 1991.

21.   McVeigh, M., Grauer, W., and Paisley, D., "Rotor/Airframe Interactions on Tiltrotor Aircraft," Journal of the American Helicopter Society, Volume 35-Number 3, July 1990.